THE RELATIONSHIP OF ICE WATER CONTENT TO ATMOSPHERIC AND MICROPHYSICAL PROPERTIES IN CIRRUS CLOUDS BASED ON IN SITU MEASUREMENTS

by

ANNA ELIZABETH LUEBKE

B.A., University of Colorado, 2008

A thesis submitted to the

Faculty of the Graduate School of the

University of Colorado in partial fulfillment

of the requirement for the degree of

Doctor of Philosophy

Department of Atmospheric and Oceanic Sciences

2013

This thesis entitled:

The relationship of ice water content to atmospheric and microphysical properties in cirrus clouds based on in situ measurements

written by Anna Elizabeth Luebke

has been approved for the Department of Atmospheric and Oceanic Sciences

Dr. Linnea M. Avallone

Dr. John J. Cassano

Dr. Martina Krämer

Dr. Shelly L. Miller

Dr. Darin W. Toohey

Date_____

The final copy of this thesis has been examined by the signatories, and we
Find that both the content and the form meet acceptable presentation standards
Of scholarly work in the above mentioned discipline.

Luebke, Anna Elizabeth (Ph.D., Department of Atmospheric and Oceanic Sciences)
The relationship of ice water content to atmospheric and microphysical properties in cirrus clouds based on in situ measurements

Thesis directed by Professor Linnea M. Avallone

Abstract

Ice clouds are known to be major contributors to radiative forcing in the atmosphere, yet understanding and describing their microphysical properties remains challenging. The ice water content (IWC) of cirrus clouds is of particular interest because it can be directly related to a number of other radiatively important variables such as extinction and effective radius. This dissertation explores data obtained from numerous airborne research campaigns to elucidate the dominant factors that determine the IWC and crystal concentration (Ni) characterizing cirrus clouds.

The first part of this study uses a new merged dataset to obtain a representation of the IWC-temperature relationship using probability distribution functions (PDFs), which allows for the variability of IWC within a temperature band to be visualized. The IWC-PDFs are observed to be bimodal over the whole cirrus temperature range. This bimodality is also found in Ni-PDFs and might be attributed to different cirrus formation mechanisms such as heterogeneous and homogeneous freezing.

Next, two midlatitude datasets (MACPEX and MidCiX) with differing IWC and Ni distributions are used to explore how cloud formation processes contribute to the resulting cirrus characteristics. Starting with large-scale processes, a case study analysis demonstrates the link between synoptic-scale dynamics and the differences observed between the MACPEX and

MidCiX datasets. However, that link is not always clear, indicating that additional information is required to explain it. This is particularly evident when considering the Ni observations from MACPEX, which appear unaffected by factors such as vertical velocity. This result is unexpected considering the relationship between vertical velocity and nucleation processes.

The final component of this analysis explores the cirrus formation processes at the nucleation level, while continuing to examine why the data in MACPEX and MidCiX are different from each other. A comparison to model simulations reveals that heterogeneous nucleation and subsequent homogeneous nucleation suppression are responsible for the Ni distribution in MACPEX. Conversely, the MidCiX IWC and Ni datasets exhibit a compatibility with model results showing heterogeneous nucleation followed by a secondary homogeneous nucleation event. Thus, it is likely that the differences observed in MACPEX and MidCiX mostly stem from differences in ice nuclei concentrations.

Acknowledgements

First and foremost, I would like to thank my advisor, Linnea Avallone for the support, advice, and opportunities that she has given me from the time that I was a somewhat lost undergraduate with an interest in Atmospheric Science to now. I feel very fortunate to have had her as a mentor these past several years and my gratitude for all that she has taught me is immeasurable. I would also like to thank Martina Krämer for being a "second advisor" to me. She has been a great source of support and guidance throughout my graduate career and influential in my success as a researcher. I could not ask for two better people to work with and learn from.

I would also like to thank my committee members, Darin Toohey, John Cassano, and Shelly Miller for their contributions to my academic and research goals throughout the years, and for their continued support. Additionally, I would like to acknowledge Carl Schmitt, Darrel Baumgardner, and Jonathan Dean-Day for taking the time to work with me on using their data correctly and effectively in my analysis endeavors. In regard to the content in this dissertation from Luebke et al. (2013), I wish to acknowledge the remaining co-authors, Christian Rolf and Jessica Meyer, for their contribution and hard work. For the grant support to accomplish my research goals, I would like to thank the NASA Earth Science Division Radiation Sciences Program and Upper Atmosphere Research Program.

Lastly, to my friends and family for their love and support to keep me going when things got tough, I am immensely grateful. In particular, to my mom and dad, the most enthusiastic members on "Team Anna", I couldn't have done it without you.

Table of Contents

Tables

Figures

Chapter 1 Introduction

1.1 Clouds and Climate Change

The causes, effects (both known and potential), and the uncertainties associated with climate change are well documented. As the 2007 Fourth Assessment of the Intergovernmental Panel on Climate Change (IPCC) report indicates, the complexity of the climate system and the numerous feedback loops ensure that all components within the climate system have some role to play as changes to the system occur. For example, the increase in greenhouse gas concentrations has widespread effects in the atmospheric, oceanic, and terrestrial domains that in turn set off other feedbacks and effects in chemical and radiative balances. The IPCC report makes note of a general warming trend, changes in frequency and intensity of drought and precipitation events, and an increase in sea level, for instance. Each of those phenomena then impacts sectors of society such as agriculture, water resources, human health, industry, and settlement, thus demonstrating the widespread impact on the social, economic, environmental, and governmental spheres.

Since 1988, the IPCC has produced reports detailing the status of climate research, including discussions of what is known and unknown. Based on this information, decisions can be made on how best to prevent and/or manage the causes of climate change and how to adapt to current and projected impacts. Courses of action have taken place on different policy platforms and through developments of new or improved technologies. However, the complexity of these

issues and the uncertainties that exist at the scientific level make creating a fitting, effective response to climate change difficult.

In what is now a well-known and often referenced figure produced in the 2007 IPCC report (shown here in Fig. 1.1), the radiative forcing impacts of various atmospheric components are shown. Among the most significant is the effect from clouds.

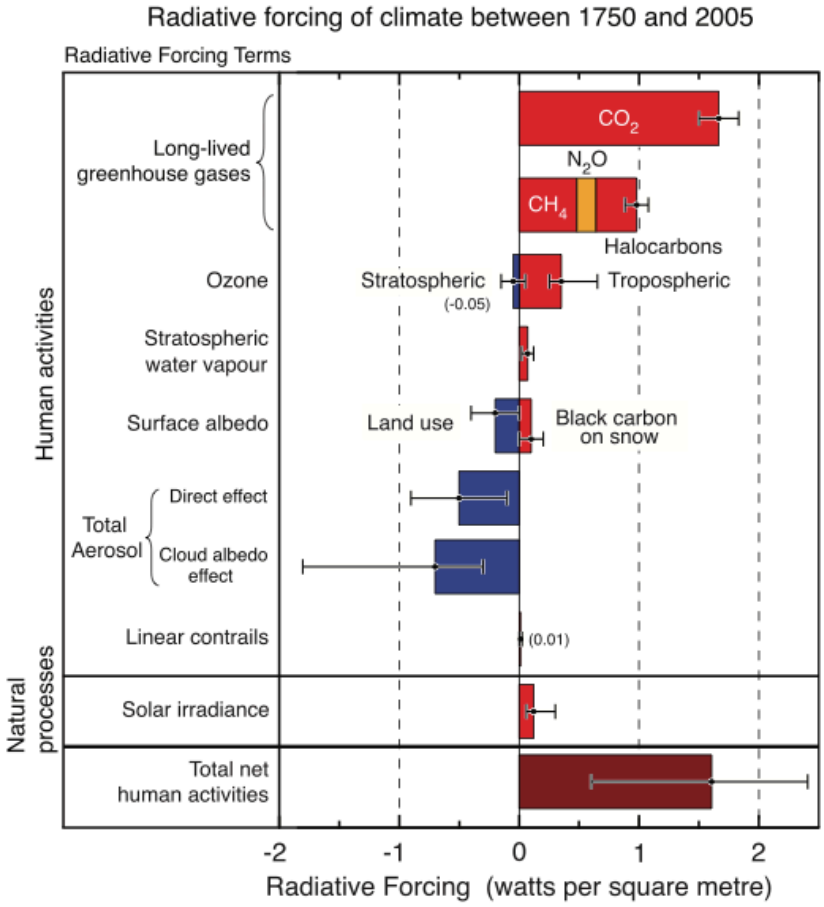

Figure 1.1. A representation of the radiative forcing impacts and uncertainties from various constituents as noted in the 2007 IPCC report. This figure is copied from FAQ 2.1, Fig. 2 of that report.

As the report states, “Clouds play an important role in regulating the flow of radiation at the top of the atmosphere and at the surface”, an impact that is global in scale. More noteworthy are the

declarations that the radiative impact of clouds has the largest uncertainty among those of the atmospheric constituents and that the scientific understanding of the radiative impact is low. The report goes on to describe how anthropogenic activities have led to an increase in aerosols and what kind of influence that increase has on cloud properties. As explained in a review by Lohmann and Feichter (2005), though aerosols directly and significantly affect the radiation budget of the atmosphere in their own right, they also have numerous indirect effects. For example, an increase in aerosols means that there is an increase in cloud condensation nuclei (CCN). This in turn can lead to an increase in cloud optical depth (via the Twomey effect) and an increase in the lifetime of a cloud, both of which have a cooling effect. A summary of the aerosol, cloud, and radiation interactions noted in the IPCC report is shown in Fig. 1.2.

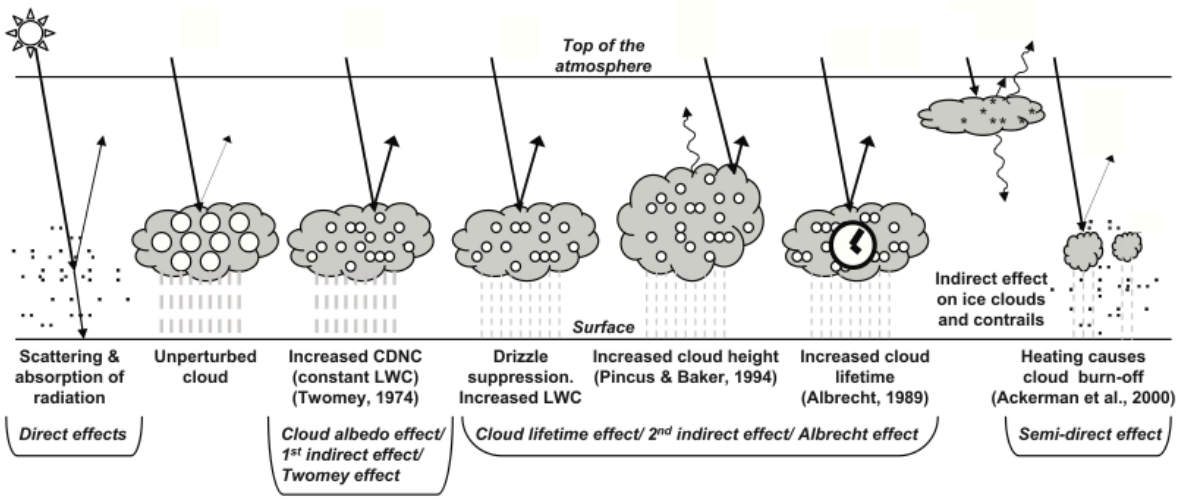

Figure 1.2. A demonstration of the interactions between clouds and aerosols and their radiative impacts. As noted in the 2007 IPCC report, the small black dots are representative of aerosols while the larger white circles indicate cloud droplets. The straight lines represent solar radiation, while wavy lines indicate terrestrial radiation. This figure has been copied from Fig. 2.10 of that report.

The effects become more complicated when narrowing the field to consider ice clouds only. Although there is a considerable amount of research on cirrus clouds, the 2007 IPCC report says little about them, focusing mostly on their interaction with aircraft emissions, another area in which very little is known. Cirrus clouds have the ability to both trap infrared terrestrial radiation and reflect solar radiation. Therefore, they are able to produce either a warming or a cooling effect on the Earth, depending on the balance between these two processes. The microphysical properties of an individual cirrus cloud, such as the cloud particle sizes (Liou et al., 2008) and the crystal habits (van Zadelhoff et al., 2007), determine whether absorption or reflection will dominate for a particular cloud. For example, Kinne and Liou (1989) found that a large number of small ice crystals are more effective at scattering radiation than a small number of large ice crystals. This example illustrates why having a good understanding of the properties of a cirrus cloud is critical to understanding that cloud's radiative role. However, as discussed below, the overall role of cirrus in the radiation budget of the atmosphere is difficult to determine owing to the number and variability of the microphysical and macrophysical, and thus radiative, properties involved, as well as to the current lack of understanding of how and why some of those variations occur.

1.2 Cirrus Clouds

Cirrus clouds are clouds that consist entirely of ice crystals and are found globally in the upper troposphere at altitudes where temperatures range from about 235 K to 185 K. They have been observed to cover close to 40% of the Earth at any given time, with the greatest coverage at the tropics and along the midlatitude storm tracks (Wylie and Menzel, 1999). In earlier years, the lack of aircraft with the ability to fly high into the troposphere as well as the unavailability of

remote sensing equipment designed for this kind of work made examining and understanding cirrus more difficult (Liou, 1986).

Now that the proper equipment is more readily available, cirrus are a prime candidate for research given the fact that they are globally accessible and occur in a variety of atmospheric conditions. As a result, entire research projects have been dedicated to providing better representation of cirrus clouds for use in general circulation models (GCMs) and for improving the existing technologies used to obtain in situ measurements of cirrus properties. Airborne measurements through campaigns like the Midlatitude Airborne Cirrus Properties Experiment (MACPEX) provide observations of many cirrus properties at one time, on small temporal and spatial scales that are comparable to the scales on which cirrus dynamics occur, and with instrumentation that is complementary and useful for comparisons of different sensing methodologies.

Remote sensing is another useful tool for cirrus research. One example of this is the Atmospheric Radiation Measurement (ARM) Climate Research Facility (ACRF) in Oklahoma. The benefit of stationary instrument suites is that they are able to capture more long-term measurements than can be acquired in an airborne campaign, which typically only lasts for a few months at most. The measurements are excellent time series for a particular location and useful statistics can be derived from such data. One downside is that, since the instrumentation is stationary, only a single location is represented in the dataset. An analysis based on such a dataset may not accurately depict the properties of cirrus in other locations. The use of satellites overcomes some of these challenges, as demonstrated by large-scale projects like the International Satellite Cloud Climatology Project (ISCCP), which provide global observations of cirrus clouds. However, there are challenges facing satellite instrumentation such as the

development of retrieval techniques and algorithms that supply reliable and accurate products from their observations (e.g. Mioche et al., 2010). In order to overcome these obstacles, the use of ground-based or aircraft data are often required for validation purposes.

1.2.1 Role of Cirrus in Chemical and Hydrologic Feedbacks

In addition to their role in the radiation budget, cirrus clouds also contribute to other important cycles in the Earth system. In terms of the chemistry of the atmosphere, the ice crystals in cirrus clouds offer optimal sites for heterogeneous chemistry to occur in the upper troposphere. For example, NO_x species can undergo hydrolysis on ice particles, which effectively removes NO_x from the atmosphere (Ravishankara, 1997). Due to the role of NO_x in ozone production in the troposphere, it is important that its atmospheric concentrations and interactions are well documented.

Cirrus clouds are also a contributor to the water budget of the upper troposphere and the lower stratosphere. The measured increase in water vapor in the stratosphere over the last few decades is of particular concern due to its ties to climate change and its potential to affect stratospheric ozone through heterogeneous chemistry and production of hydroxyl radical. Understanding how water is being transported there in the first place is a key component in determining why the increase in water vapor is occurring. In a study by Wang et al. (2009), evidence is presented suggesting that the deep convection associated with thunderstorms can transport water vapor through the tropopause and into the stratosphere in the form of cirrus clouds by a phenomenon known as “jumping cirrus” or overshooting top plumes.

1.2.2 Ice Cloud Microphysics

Cirrus Properties

Owing to the number of microphysical and macrophysical properties used to characterize cirrus clouds, there are many avenues of research that can be pursued. The macrophysical properties include features such as the altitude, thickness, and horizontal scale of the cloud. However, the analyses presented in this dissertation focus on the microphysical properties related to the ice crystals that make up the cloud. One of the microphysical properties of cirrus that is essential for describing their role in various atmospheric systems, and that is the basis for this work, is ice water content (IWC). IWC is the mass of ice per unit volume of air, often expressed in ppmv or g kg^{-1}. Currently, it is known that the IWC of cirrus varies over at least six orders of magnitude (from 10^{-3} ppmv to 10^{3} ppmv) and is influenced by factors such as the water vapor content of the air and temperature (Schiller et al., 2008).

Going back to the two cases listed above, the importance of knowing the IWC of the cirrus clouds involved is clearly essential. Starting with the atmospheric chemistry example, in order to eliminate any uncertainty concerning the amount of NO_x that could be removed by ice, it is imperative to know how much ice water there is to begin with as well as how variable that IWC can be. In the case of the "jumping cirrus" water transport, not only is it important to know how much IWC is in the cirrus that is being transported but also how the mechanism of initial cloud development influences the resulting IWC.

More central to the analyses presented here is the importance of IWC in the radiative role of cirrus clouds (Liou et al., 2008). IWC is very closely related to ice crystal number, size, and extinction and is often used as the basis for obtaining those variables in model schemes. An example of the numerical relationship between IWC and extinction is shown in Chapter 2, Eq.

(2.5) (Heymsfield et al., 2005). Therefore, it is imperative that IWC and other microphysical properties are accurately represented both in magnitude and their relationship to one another since they are all used to determine the radiative properties of a cirrus cloud.

Large-scale Dynamics

The vertical motions of the atmosphere, both large and small, have been found to play a significant role in the formation of cirrus clouds. In the late 1950s, an area of research concerning the relationship between weather and cirrus emerged. In the first published study (Stone, 1957), which was sponsored by the Air Force, surface and aircraft observations were compiled that showed a correlation between the jet stream and the occurrence of cirrus clouds, particularly in terms of where in relation to the jet stream cirrus clouds were likely to be found. As noted by Wylie (2002), it is now generally understood that three weather-related mechanisms are primarily responsible for the formation of cirrus clouds: baroclinic fronts and lows, convection, and orographic lifting. Furthermore, the in situ aircraft measurements analyzed by Heymsfield (1977) noted the relationship between vertical velocity and the resulting cirrus characteristics in terms of the IWC and ice crystal concentrations. Given that large-scale dynamics are essential for transporting the moisture and setting up the cooling rates responsible for cirrus formation or maintenance, it is not surprising that the synoptic systems characterized by more rapid ascent displayed cirrus clouds that contained more ice water and higher ice crystal concentrations. Chapter 4 contains a more thorough literature review of this topic.

Ice Nucleation

Ice nucleation is the mechanism by which ice particles are formed. This process can happen homogeneously or heterogeneously, the specifics of which are given below. For one of these ice formation pathways to begin, certain thresholds must be met in terms of the relative

humidity with respect to ice (RH_{ice}), which relies heavily on the amount of available water vapor and the rate at which the air is cooling. Ultimately, the mechanism responsible for forming the ice crystals is a major determinant of the ice crystal concentration. As discussed in Section 1.1.2, a good grasp of the ice concentrations found in cirrus clouds is critical to understanding the radiative role of those clouds.

The homogeneous nucleation mechanism takes place when pure liquid solutions freeze. This typically takes place between at RH_{ice} values of 140 – 180% and at temperatures in the range of 180 – 240 K (Koop et al., 2000). Homogenous ice nucleation will take place at temperatures no lower than 235 K from water drops on the order of a micrometer in size, but the addition of high concentrations of solutes will lower that temperature threshold. Through theoretical work, Koop et al. (2000) found that this process is independent of the solute itself, and instead relies on the water activity of the solution, which is dependent on concentration, pressure, and temperature. Modeling studies have found that cooling rate and temperature are the factors on which homogeneous freezing is dependent (Kärcher and Lohmann, 2002). This freezing mechanism typically results in high concentrations of ice crystals.

Heterogeneous ice nucleation, on the other hand, takes place when ice freezes on an ice nucleus containing a water-insoluble core such as soot, dust, or biological particles. In this case, the supersaturation freezing threshold is dependent on the material, but generally these thresholds are lower than those for homogeneous freezing (Kärcher and Lohmann, 2002). For instance, Mangold et al. (2005) found that ice nucleation via deposition could begin at RH_{ice} values of 102 – 105% for temperatures between 209 and 224 K. In contrast to homogeneous freezing, this mechanism yields smaller concentrations of larger ice crystals. However, studies

like that from DeMott et al. (1997) show that the concentration, size, and type of ice nuclei are determining factors of how many ice crystals are successfully produced by this mechanism.

Hoyle et al. (2005) and Heymsfield and Sabin (1989), for example, suggested that homogeneous freezing is the dominant freezing mechanism for cirrus formed in situ. However, recent analyses have suggested that heterogeneous nucleation is a more prevalent mechanism than it was previously thought to be (Kärcher et al., 2009; Spichtinger and Krämer, 2013; Jensen et al., 2013; Luebke et al., 2013). In fact, it has been demonstrated both in models and through observations by the aforementioned analyses that initial freezing events are the result of heterogeneous freezing due to the low RH_{ice} threshold and that homogeneous nucleation occurs in subsequent events. However, the competition for water vapor among ice crystals can block or delay later homogeneous freezing events by keeping the RH_{ice} values below the homogeneous freezing threshold (e.g. Gierens, 2003; Spichtinger and Cziczo, 2010). Additionally, the number of ice crystals than can be produced by a subsequent homogeneous freezing event can be reduced. Spichtinger and Cziczo (2010) note that these findings are likely to be most important for cirrus development in the midlatitudes.

Another process that is noteworthy in terms of its influence on cirrus is sedimentation. As ice crystals grow, they may reach a large enough size and fall to a lower region in the cloud or out of the cloud entirely, producing the virga streaks so commonly associated with cirrus clouds. Spichtinger and Gierens (2009b) demonstrated with their modeling scheme that sedimentation of ice crystals leads to a change in the concentration of ice crystals in the cirrus cloud and alters the RH_{ice} values throughout the cloud depending on where the larger crystals settle. For instance, as large crystals leave the upper layers of a cirrus cloud, RH_{ice} may increase, allowing a homogeneous nucleation event to occur. Conversely, at the lower layers where

homogeneous nucleation may have been taking place, the arrival of large crystals may block any further homogeneous nucleation by reducing the RH_{ice} below homogeneous threshold values. In addition to modifying the concentration of ice crystals, sedimentation also has a significant effect on the IWC by removing water from the cloud (Heymsfield and Donner, 1990).

1.3 Dissertation Overview

Currently, one of the main weaknesses in numerical models is the parameterization of cloud processes (Koop et al., 2000). This is due in part to the fact that the grid scales on which models are based are not compatible with the scales at which cirrus processes occur (Marchand et al., 2006). However, as this dissertation demonstrates, through the use of in situ observations, we can create datasets that can be used to more accurately describe the properties of cirrus clouds, understand relationships that exist between those properties, and also to determine the relative importance of different factors that determine the properties of cirrus.

In Chapter 2, I begin by exploring the instrumentation used to obtain the cirrus observations used in the following analyses. This chapter not only discusses the technology that is currently being used, but also introduces some of the challenges associated with measuring cirrus microphysical properties. Furthermore, a discussion of the data processing techniques exhibit some of the ways in which those challenges are overcome.

The next three chapters present a series of analyses that build upon one another to examine the relationship of IWC to atmospheric parameters, such as temperature and vertical velocity, and the relationship to cirrus microphysical properties, namely ice crystal concentration. Starting with the most basic relationship, Chapter 3 presents an analysis of the relationship between IWC and temperature that is based on the combination of several European and U.S. datasets to create a comprehensive database. One of the toughest challenges in

describing the relationship of IWC to temperature is the large variation in IWC over any given temperature range, thus suggesting that the relationship is not simple. The relationship between IWC and temperature is further investigated using the new merged dataset and probability distribution functions (PDFs). A PDF-based formulation allows for representation of not only the mean values of IWC, but also the variability of IWC within a temperature band. The IWC-PDFs are observed to be bimodal over the whole cirrus temperature range. This bimodality is also found in ice crystal number PDFs and is hypothesized to be attributed to different cirrus formation mechanisms such as heterogeneous and homogeneous freezing.

The results from Chapter 3 clearly demonstrate the complexities of the IWC-temperature relationship and provide a clear indication that other factors must be considered, namely those associated with cirrus formation. However, as described in Section 1.2.2, cirrus properties are developed and influenced by processes that occur on large and small scales. Starting with the large scale, Chapter 4 introduces the influence of weather-related processes on IWC and ice crystal concentration. The analysis is based on the comparison of two midlatitude datasets from similar airborne campaigns, MACPEX and MidCiX. Considering the influence of dynamics from weather patterns to updraft velocities, a case study analysis of observations from different dynamic regimes shows that differences in the dynamics will also be represented by differences in the observed microphysics. However, differences in the ice crystal concentration are not fully explained using this large-scale point of view.

In Chapter 5, the analysis started in Chapter 4 is continued, but is instead based on what is occurring at the nucleation level. While temperature and vertical velocity make important contributions to nucleation processes, the influences of ice nuclei (IN) are also introduced. The resulting analysis provides an assessment of the homogeneous and heterogeneous nucleation

mechanisms and how they interact based on atmospheric conditions, while ultimately providing a more thorough explanation for why the data from MACPEX and MidCiX are different. Using the results from the Model for Aerosol and Ice Dynamics (MAID), the effects of temperature, vertical velocity, and IN concentration can be explained and are then demonstrated by the observations from MACPEX and MidCiX. The final result establishes the importance of IN as a strong driver for determining both IWC and Ni characteristics in cirrus clouds.

In the concluding Chapter, I summarize the key results of this dissertation research and explore the implications of those results. Additionally, remaining questions are discussed as are my suggestions for ways to address those issues in future work.

Chapter 2 Instrumentation, Data and Analysis Methods

2.1 Introduction

While model studies are ultimately used to simulate past, current, and future projections of the role of cirrus clouds in the climate system, measurements of the factors involved are absolutely necessary for model validation and for providing modelers with physically meaningful, representative parameters. On their own, they also provide a real-time look at cirrus dynamics. Thus, given the discussion in Chapter 1 of the significant uncertainty that exists in this area of study, observational studies continue to be essential to better quantifying cirrus dynamics and their role in a changing climate.

The data used in the analyses presented in Chapters 3, 4, and 5 are entirely derived from in situ measurements. One advantage of in situ instrumentation is that they are able to provide measurements on a subkilometer scale relative to satellite or other methods, which is more compatible with the scale on which cirrus formation processes occur. Three major categories of instrumentation are used here as a means of obtaining a thorough picture of the cirrus clouds and the conditions in which they were sampled. As indicated in Chapter 1, the focus of this dissertation is the ice water content (IWC) of cirrus clouds, thus this chapter begins with an exploration of the instrumentation used to quantify IWC (Section 2.2). In Section 2.3, a different set of instrumentation is discussed, which provides the measurements of the second cirrus property important for my analysis, ice crystal number. The final instrument discussed is the

Meteorological Measurement System (MMS) that provides data detailing general atmospheric conditions.

In addition to the survey of instrumentation and measurement techniques, this chapter also contains information on the methods used to prepare the data for analysis. The methods that are discussed as a part of the instrumentation sections are procedures that are regularly performed as a part of the data processing techniques used by each instrument group. The purpose of Section 2.5 is to demonstrate my own preparation of the data for the purposes of my intended analyses to ensure that the data is of good quality and being used properly.

2.2 Water Instruments

Accurate measurements of water vapor are an important component of any study exploring cloud microphysics, as water vapor clearly plays a key role in the formation and maintenance of cloud particles. In this section, I describe instrumentation from two classes of sensors for quantifying atmospheric water – those capable of measuring so-called "total water" (sections 2.2.1 and 2.2.2) and those designed to observe only water vapor (section 2.2.3). Additionally, the instruments discussed here represent some of the most common, reliable measurement techniques used today, but are not necessarily a comprehensive representation of the available methodologies. Data from all of these instruments is used in the analyses presented in Chapters 3, 4 and 5, but here I describe their basic measurement principles, detection limits and accuracy.

2.2.1 Closed-path Laser Hygrometer (CLH)

The main instrument used for determining the IWC of cirrus clouds in each of the three analyses presented here is the University of Colorado Closed-path Tunable diode laser Hygrometer (CLH). This instrument was developed as a closed-path modification of the near-

infrared tunable diode laser spectrometer created at the Jet Propulsion Laboratory (JPL; May, 1998). Due to the narrow line width, the ability to easily tune with temperature or current, and the compact size of the laser, this system is an excellent option for use in airborne water vapor measurements (Davis et al., 2007a). Figure 2.1 depicts a block diagram of the CLH.

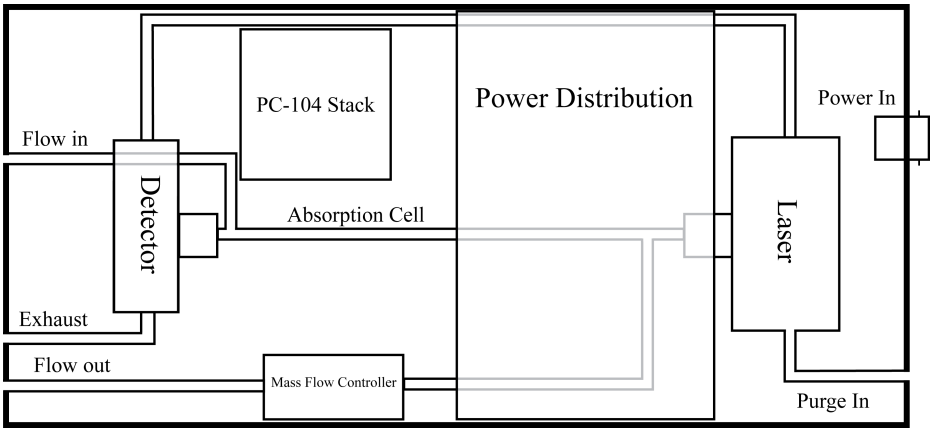

Figure 2.1. Block diagram of the CLH (Davis et al., 2007a, Fig. 1).

The CLH has been a contributor to the instrument payload on the NASA WB-57F aircraft or the NSF/NCAR Gulfstream G-V aircraft, depending on the airborne campaign. The instrument measures the total water amount of the sampled air parcel, which is the gas-phase water plus the water vapor that results from evaporating cloud particles. A heated inlet and flow path are used for sampling, both to aid in the evaporation of the cloud particles and to minimize contamination from desorption of water off the instrument surfaces. Water vapor is detected by second harmonic (2f) infrared spectroscopy for smaller mixing ratios and by direct absorption for larger mixing ratios. Both measurements are made at about 8 Hz and are taken continuously throughout a flight. The instrument has the ability to measure water vapor quantities ranging

from about 50 ppmv to more than 20,000 ppmv, with an accuracy of about 10% (Davis et al., 2007a).

One of the key features of this instrument is that it is coupled to a subisokinetic inlet. The inlet is forward-facing and is situated on the rightwing-pod of the WB-57F aircraft with the CLH mounted behind it or on the top of the fuselage of the G-V, with the CLH in a rack inside the cabin. A consequence of sub-isokinetic sampling is that condensed-phase concentrations measured by the instrument are significantly enhanced over ambient amounts, which occurs because the particles cannot follow streamlines around the inlet (Davis et al., 2007a; Hallar et al., 2004). The cloud particles are therefore enhanced by a known, size-dependent factor and result in a value called enhanced IWC (eIWC). Since the CLH also detects the gas-phase water in addition to eIWC, an enhanced total water (H_2O_{enh}) value is the actual measurement made by this technique.

In its simplest form, the enhancement factor (EF) of cloud particles can be determined from the ratio of the true aircraft speed to the instrument inlet speed. However, a more refined and accurate enhancement factor that takes into account two additional variables was used in the analyses here. First, a size-dependent particle enhancement curve provides a more accurate prediction of inlet efficiency (see Fig. 2.2). The particle enhancement curve consists of a ratio detailing the number of particles per unit volume per diameter entering the CLH as compared to the number of particles per unit diameter in ambient air. The development of this curve involves the use of three-dimensional computational fluid dynamics (CFD) and three-dimensional particle dynamics simulations as described by Engblom and Ross (2003). Unique CFD calculations were done by Engblom for CLH installations on both the WB-57F and G-V aircraft. The second component of the EF is a particle size distribution, which is created from observations of

particles made by imaging probes flown in tandem with the CLH such as the Cloud, Aerosol, and Precipitation Spectrometer (CAPS, Baumgardner et al., 2001), the 2-Dimensional Stereo (2D-S) probe (Lawson et al., 2006), and the Video Ice Particle Sampler (VIPS, Schmitt and Heymsfield, 2009). Each of these instruments is described in more detail below in Section 2.3. The particle size distribution is integrated with the particle enhancement curve to determine the EF for each observation made by the CLH. For instance, as seen in Fig. 2.2, an observation dominated by small particles will be enhanced to a lesser degree than an observation dominated by large particles. A more exhaustive description of the calculations involved can be found in Davis et al. (2007a).

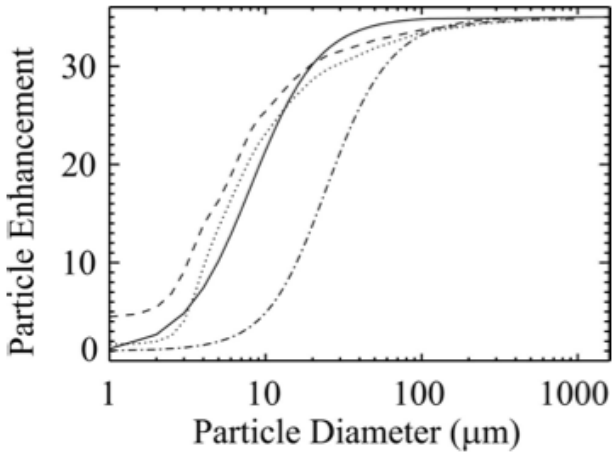

Figure 2.2. Particle enhancement curve for CLH. This figure is copied here from Fig. 4 of Davis et al. (2007a). This curve was calculated for a true aircraft speed of 160 m s^{-1} and an instrument inlet speed of 4.57 m s^{-1}. The different lines denote different calculations as described in Davis et al. (2007a).

In order to calculate the IWC from the H_2O_{enh} directly measured by the instrument, the ambient water vapor (H_2O_{gas}) must first be removed from the H_2O_{enh} measurement. Water vapor measurements made by the Jet Propulsion Laboratory (JPL) tunable diode laser hygrometer (JLH) or the Harvard Water Vapor (HWV) instrument (both described below in Section 2.2.3),

which were flown in tandem with the CLH during the flight campaigns, were used as sources for H_2O_{gas}. The result of this calculation is the enhanced IWC (eIWC). From this point, simply dividing that quantity by EF provides the final IWC value in units of density (mg m^{-3}). This process can be defined in the following equation

$$IWC = \frac{H_2O_{enh} - H_2O_{gas}}{EF} \quad (2.1)$$

A pictorial description of the data analysis process is shown in Fig. 2.3, where key variables that go into the IWC calculation are highlighted (Fig. 11 from Davis et al., 2007a).

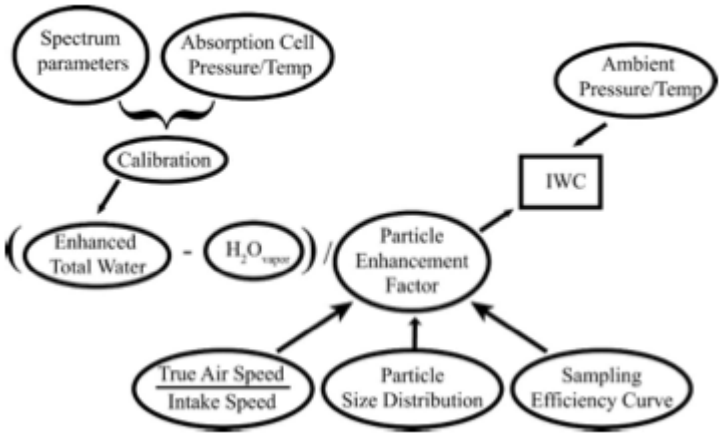

Figure 2.3. IWC calculation schematic. This figure is copied from Fig. 11 of Davis et al. (2007a).

For a few flights during the Midlatitude Airborne Cirrus Properties Experiment (MACPEX; discussed in Chapters 4 and 5), water vapor measurements from the JLH were not available. Although water vapor measurements from the HWV instrument were available, they were not used in order to maintain consistency of the analysis within and between campaigns. Instead, for flights without JLH water vapor, the baseline water vapor was removed manually from H_2O_{enh}. This was accomplished using knowledge of clear air segments of the flight, based

on an absence of cloud particles, and an indication of the baseline water vapor value, based on comparison between CLH and HWV measurements.

2.2.2 Fast In Situ Stratospheric Hygrometer (FISH)

In the analysis of the large dataset of cirrus ice water found in Chapter 3, data from the Fast In Situ Stratospheric Hygrometer (FISH; shown in Fig. 2.4), developed by Forschungszentrum Jülich, is used. Similar to the CLH, FISH measures enhanced total water, but in the range of 1 – 1000 ppmv and with an uncertainty of 6% ± 0.2 ppmv. FISH is regularly calibrated between flights using a portable calibration bench to simulate realistic atmospheric conditions at varying H_2O mixing ratios and pressures.

Figure 2.4. Picture of FISH (right) and the dew point generator (left) used for calibrations between flights.

First described in Zöger et al. (1999), this instrument utilizes the Lyman-α photofragment fluorescence technique for measuring water in the atmosphere. This technique, originally developed by Kley and Stone (1978) and Bertaux and Delannoy (1978), involves the detection of the fluorescence of electronically excited OH molecules that are produced by photodissociation of H_2O molecules. In order to minimize the effects of the oxygen absorption cross section in that

spectral region, the Lyman-α line at λ = 121.6 nm, generated by emission from hydrogen atoms, is used to initiate the photodissociation.

Equation (3') in Zöger et al. (1999), reproduced here as Eq. (2.2), demonstrates the relationship between the number of fluorescence photons, N_f, and the concentration of H_2O molecules, $[H_2O]$, for measurements in the troposphere and lower stratosphere and is given by

$$N_f = C \cdot \frac{[H_2O]}{[air]} \tag{2.2}$$

The coefficient C contains factors representing the photodissociation rate of reaction, the quantum efficiency for OH production, the Einstein coefficient of reaction for the OH molecule relaxing to ground state, and the quenching coefficient of the OH radical in air. Those coefficients are all known, thus C is assumed to be a constant and the H_2O mixing ratio is proportional to the number of fluorescence photons.

The data used in the analyses presented here comes from the work done when the instrument was aboard the Russian high-altitude M55 Geophysica aircraft and the GFD Lear Jet. Though the instrument may be adapted to fit different aircraft, the closed-cell instrument typically resides within the pressurized cabin when aboard research aircraft and uses a forward-facing, heated inlet to sample total water. Similar to the CLH, the resulting measurements from FISH are enhanced due to the geometry of the anisokinetic inlet. Schiller et al. (1999) explain that, based on computational fluid dynamics modeling, the enhancement factor can be determined for the different inlets used with FISH aboard different aircraft. Krämer and Afchine (2004) go on to demonstrate that particles with radii smaller than 0.3 μm typically exhibit the lowest enhancement factors around 1 – 2, while particles larger than 3 – 4 μm in radius reach the maximum enhancement values. On the Lear Jet, the maximum enhancement value is approximately 3, while it is between 8 and 10 on the Geophysica. Similar to the procedure used

to process CLH observations, the FISH also relies on water vapor measurements made by other instruments to calculate IWC from the total water measurement. In the datasets used here, the water vapor measurements come from the Central Aerological Observatory Lyman-α Stratospheric Hygrometer (FLASH) and the Forschungszentrum Jülich open-path tunable diode laser spectrometer (OJSTER), both of which are discussed in Section 2.2.3.

2.2.3 Water Vapor Instruments

Water vapor measurements in the atmosphere are particularly important due to the contribution of water to the radiative balance. In terms of cirrus clouds, these measurements are important for determining the relative humidity with respect to ice, RH_{ice}, which was explained in Chapter 1 to be a key factor for cirrus formation. As mentioned in Sections 2.2.1 and 2.2.2, water vapor measurements are also necessary for deriving IWC from the total water measurements of CLH and FISH. The instruments themselves are quite similar and use the same basic techniques employed by CLH or FISH. The four water vapor instruments used in the analyses presented here are discussed below.

Though a more thorough treatment of the details is beyond the scope of this dissertation, it is worth mentioning that there are often discrepancies between instruments when it comes to measurements of water vapor. As a result, several comparisons and experiments have taken place with the goal of minimizing and determining what causes those differences. For example, the Stratospheric Processes and Their Role in Climate (SPARC) Assessment of Upper Tropospheric and Stratospheric Water Vapour (2000) report is a compilation of in situ, ground based, and satellite measurements of water vapor and includes data from the FISH, HWV, and JLH instruments discussed here. The authors of the assessment note in a summary of instrument comparisons that significant variability is observed among instruments sampling in similar

conditions, but that, given the small sample size, the statistical significance of those differences cannot be determined. The SPARC Assessment also notes that biases between instruments have been observed, but that their origin has not been explained nor have these differences been resolved.

Jet Propulsion Laboratory Laser Hygrometer (JLH)

The JLH is the primary source for the water vapor measurements used in calculating IWC from the total water measurements of the CLH since they are often flown in tandem and operate based on the same measurement principles. Except for the cases mentioned in Section 2.2.1, all IWC data stemming from CLH measurements were calculated using JLH measurements. Developed by the Jet Propulsion Laboratory, May (1998) explains that the instrument uses the technique of infrared absorption spectroscopy, employing the second-harmonic technique to achieve high accuracy and precision when measuring the small amounts of water vapor characteristic of the stratosphere. The measurement technique is quick, direct, and noninvasive and without the problems that can plague closed-path instruments such as wall reactions and flow issues. Typically, the instrument is mounted on the wing of the research aircraft. An open-path, multipass "Herriot" cell is the external piece of the instrument and has been designed to sit outside of the aircraft's boundary layer. A picture of JLH mounted to an aircraft and a schematic illustrating some of the components of JLH are shown in Fig. 2.5. May (1998) reports a measurement precision of ± 0.05 ppmv for a 2 s measurement in the stratosphere.

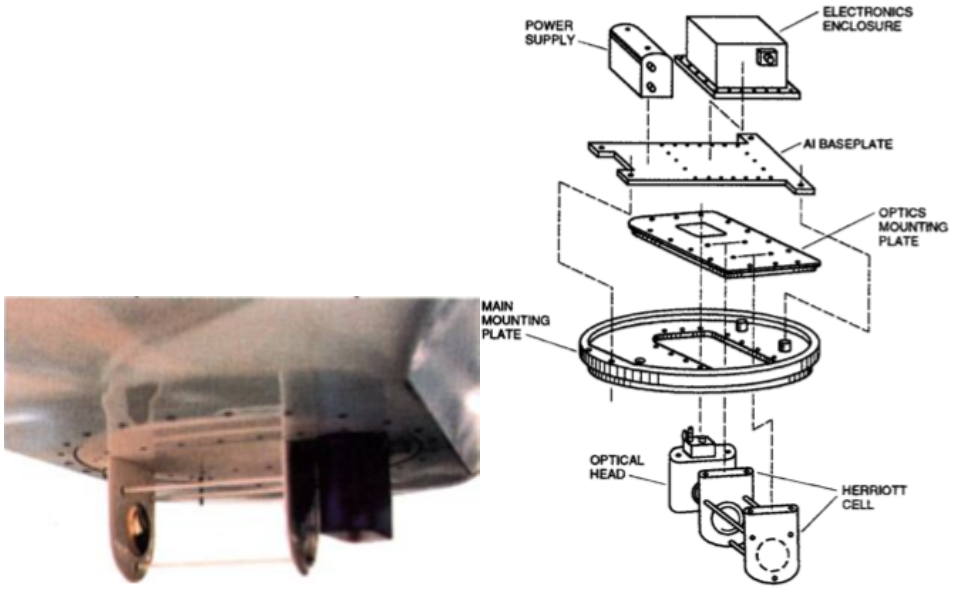

Figure 2.5. Picture of JLH instrument mounted to aircraft (left) and basic schematic of JLH components (right). This figure is copied from Plate 1 of May (1998).

Harvard Water Vapor Instrument (HWV)

The second instrument often flown on the WB-57 at the same time as the CLH is the HWV, shown in Fig. 2.6. This instrument utilizes the photofragment fluorescence technique described in Sect 2.2.2 for measuring water vapor in the troposphere and stratosphere. Similar to the previous description of FISH, Weinstock et al. (1994) explain that the instrument works by using Lyman-α radiation to dissociate water vapor molecules. The fluorescence of the resulting OH is collected at a right angle to the radiation beam and then detected by a photomultiplier tube to determine water vapor mixing ratio. Water vapor concentration measurements can also be made by direct absorption in the middle and upper troposphere using scattered lamp and solar radiation. Briefly, the instrument is calibrated in the laboratory before and after field campaigns and also in-flight by comparing the measurements made via the fluorescence method to those made by direct absorption. Weinstock et al. (1994) report that the instrument is able to measure

water vapor mixing ratios in the range of 2 – 300 ppmv with an accuracy of ±10% based on laboratory and in-flight calibrations. An updated analysis of the instrument from Hintsa et al. (1999) indicates that the accuracy of the instrument is ±5% with an additional offset of 0.1 ppmv.

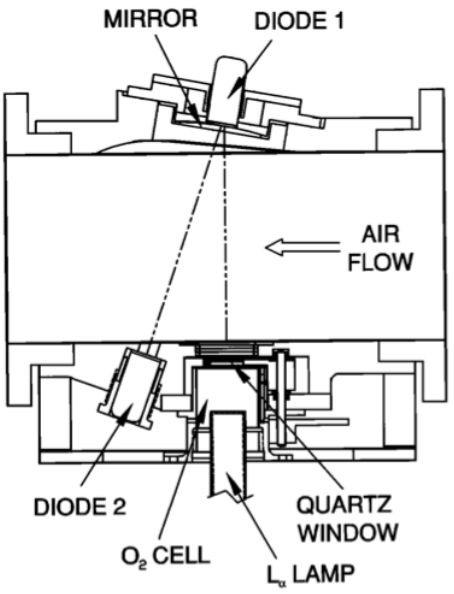

Figure 2.6. Schematic of the Harvard Lyman-α instrument copied from Fig. 1 of Hintsa et al. (1999).

Fluorescent Airborne Stratospheric Hygrometer (FLASH)

The FLASH instrument is the first of two instruments used in conjunction with FISH. As explained by Sitnikov et al. (2007), FLASH also takes advantage of the photofragment fluorescence technique previously described for FISH and HWV. The instrument was originally developed by the Central Aerological Observatory for upper tropospheric and lower stratospheric measurements. As shown in Fig. 2.7, copied from Fig. 1 in Sitnikov et al. (2007), this is a closed-path instrument. The inlets are cut at a 45º angle and turned away from the airplane, which results in a kinetic separation of ice crystals from the water vapor. This design is based on calculations from fluid dynamic simulations. Sitnikov et al. estimate that at a speed of ~700 km

h^{-1}, particles > 1 μm would not make it into the measuring chamber. Laboratory calibrations show that FLASH has an accuracy of 8% and measures water vapor in the range of 0.5 – 300 ppmv.

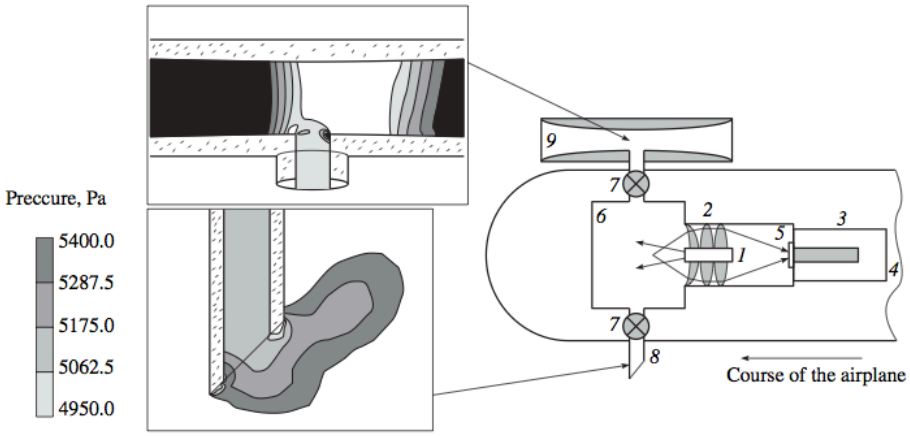

Figure 2.7. Diagram of FLASH copied from Figure 1 of Sitnikov et al. (2007). As described by Sitnikov et al.: (1) hydrogen lamp, (2) uviol lenses, (3) electronic unit, (4) PMT, (5) interference filter, (6) measuring chamber, (7) valve, (8) sucker, (9) nozzle.

Open-path Jülich Stratospheric TDL (OJSTER)

The second instrument that often supplies water vapor measurements for the IWC calculations from the FISH measurements is an open-path instrument called OJSTER. First described by Schlicht (2006), this instrument uses the same measurement technique and data analysis procedures as the JLH instrument (described above). Additionally, the instrument also works by using a Herriot multipath cell.

2.3 Ice Particle Imaging Probes

As noted in Chapter 1, accurate measurements of the size, shape, and concentration of cirrus ice crystals are of particular importance for everything from understanding and documenting ice crystal statistics to the necessary calculations for processing other cirrus

measurements, i.e. the enhancement factors of the H_2O_{enh} measurements. Currently, there are a number of different instruments and techniques available to make these measurements. In the analyses presented here, data from three instruments was used, both directly and indirectly. The following sections (Sections 2.3.1 – 2.3.4) provide details on each instrument, where and how they were utilized for the purposes presented here, and brief discussions of the advantages and disadvantages to using each.

An important issue to keep in mind with any measurement of atmospheric particles is the potential for creating shattered particles and the error that can be introduced to the measurements. These shattered particles come from large ice crystals hitting the aircraft or the imaging probes themselves and then shattering into many smaller particles. This results in a false measurement of a large concentration of small ice crystals (< 50 μm diameter). The subsequent use of those measurements can then lead to incorrect assumptions of the role of small particles in cirrus clouds, and as McFarquhar et al. (2007) point out, overestimates of shortwave reflection and therefore incorrect calculations of the contribution of cirrus to radiative forcing. The techniques and steps taken to correct for this artifact for each of the instruments prior to the start of the analyses presented here are discussed in Section 2.3.4.

2.3.1 Cloud, Aerosol, and Precipitation Spectrometer (CAPS)

CAPS is an airborne particle spectrometer developed by Droplet Measurement Technologies (DMT, Baumgardner et al., 2001). One of the most useful features of this particular spectrometer is that it incorporates five kinds of probes into a one integrated system as shown in Fig. 2.8. This essentially eliminates the aircraft co-location issues that other probes may have when trying to cover a large crystal size spectrum. Two of the CAPS probes make measurements related to the particles while two additional sensors measure temperature and air

speed, which are necessary for data processing. The fifth sensor, the liquid water content detector (LWCD), measures liquid water content (LWC), but will not be discussed here.

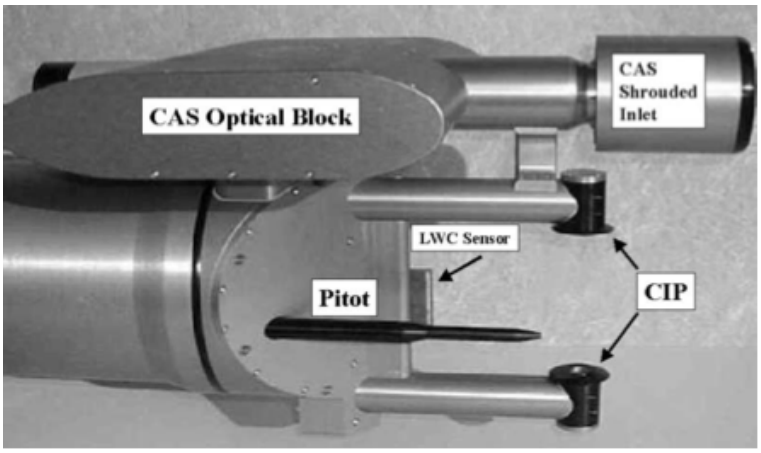

Figure 2.8. Photograph of CAPS instrument showing all major components. This photograph is copied from Fig. 1 of Baumgardner et al. (2001). It should be noted that this photo is not up to date as the CAS inlet is no longer shrouded.

The first sensor is the cloud and aerosol spectrometer (CAS; shown in Fig. 2.9), which covers a particle size range of 0.6 – 50 μm. Using Mie theory and the assumption that the particles are spherical, the size of each particle that passes through a focused laser beam can be determined. The instrument incorporates its own error check by measuring and comparing the signals from both forward-scattered (4 - 13°) and backscattered (5 - 14°) light. The CAPS instrument also houses the temperature sensor and a Pitot tube used for determining airspeed. The latter feature enables sample volume calculations to be made and is used for controlling the cloud imaging probe (CIP).

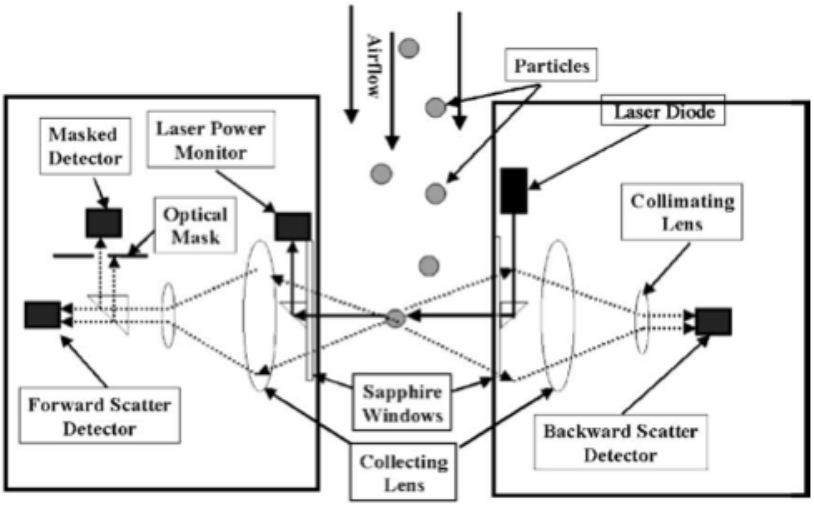

Figure 2.9. Schematic demonstrating the configuration of CAS. This figure is copied from Fig. 2 of Baumgardner et al. (2001).

The CIP instrument, shown in Fig. 2.10, measures particles in the larger size range, with diameters from 25 – 1550 μm, which overlaps with the size range covered by the CAS. Using a different technique than the CAS, a collimated laser beam positioned on a linear array of 64 diodes is used to capture the shadow of particles passing through the beam. The instrument begins counting when the diode state is recorded as "on". This occurs when the light level has decreased by 70%. Probes like the 2D-S (discussed below) use a threshold of 50%, but Korolev et al. (1998) found that a 70% threshold was necessary for decreasing sizing uncertainty. In combination with the CAS, a full particle size range of 0.35 – 1550 μm can be obtained by a single system. This range adequately and easily captures the range of ice crystal sizes found in cirrus clouds.

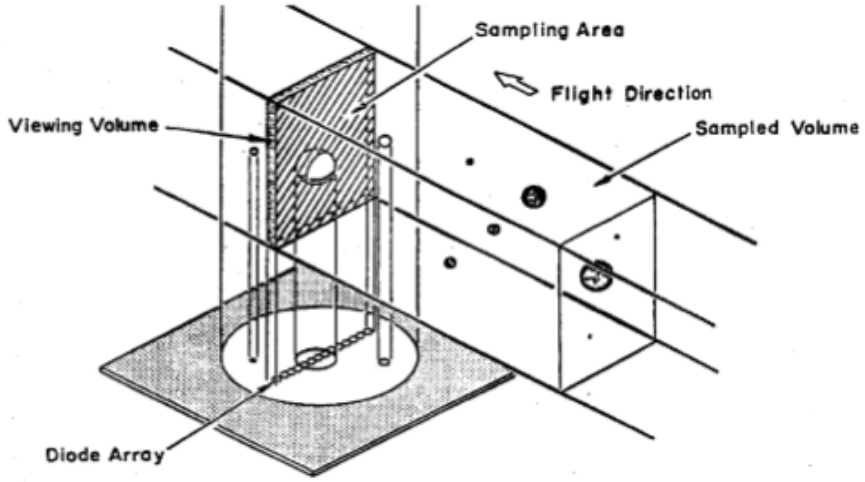

Figure 2.10. Schematic drawing of CIP demonstrating the basic function of the instrument. This figure is copied from Fig. 3 of Baumgardner et al. (2001).

The measurements from the CAPS system are utilized and discussed in the analyses presented in Chapters 4 and 5. The data used directly in the analyses presented here are the ice crystal concentrations (Ni) from the Midlatitude Cirrus Experiment (MidCiX). Additionally, CAPS particle size distributions were incorporated into the enhancement factor calculation as described in Section 2.2.1 for MidCiX, the 2006 Tropical Composition, Cloud, and Climate Coupling mission (TC4), the 2008 Stratosphere-Troposphere Analyses of Regional Transport (START08) campaign, and the 2002 Cirrus Regional Study of Tropical Anvils and Cirrus Layers – Florida Area Cirrus Experiment (CRYSTAL-FACE).

2.3.2 2-Dimensional Stereo Probe (2D-S)

The 2-Dimensional Stereo Probe is an optical particle imaging instrument that has often been flown in tandem with the CLH. Data from this instrument is used to determine the ice crystal concentrations observed during the MACPEX campaign, which is discussed in Chapters 4 and 5.

Lawson et al. (2006) describe the basic design of the probe, shown in Figure 2.11, to include the use of two diode laser beams crossing at right angles (vertically and horizontally depending on the instrument's orientation while mounted on the aircraft) that are used in conjunction with 128-photodiode arrays to detect the shadow of particles as they pass over the array. Particles are counted when the light has decreased by ≥50% over any pixel; particle counting stops when none of the photodiodes are shadowed. The use of two beams allows for two independent images of a particle to be recorded when the particle is in the overlap region of the beams. If the particle is outside of the overlap region, a single image will be recorded. Lawson et al. report a resolution of 10 μm at jet aircraft speeds and an improvement in sizing of small particles (< 100 μm) in comparison to older optical probes. The sample volume achieved by the probe is equal to that of the CIP (described in Section 2.3.1).

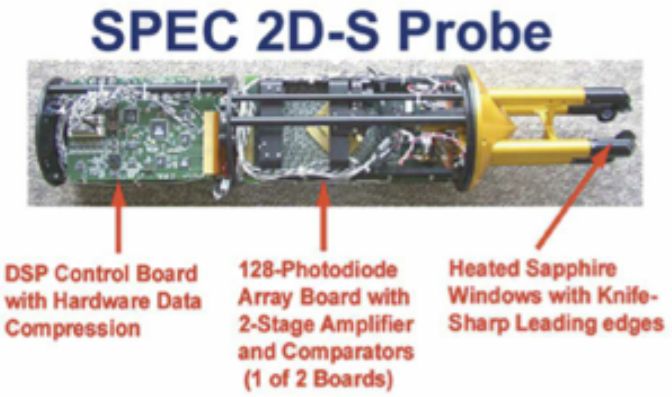

Figure 2.11. Copied from Fig. 1 of Lawson et al. (2006), this figure shows a photograph of the 2D-S probe and provides details on some of the major components.

One of the issues that this instrument has is that as the particle sizes decrease, the sample volume of the instrument also decreases (Jensen et al., 2009). In order to compensate for this issue, it is assumed that the depth of field is proportional to the square of the particle radius. However, Jensen et al. (2013) point out that this creates a lot of uncertainty in the smallest

particle size bin, and the result is a significant increase in the ice crystal concentrations in that bin compared to the larger size bins. Thus, it is suggested that the first size bin (5 – 15 μm) in the 2D-S dataset be removed. Jensen et al. (2013) go on to say that they expect that particles smaller than 15 μm would not contribute significantly to a particle size distribution in general. They suggest that particles in that size range are likely to either grow or sublimate rapidly and therefore will not persist. The potential effects of removing this size bin are discussed in the analysis presented in Chapter 5.

2.3.3 Video Ice Particle Sampler (VIPS)

The Video Ice Particle Sampler probe is ideal for thin clouds, since thick clouds can quickly overwhelm the field of view on the instrument (Schmitt and Heymsfield, 2009). The instrument is able to determine particle properties such as projected area and maximum dimension and then put each particle image into the appropriate size bin (10 – 350 μm). Instead of taking direct images with the use of lasers like the other two particle imaging probes discussed here, the instrument works by taking images with a high-resolution video microscope on a clear plastic belt coated with silicone oil. As particles hit the belt, they can be imaged and recorded, then analyzed by hand and with the help of image analysis software.

As indicated, the instrument is designed for measuring small ice crystals, but Schmitt and Heymsfield (2009) also point out that the collection efficiency of the instrument is reduced for particles smaller than 10 μm. Also, McFarquhar and Heymsfield (1997) report that crystals larger than 150 μm would often break on impact with the plastic belt, therefore making it difficult to determine their original shapes.

VIPS data is not directly used in any of the analyses, but has indirectly contributed through its use in processing CLH data from the MACPEX campaign. As mentioned in Section

2.3.1, data from the CAPS instrument is typically used for this purpose, but CAPS was not involved in MACPEX. Ice crystal concentration data was available from the 2D-S instrument, as indicated in Section 2.3.2, but the removal of the size bin below 15 μm made this dataset a less favorable candidate in comparison to the VIPS dataset. As shown in Fig. 2.2, the particle enhancement curve from Davis et al. (2007a) for the CLH reveals that the enhancement is significantly affected by particles with diameters at those small sizes. Thus, the range of sizes sampled by the VIPS instrument is better suited for the enhancement factor calculation.

2.3.4 Shattering Corrections

Both the 2D-S and CAPS instruments have been used to study shattering of large particles on particle probes. For instance, McFarquhar et al. (2007) compared in situ measurements from the Tropical Warm Pool International Cloud Experiment (TWP-ICE) for two instruments in order to investigate this issue. In comparison to the Cloud Droplet Probe (CDP), the CAS instrument (the small particle probe from the CAPS instrument) was shown to be measuring Ni values in the 3 – 50 μm range that were significantly larger than those observed by the CDP. The cause of this difference was discovered to be consistent with the shattering of ice crystals on the CAS inlet. Around this time, a shroud was also added to the CAS inlet as a means of straightening the airflow and minimizing measurement issues associated with the aircraft angle of attack (Jensen et al. 2009). McFarquhar et al. (2007) indicate that the shroud was particularly prone to inducing particle shattering. They conclude that this artifact could be resulting in an overestimation of Ni by as much as 300%. In a comparison by Jensen et al. (2009), Ni observations from the CAS and 2D-S reveal similar results.

As a result of these findings, modifications have been made to the instruments and to the data processing methods to minimize and/or eliminate this artifact from their datasets. For

example, Jensen et al. (2009) note that shattering is less likely for the 2D-S and CIP (the CAPS probe measuring in the larger particle size range) due to the long, protruding arms of the detector. Also, they report that the sharp disks on the detector arms of the 2D-S are used for deflecting shattering artifacts away from the Ni sample. Additionally, an algorithm described by Baker et al. (2009) that was originally intended for use with raindrop splatter has been included in processing 2D-S data, which allows for shattered fragments that are included in the sample volume to be removed. Similarly, an algorithm based on particle interarrival times is used to correct for shattering artifacts on the CIP instrument. The CAS instrument is corrected by matching the overlapping size bins from the CIP and then using a best fit approach to extrapolate down to the smallest size bins only observed by the CAS (D. Baumgardner, personal communication). For the VIPS instrument, Schmitt and Heymsfield (2009) note that it is possible for particles larger than 250 μm in diameter to break up, but it is unclear what the corrections are for those cases.

2.4 Atmospheric Measurements

Additional measurements of atmospheric parameters such as temperature, pressure, and vertical velocity are needed for data processing and analysis purposes. While temperature and pressure measurements are standard on all research aircraft, measurements of vertical velocity are relatively novel. This section includes a brief discussion of the MMS instrument used to acquire these variables for use with the CLH measurements.

Originally developed for a NASA U-2 aircraft in the early 1980's, the Meteorological Measurement System (MMS) went through several iterations before becoming the system that it is today. As described by Scott et al. (1990), the purpose of this airborne system is to record and provide accurate, quick, in situ measurements of the meteorological variables used in all areas of

atmospheric research such as temperature, pressure, and wind velocity. Other variables relating to aircraft location and various flight angles (pitch, yaw, heading, etc.) are also recorded for research purposes.

Temperature is one of the key meteorological factors used throughout the analyses due its significant role in cirrus formation and maintenance processes. Briefly, temperature measurements aboard the WB-57 are made using two platinum-resistance total air temperature sensors, one with a fast time constant and one with a slow time constant (Scott et al., 1990). The sensor with the long time constant measures between -70 and 0°C, while the sensor with the short time constant measures temperatures in the range of -100 - 0°C. As of the report from Scott et al. (1990), both sensors were measuring with an accuracy of ±0.25°C and with a resolution of 0.05°C. However, more recent measurements from the 2011 MACPEX campaign report an accuracy of 0.03°C (cloud1.arc.nasa.gov/airborne/).

Vertical velocity is another key variable involved in cirrus dynamics and is used in the analyses presented in Chapters 4 and 5. This quantity is the result of a calculation based on other MMS measurements. Scott et al. (1990) report that a resolution better than ±0.1 m s^{-1} can be achieved, and more recent data indicates an uncertainty of ±1 m s^{-1} at 1-sigma for 1Hz measurements (http://cloud1.arc.nasa.gov/airborne/archive/browse/MACPEX). Section 2.5.3 provides more information on how vertical velocity is calculated, as well as the additional data processing that took place before including the data in the analyses.

2.5 Analysis Preparation Methods

It is important with any dataset to ensure that the data are of good quality and that they are used in a way that is appropriate in regards to the limitations of the instrument that they come

from and the quantity being measured. The final section of this chapter focuses on the procedures and methods used to achieve both of those criteria.

2.5.1 Determining if Data are In-Cloud

A critical piece of the analysis that underlies the results presented in Chapters 3, 4 and 5 was the development of a method that could be used to determine whether the aircraft was in or out of clouds and thus where the data are representative of cirrus versus clear air. The method employed here is based on those described in Krämer et al. (2009) and Schiller et al. (2008) for the FISH, FLASH, and OJSTER instruments and involves comparisons between the CLH data and the water vapor measurements from the JLH. It should be noted that because these procedures have been previously applied to the datasets acquired by the FISH instrument those data were incorporated here without further processing.

The first step is to perform a data quality check on the water vapor measurements. This is done by comparing H_2O_{gas} and H_2O_{enh} to one another. During periods of the experiment spent in clear air, the two measurements should agree within their respective uncertainties. During periods of the flight spent in cloud, H_2O_{enh} should be greater than H_2O_{gas}. Flights with good fidelity to those rules are used for the analysis while flights that do not pass the test are left out. Before they are removed, however, an attempt is made to adjust the value of H_2O_{enh} to ensure that H_2O_{enh} and H_2O_{gas} match in cases where the IWC is equal to zero. This is a reasonable procedure because the CLH has a higher detection limit than the JLH as a result of its short path length. When the ambient water vapor is 5 ppmv, for example, the CLH will report an H_2O_{enh} measurement that is at least 20 ppmv. Davis et al. (2007b) discuss this in more detail. In cases where the H_2O_{enh} from CLH in clear air exceed H_2O_{gas}, the H_2O_{enh} value was adjusted with

respect to the H_2O_{gas} value. This was done by first calculating an adjusted water vapor measurement ($H_2O_{gas,adj}$) using the expression

$$H_2O_{gas,adj} = H_2O_{enh} - eIWC \quad (2.3)$$

Remembering that eIWC is the value calculated by subtracting H_2O_{gas} from H_2O_{enh} without removing the enhancement factor, Eq. (2.3) comes from a simple rearrangement of that relationship. Since H_2O_{gas} is a measured value and $H_2O_{gas,adj}$ is a value calculated from the enhanced CLH measurement, they will not likely be equal, particularly in cases of low ambient water vapor due to the limitations of the CLH as previously mentioned. What this calculation does is adjust the value of H_2O_{gas} relative to H_2O_{enh} so that it passes the data quality check. However, the value of $H_2O_{gas,adj}$ is not physically meaningful since the adjusted water vapor measurement will always be greater than the saturation water vapor mixing ratio, indicating that the aircraft is always inside cloud. To correct for this, the original enhanced total water measurement, H_2O_{enh} is adjusted relative to $H_2O_{gas,}$ thus creating $H_2O_{enh,adj}$, which is defined here as

$$H_2O_{enh,adj} = H_2O_{enh} - (H_2O_{gas,adj} - H_2O_{gas}) \quad (2.4)$$

The difference between the adjusted water vapor and the measured water vapor should be the same value as the difference between the adjusted and measured enhanced total water, thus it can be used in the above calculation. As a result, $H_2O_{enh,adj}$ and H_2O_{gas} are both physically meaningful values that can potentially pass the data quality check. There is still the chance that the adjustment will yield results with a large variation between the adjusted and measured values indicating a poor agreement on the characteristics of the measurement between the CLH and JLH, and in that case, the data are taken out of the analysis. An example graphical representation of these values and the adjustment can be seen in Fig. 2.12, where H_2O_{gas} (red), H_2O_{enh}

(turquoise), and $H_2O_{enh,adj}$ (dark blue) are shown. The water vapor saturation mixing ratio (H_2O_{sat}, black) is also shown to illustrate that H_2O_{gas} and $H_2O_{enh,adj}$ are physically meaningful values.

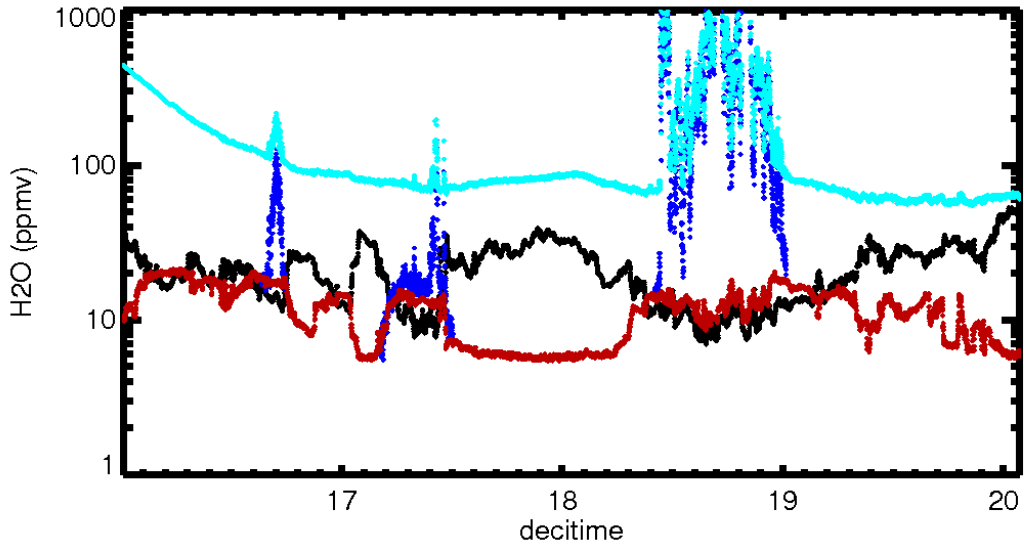

Figure 2.12. This figure illustrates the H_2O data quality check using data obtained by the CLH during the CRYSTAL-FACE campaign on July 9, 2002. The black line is H_2O_{sat}, the red line is H_2O_{gas}, the turquoise line is H_2O_{enh}, and the dark blue line is $H_2O_{enh,adj}$.

After completing the data quality check, the water vapor data are usable for calculating the relative humidity with respect to ice (RH_{ice}) and the enhanced relative humidity with respect to ice (eRH_{ice}), which together is the basis for the method used to determine whether a particular data point was measured "in-cloud" or in clear air. The parameter RH_{ice} was chosen to distinguish between clouds and clear air because it is more sensitive to the changes associated with the status of cirrus formation conditions than water vapor (Krämer et al., 2009). eRH_{ice} is calculated from the H_2O_{enh} measurement while RH_{ice} is calculated from H_2O_{gas}. The ratio of eRH_{ice} to RH_{ice}, termed here a "cloud limit", is the parameter that defines where a cloud exists

and is instrument specific. When eRH_{ice}/RH_{ice} is greater than 1, and eRH_{ice} is greater than 100%, saturated or supersaturated cirrus is being sampled. However, due to measurement uncertainties and data scatter, when the ratio is barely greater than 1, it is difficult to determine with confidence whether the sample is in cloud or not (Krämer et al., 2009). Thus, a cloud limit value that is greater than, but not equal to, 1 must be employed. A second, higher cloud limit is also needed for cases where the eRH_{ice} values are less than 100%, which could indicate subsaturated cirrus. For example, in Krämer et al. (2009), the cloud limits used are 1.03 and 1.3. When those specific values are applied to the IWC data from the CLH instrument, IWC measurements smaller than the detection limits of the instrument remain included in the dataset as measurements from inside a cloud. However, because those measurements cannot be confidently determined to be in cloud, they should not be included in the dataset. In order to remove those values, higher cloud limits were put in place. In the case of the CLH data, the cloud limits were determined to be 1.3 and 3.

There are three possible scenarios for each data point, which are as follows. The first is a scenario indicating that the data point definitely represents a measurement taken inside a cirrus cloud. In this scenario, RH_{ice} and eRH_{ice} are both greater than 100% and eRH_{ice}/RH_{ice} is greater than 1.3. In the second scenario, eRH_{ice} is greater than 100% but RH_{ice} is not. As long as eRH_{ice}/RH_{ice} is greater than 1.3, the data point is most likely in cloud. The last scenario is for data points where neither eRH_{ice} nor RH_{ice} is greater than 100%. For this case, the larger cloud limit is used to ensure that if a data point is to be included and labeled “in-cloud”, it is definitely a cirrus measurement. Thus, in order for it to be included, eRH_{ice}/RH_{ice} must be greater than 3. Results that do not fall into one of these three categories are assumed to be measurements made

in clear air and are not included in the climatology. An example of the results of this process is given in Figure 2.13.

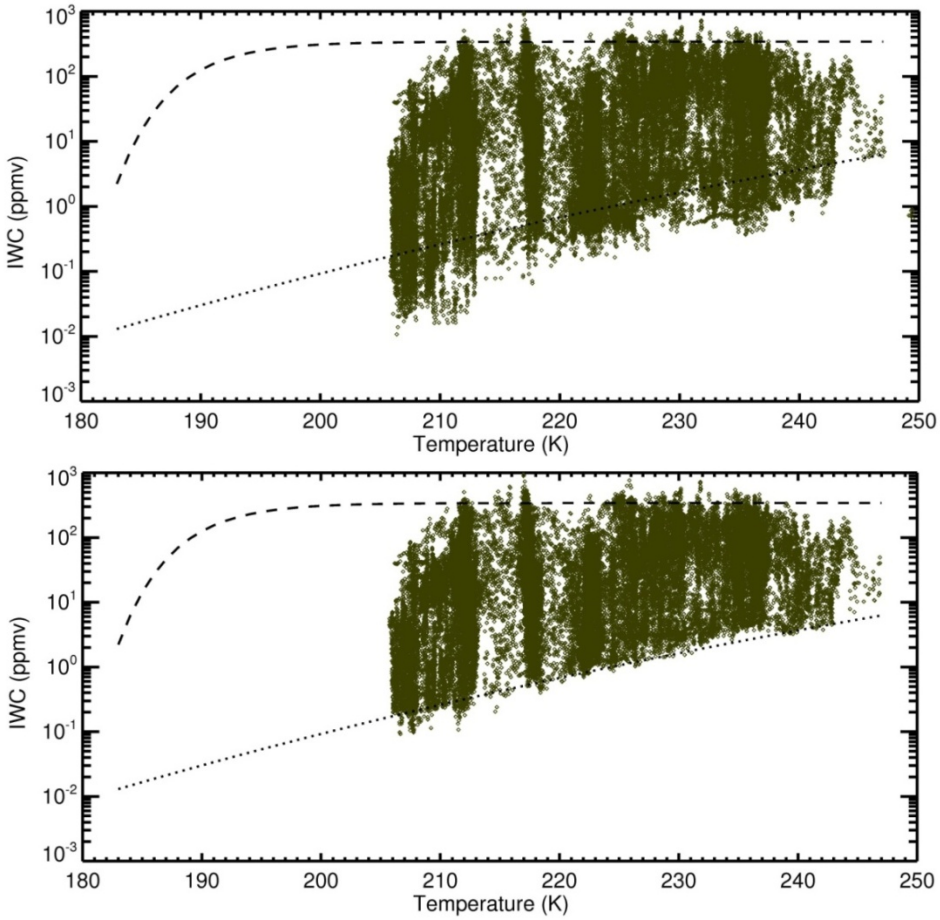

Figure 2.13. The top plot illustrates the IWC data that is considered "in-cloud" when the wrong cloud limits are used. The bottom plot illustrates the situation when the right ones are used. The dashed and dotted black lines represent the maximum and minimum IWC values, respectively, as determined in Schiller et al. (2008). The data being used come from the MidCiX campaign.

2.5.2 Comparison of Leo-Lidar with FISH-CLH

In cases of thin and subvisible cirrus clouds, the water content values are often close to or below the lower detection limit of the instruments discussed in Section 2.2, presenting a

significant challenge to their capabilities. However, there are alternative measurement techniques, such as lidar, that are better suited to those situations. In this section, measurements from a lidar system are used to verify that the low IWC values observed by CLH and FISH are likely to be indicative of thin clouds, rather than artifacts of the measurement techniques.

Lidar (Light Detection and Ranging) is an active remote sensing instrument measuring the optical properties of atmospheric particles. The backscatter and extinction coefficients as well as the depolarization of a particle ensemble (e.g. cirrus ice particles) can be determined from the backscattered light. The lidar used here is a commercial mobile backscatter lidar system (Leosphere), named Leo-Lidar, that works at a wavelength of 355 nm with a repetition rate of 20 Hz. Because the extinction coefficient as well as the IWC depends upon the particle size distribution of an ice particle ensemble, IWC can be determined from extinction measurements, provided that something is known about the particle size distribution. Here, the IWC of cirrus clouds is determined by using the relation provided by Heymsfield et al. (2005)

$$IWC(g/m^3) = a \cdot \sigma(m^{-1})^{\,b} \qquad (2.5)$$

which is derived from extinction and IWC measurements from aircraft in situ sensors compared with data from the spaceborne instruments CloudSat radar and Calipso Lidar. The parameters a and b are given by $89 + 0.6204 \cdot T(°C) g/m^2$ and $1.02 – 0.00281 \cdot T(°C)$, respectively.

The extinction (σ) of a cirrus cloud observed by lidar, and thus IWC, is determined as follows. First, the Leo-Lidar measurements are averaged in time over the whole observed cirrus cloud with a vertical resolution of 60 m. This gives a cloud profile with a high signal-to-noise ratio to be used in further analysis. To determine the extinction profile, a fixed lidar ratio has to be assumed. This ratio is usually constant for one ice particle composition, shape, and particle size distribution within a cirrus layer. Under the assumption of a particle-free atmosphere

directly below and above the cirrus cloud, the lidar ratio is estimated as described by Seifert et al. (2007). In the vicinity of clouds this assumption is valid for wavelengths $\lambda \leq 532$ nm as reported in Ansmann (2002). A multiple scattering correction is also applied to the cirrus extinction profile. The particle size-dependent multiple scattering occurs when the forward-scattered laser light is scattered again by an ice particle, which leads to an underestimation of the extinction coefficient (for more details see Rolf et al., 2012).

The Leo-Lidar measures IWC in the range 0.01 - 400 ppmv with a mean uncertainty of 12%. Thus, the upper detection limit is below those of CLH and FISH, but the lower detection limit is below the minimum IWC that can be detected with certainty by CLH and FISH (Schiller et al., 2008; see red dotted line in Fig. 2.14). For lower IWC from CLH and FISH it is uncertain if the signal stems from instrument uncertainties or from a cloud (see Krämer et al., 2009, their in-cloud definition is applied to the IWC measurements). Thus, the consideration of Leo-Lidar cirrus observations provides the opportunity to assess the validity of small IWC values from CLH and FISH measurements.

During the period of Spring 2011 to Spring 2012, 142 ground-based cirrus observations were performed with the Leo-Lidar over mid-latitude Jülich, Western Germany (50° 54' North, 6° 24' East). In Fig. 2.14 the complete CLH and FISH IWC datasets, which are presented in more detail in Chapter 3, are shown as a function of temperature in blue and grey, respectively. The Leo-Lidar measurements are plotted in orange. The upper IWC detection limit of the Leo-Lidar is clearly visible. The lower Leo-Lidar IWC values coincide nicely with those of the in situ dataset for temperatures > 230 K. Most notable is the agreement of the data below the red dotted line, the minimum IWC that can be detected with certainty by CLH and FISH. At temperatures

below 230 K, CLH and FISH measured IWCs even smaller than those detectable by the Leo-Lidar, but that is with low certainty.

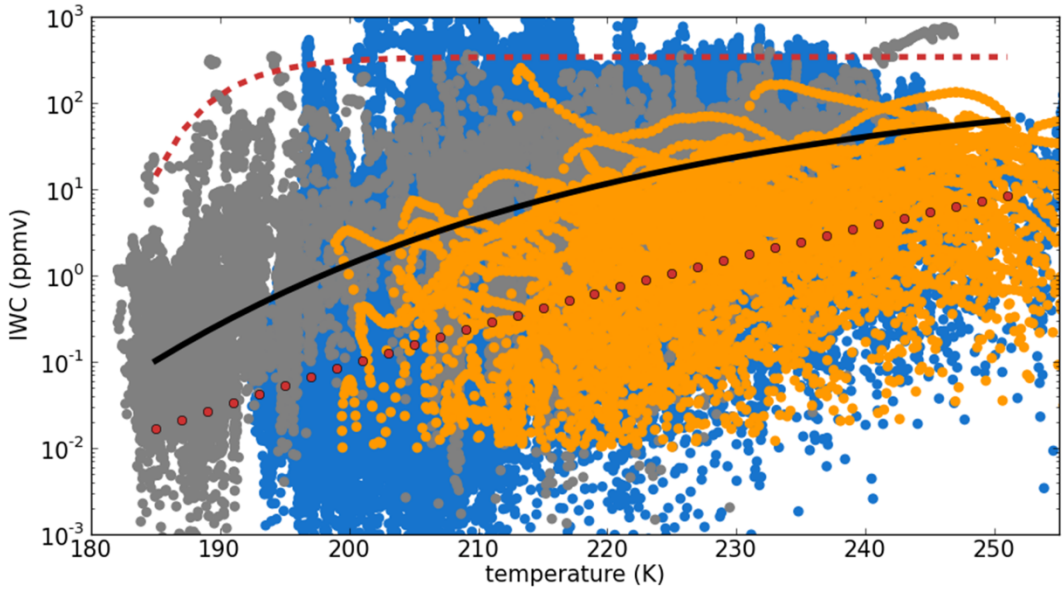

Figure 2.14. IWC as a function of temperature for CLH (blue), FISH (grey) and Leo-Lidar (orange). The red dotted lines represent the IWC maximum and the minimum that can be detected with certainty by CLH and FISH (Schiller et al., 2008; Krämer et al., 2009), respectively. The back solid line is the median of the merged CLH and FISH dataset that is discussed in more detail in Chapter 3.

The Leo-Lidar IWC dataset is not merged with that of CLH and FISH for the remaining analyses presented here since high IWC values are not included in the Leo-Lidar observations, thin cirrus are missed in the temperature range 200 - 230 K and no measurements exist below 200 K. However, from the comparison of the lidar and in situ IWC climatologies there is a strong indication that the low IWC data measured with the in situ instruments are representative of cirrus clouds and not instrument artifacts. Moreover, it seems that the in situ instruments do not miss very thin cirrus clouds but cover the whole atmospheric cirrus IWC range.

2.5.3 Vertical Velocity Data Processing

Vertical velocity measurements from the MMS are used in the analyses presented in Chapter 4 and 5 for the MidCiX and MACPEX campaigns. As explained in Jensen et al. (2009), vertical velocity is calculated by combining two measurements. The first measurement concerns the motion of the aircraft, which is determined by Inertial Navigation System's vertical accelerometer. The second measurement uses differential pressure air motion sensors to calculate airflow with respect to the aircraft. However, they also note that the integration of the vertical accelerometer measurements results in an error that is large in comparison to the vertical velocities at low frequencies. Thus, the average vertical velocity over a short timescale may be biased.

In order to remove this bias, a number of steps were taken (J. Dean-Day, personal communication). First, flight segments associated with ascents and descents were removed due to the measurement challenges accompanying those maneuvers. Turns in the flight path that were greater than 90° were also removed for similar reasons. Of the remaining level flight legs, horizontal distances shorter than 75 km were removed as well, since mesoscale phenomena may also contribute their own bias. Finally, for each flight segment that passed the previous criteria, the average vertical velocity was calculated and removed. While this procedure is necessary for providing more accurate measurements, it diminishes the amount of data available for analysis. The degree to which data are removed is different on a flight by flight basis.

2.6 Conclusion

The information discussed in this chapter provides details on the instrumentation and analysis methods that are used throughout Chapters 3, 4, and 5. Given the importance of field measurements to the overall accumulation of knowledge in regards to cirrus properties and

processes, measurements that are accurate and techniques that are suited to providing a comprehensive survey of the variables involved are absolutely necessary. The instruments surveyed in this chapter demonstrate the methods and techniques that are in use today, including the ways in which uncertainty may be introduced. However, as also demonstrated, a number of processing methods have been used to provide data that are of the quality necessary to perform the thorough and representative analyses found in the following chapters.

Chapter 3 Ice Water Content of Arctic, Midlatitude, and Tropical Cirrus: Extension of a Database and New Statistical Analysis

3.1 Introduction

One of the most common ways to parameterize ice cloud properties in models is to use IWC (Heymsfield and Platt, 1984). For example, Liou et al. (2008) used IWC to determine the mean effective crystal size, which was then used for radiative transfer calculations. In this case, IWC was calculated based on an assumed ice crystal density, in situ measurements of the ice crystal size distribution, and the measured volumes of individual ice crystals. Though the authors take into account the differences between tropical, midlatitude, and arctic regions in terms of cloud formation processes, the datasets used for their parameterization come from only a few experiments, and measured variability of IWC is not considered.

A number of published studies present parameterizations of IWC as a function of temperature, but most have had relatively little data at their disposal to create these relationships (McFarquhar and Heymsfield, 1997; Mace et al., 2001). Although they have described the general behavior of IWC with respect to temperature, these studies have concluded that the variability of IWC measurements is difficult to parameterize on the basis of temperature alone and that using mean IWC values for each temperature in a parameterization masks the natural variability of IWC measurements. Heymsfield and Donner (1990) parameterized IWC as a function of large-scale meteorological variables that could be used in climate models for evaluating optical cloud properties. By including vertical velocity, they added a focus on the

conditions necessary for cloud formation to their parameterization. Their results showed that while each IWC-temperature relationship at a given vertical velocity represented the in situ data well, the use of multiple expressions for a range of vertical velocities provided a more complete picture of the variability of IWC with temperature. However, the addition of more variables into a parameterization makes its implementation more complex.

While efforts have been made to obtain more comprehensive datasets through projects such as the Cirrus Regional Study of Tropical Anvils and Cirrus Layers – Florida Area Cirrus Experiment (CRYSTAL-FACE), logistical considerations dictate that a particular campaign focuses on a specific geographic region (e.g., the tropics, midlatitudes, or poles) and there is little to no overlap. Schiller et al. (2008) created an extensive dataset of IWC values by combining data from ten European airborne field campaigns. In this chapter, I report the extension of that dataset by including measurements from four US field campaigns of similar design.

In the following chapter, the new, extended IWC dataset is introduced. First, the instrumentation and data processing methods are briefly discussed (Section 3.2). Next, the comprehensive nature of the merged datasets is established and the differences between the original and merged climatologies are described (Section 3.3.1). From the merged dataset, it is possible to perform a more detailed statistical analysis of IWC than that provided by Schiller et al. (2008). In Sect. 3.3.2, I explore the analysis of IWC solely as a function of temperature, based on probability distribution functions. This analysis method captures the measured variability of IWC and allows the IWC-temperature relationship to be more thoroughly examined. This exploration is further expanded with the inclusion of ice particle number observations, which may offer some explanation for the distribution of IWC in a given temperature range.

3.2 Instruments and Field Campaigns

The in situ IWC climatology obtained from aircraft presented in this study is the result of merging two large datasets, one provided by the University of Colorado Boulder and one from the Forschungszentrum Jülich, Germany. In situ data from 13 flight campaigns, comprising 67 flights and totaling approximately 38 hours of cirrus observations, and from two different total water instruments are included.

3.2.1 CLH Instrument

Four of the thirteen campaign datasets are the result of measurements by the University of Colorado closed-path laser hygrometer (CLH), which was situated aboard the NASA WB-57F aircraft or the NCAR Gulfstream G-V aircraft, depending on the campaign. See Chapter 2 for a full description of this instrument.

The CLH was used in the 2002 CRYSTAL-FACE (Jensen et al., 2004), the 2004 Midlatitude Cirrus Experiment (MidCiX), the 2006 Tropical Composition, Cloud, and Climate Coupling mission (TC4, Toon et al., 2010), and the 2008 Stratosphere-Troposphere Analyses of Regional Transport (START08) campaign (Pan et al., 2010). The IWC measurements from these campaigns were taken primarily in the midlatitudes and the northern tropics. Table 3.1 provides details on the number of flights, hours of in-cloud data, and the temperature and latitude ranges sampled for each campaign.

Table 3.1. Description of the Flight Campaigns Used to Develop the IWC Dataset

Instrument	Campaign	Date	# of flights	Time in cloud (h)	Temperature Range (K)	Latitude Range
CLH	CRYSTAL-FACE	July 2002	11	9.74	195 – 229	14°N - 27ºN
	MidCiX	April – May 2004	9	11.31	205 – 247	26°N – 38°N
	START-08	April – June 2008	13	1.32	203 – 273	33°N – 53°N
	TC4	August 2008	5	6.01	192 – 229	1°N – 37°N
FISH	APE-THESEO	Feb. – March 1999	1	0.28	182 – 191	4°S – 0°
	Cirrus 2003	December	2	1.20	203 – 242	53°N – 63°N
	Cirrus 2004	November	2	1.58	205 – 246	55°N – 64°N
	Cirrus 2006	November	4	1.63	210 – 235	47°N – 66°N
	Envisat 2002	October	1	0.04	211 – 232	44°N – 45°N
	Envisat 2003	March	2	0.05	198 – 205	61°N – 66°N
	Euplex 2003	Jan. – Feb.	2	0.09	206 – 236	67°N – 68°N
	Scout 2005	Nov. – Dec.	11	4.17	182 – 247	15°S – 18°N
	Troccinox 2005	Jan. – Feb.	4	0.95	188 – 224	22°S – 12°S
Total	13 campaigns		67	38.38	182 - 273	22°S – 68°N

Table 3.1. CLH: Closed-path Laser Hygrometer; FISH: Fast In Situ Stratospheric Hygrometer; for details of FISH and the corresponding field campaigns see Schiller et al. (2008). The temperature and latitude ranges and the time spent in cloud are in reference to all in-cloud measurements.

3.2.2 FISH Instrument

Data from the remaining nine campaigns were obtained by using the Fast In Situ Stratospheric Hygrometer (FISH), which spent time aboard the Russian high-altitude M55 Geophysica aircraft and the GFD Lear Jet throughout various campaigns. This instrument has also been previously described in Chapter 2.

The campaigns in which FISH was utilized cover the tropics, higher midlatitudes, and the polar latitudes. The tropical measurements come from the Airborne Platform for Earth Observation's Third European Stratospheric Experiment on Ozone in 1999 (APE-THESEO, Stefanutti et al., 2004), the 2005 Stratospheric-Climate Links with Emphasis on the UTLS campaign (SCOUT-O3, Vaughan et al., 2008), and the 2005 Tropical Convection, Cirrus, and Nitrogen Oxides Experiment (TROCCINOX). The midlatitude data used by Schiller et al. and in this study are a result of the 2003, 2004, and 2006 CIRRUS experiments and the 2002 ENVISAT validation experiment. The field campaigns that yielded the arctic measurements for the climatology were the 2003 ENVISAT validation experiment and the 2003 European Polar Stratospheric Cloud and Lee Wave Experiment (EUPLEX). It should be noted that the FISH data that were included in this analysis are a subset of that from Schiller et al. (2008), coming from the 29 flights where water vapor (H_2O_{gas}) was measured separately and could be used to calculate IWC from the enhanced total water (H_2O_{enh}) measurement. The full Schiller climatology contains data in which IWC was determined by the difference between the total water measurement made by FISH and the water vapor saturation mixing ratio (see Schiller et al., 2008, for additional information). Table 3.1 contains additional details for each of the field campaigns in which the FISH instrument was used.

3.2.3 FISH and CLH Analysis Methods

One of the screening methods that was applied to the data for this analysis is the determination of geographic location for each of the datasets. It is understood that cirrus properties vary from region to region due to the differences in atmospheric conditions that exist between them (McFarquhar and Heymsfield, 1997). Similar to Schiller et al. (2008), the divisions between regions were made based on familiar latitudinal definitions. The tropics were defined to be between the Tropics of Cancer and Capricorn at 23.5°N and 23.5°S, respectively; the midlatitudes are between 23.5° and 60° in either hemisphere; and the polar region was considered to be latitudes greater than 60° in either hemisphere. In general, these definitions work well. However, in the case of the START-08 dataset, there was cause for some uncertainty, because this campaign began in the late spring and ended in the early summer, a time during which atmospheric conditions change because of the increasing height of the tropopause with the heating of the atmosphere. Since the tropical region is partly defined by a high tropopause, a shift in the latitudes where the tropopause is highest makes using a rigid latitudinal definition of geographic regions questionable. To accommodate this, a different scheme was developed to use the polar and subtropical jet streams as boundaries between the arctic and the midlatitudes, and between the midlatitudes and tropics, respectively. Since the jet streams change locations depending on the season, they were ideal for this analysis. The geographic region for each dataset from the START-08 campaign was determined using upper-level weather maps, which revealed the positions of the jet streams for that day. The data were then labeled and separated accordingly. For data points falling in the midst of a jet stream, the assumption is made that those points display the characteristics of both geographic regions and

they are thus displayed as part of both. Additional information on the analysis methods used to prepare the dataset can be found in Chapter 2.

3.3 Results and Discussion

3.3.1 Extended Cirrus Dataset

One major result of this study is the merging of two large datasets, which yields an even larger and more comprehensive picture of cirrus IWC than that published by Schiller et al., and one that is representative of nearly all latitudes. The latitudinal coverage of the data is illustrated by Fig. 3.1; combining the US and European datasets minimized the gaps in latitudinal sampling. For example, the MidCiX, CRYSTAL-FACE, and START-08 data filled a hole in the Schiller data between 0 and 40 °N. In terms of longitudinal coverage, it should be noted that the data come from field campaigns that focused largely on the western hemisphere.

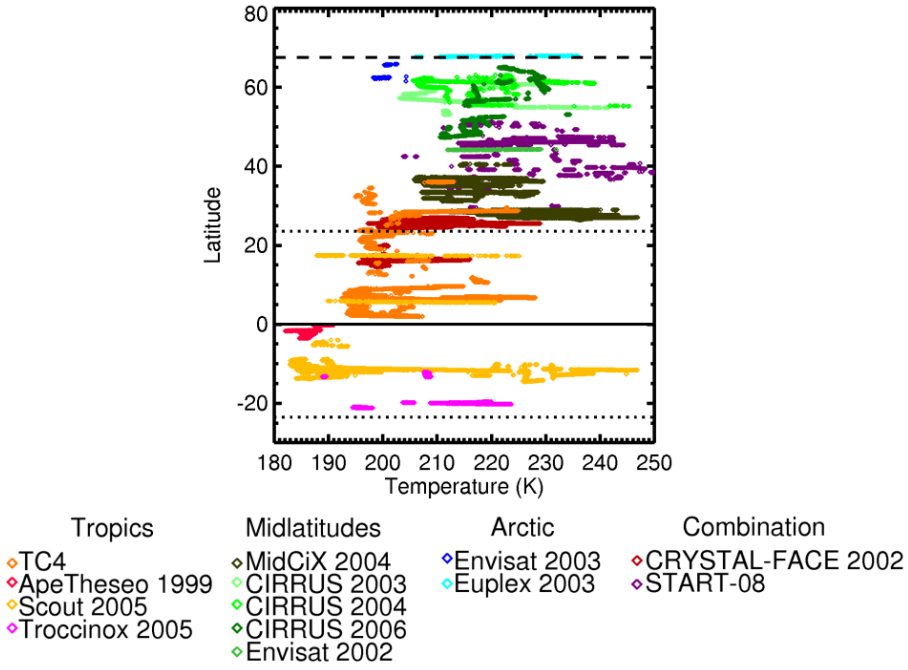

Figure 3.1. The latitudinal coverage achieved by the combined dataset. The color scheme in the legend is used consistently throughout the rest of this chapter.

To further demonstrate the comprehensive nature of the dataset, Fig. 3.2 shows the range of altitudes and temperatures that are covered. Although the Arctic data are sparser than that in the other regions, in general, observations were obtained throughout the mid and upper troposphere and even slightly above the tropopause. Thus, the temperatures and altitudes at which cirrus occur are well represented.

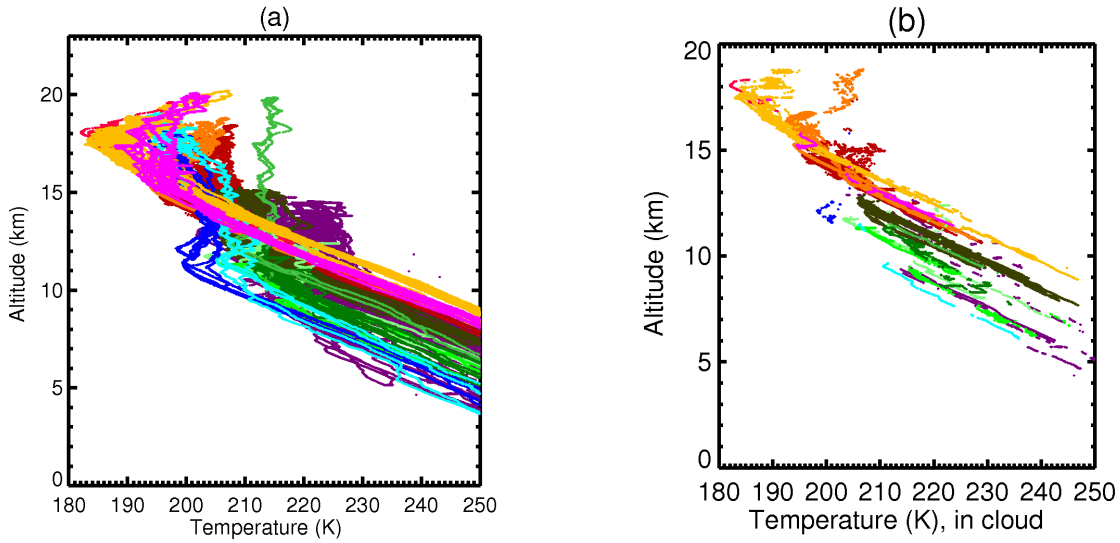

Figure 3.2. (a) Temperature and altitude coverage of all data taken during all campaigns. (b) Same as (a) but for in-cloud data only. The color scheme is the same as in Fig. 3.1.

The CLH and FISH datasets complement each other as a result of differences in instrument capabilities. For example, the lower limit of the FISH instrument allows for accurate measurements in very thin cloud not accessible by the CLH. On the other hand, the CLH has the ability to measure water vapor mixing ratios that are too large for the FISH to measure. In this regard, the two datasets are able to offer the full range of atmospheric IWC values, but only when used together.

Altogether, the dataset used in this analysis encompasses the latitude range from 22 degrees South to 68 degrees North, the altitude range from 5 to 20 km and the temperature range 182 - 249 K. It represents 38.2 hours (27,500 kilometers) of cloud sampling (137,409 data points; for more details of the 13 field campaigns between 1999 and 2008 see Table 3.1). The statistical significance of the dataset is demonstrated in Fig. 3.3, where all observed IWCs are shown as a function of temperature. The color scheme is the frequency of data points with respect to the total number of sampled data. It can be seen that the complete large temperature and IWC range of cirrus is covered by the measurements (it should be noted, however, that the TTL cirrus at temperatures < 200 K were probed with a little lesser frequency than the other temperatures due to the fact that fewer field campaigns took place in the tropics). The dataset includes samples collected only one second apart, which might not be regarded as independent from each other. However, I believe that the reliability and statistical significance of the dataset is given by the spread of IWCs over several orders of magnitude sampled in each temperature interval.

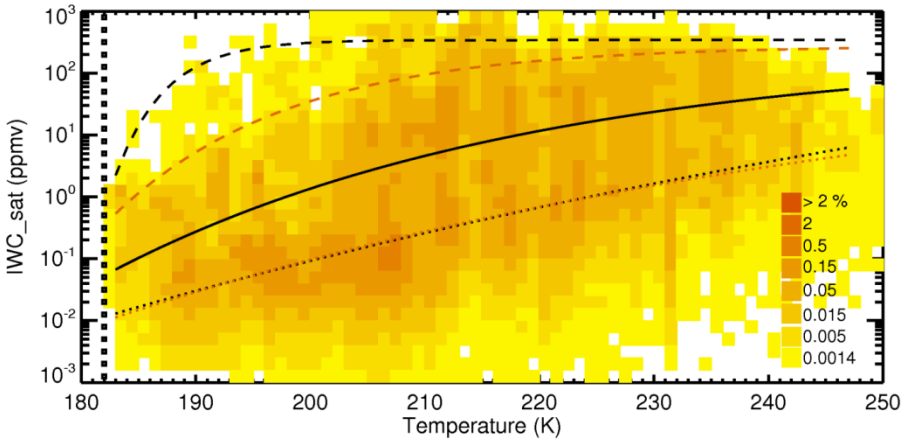

Figure 3.3. IWC as a function of temperature. Color scheme is the frequency of data points with respect to the total number of sampled data. The overall data base represents 38.4 hours (138,240 data points) of in-cloud sampling as noted in Table 3.1. Black solid/dashed/dotted lines are median/maximum/minimum IWC, red dashed/dotted lines encompasses the core IWC region of the climatology of Schiller et al. (2008).

From Fig. 3.3 it can also be seen that, as expected, IWC increases with temperature, a general relationship that is already well documented (see Fig. 5 of Schiller et al., 2008). This behavior is seen again in Fig. 3.4, which lends confidence to the use of the CLH and FISH datasets in combination. Another feature that is also obvious in Fig. 3.4 is the broad range of IWC values for a given temperature, showing that the temperature-IWC relationship is complicated and requires the use of additional variables (e.g. vertical velocity, geography, etc.) to explain it.

One variable that is known to play a role in the temperature-IWC relationship is geographic region. Thus, the dataset was divided by geographic region: arctic, midlatitude, or tropics. Figure 3.4 shows how the temperature-IWC relationship changes as a function of geographic region. By comparing the three plots, it is easily observed that for each region, the relationship has a unique shape. Median fit lines have been developed to more clearly define the relationships. The fit lines are a function of the form $10^{(ab^T + c)}$ as in Schiller et al. (2008). For this paper, the fit lines were developed using data that came only from flights where the purpose was to sample cirrus other than that associated with active tropical deep convection. The flights focused on convection include the SCOUT-O3 flights on 23, 29, and 30 November 2005, the START-08 flight on 16 June 2008, and the TC4 flights on 5, 6, 8, and 9 August 2007. Cirrus formed in association with tropical deep convection have been shown to have very high IWC values at very low temperatures (Schiller et al., 2008) so data from these flights have been removed from the development of any fit lines in this analysis. Using those data in the analysis has the potential to yield results that inaccurately depict the relationship between temperature and IWC. It should be noted, however, that all data, convective and nonconvective, are shown in Fig. 3.4, as well as in the previous figures in this chapter.

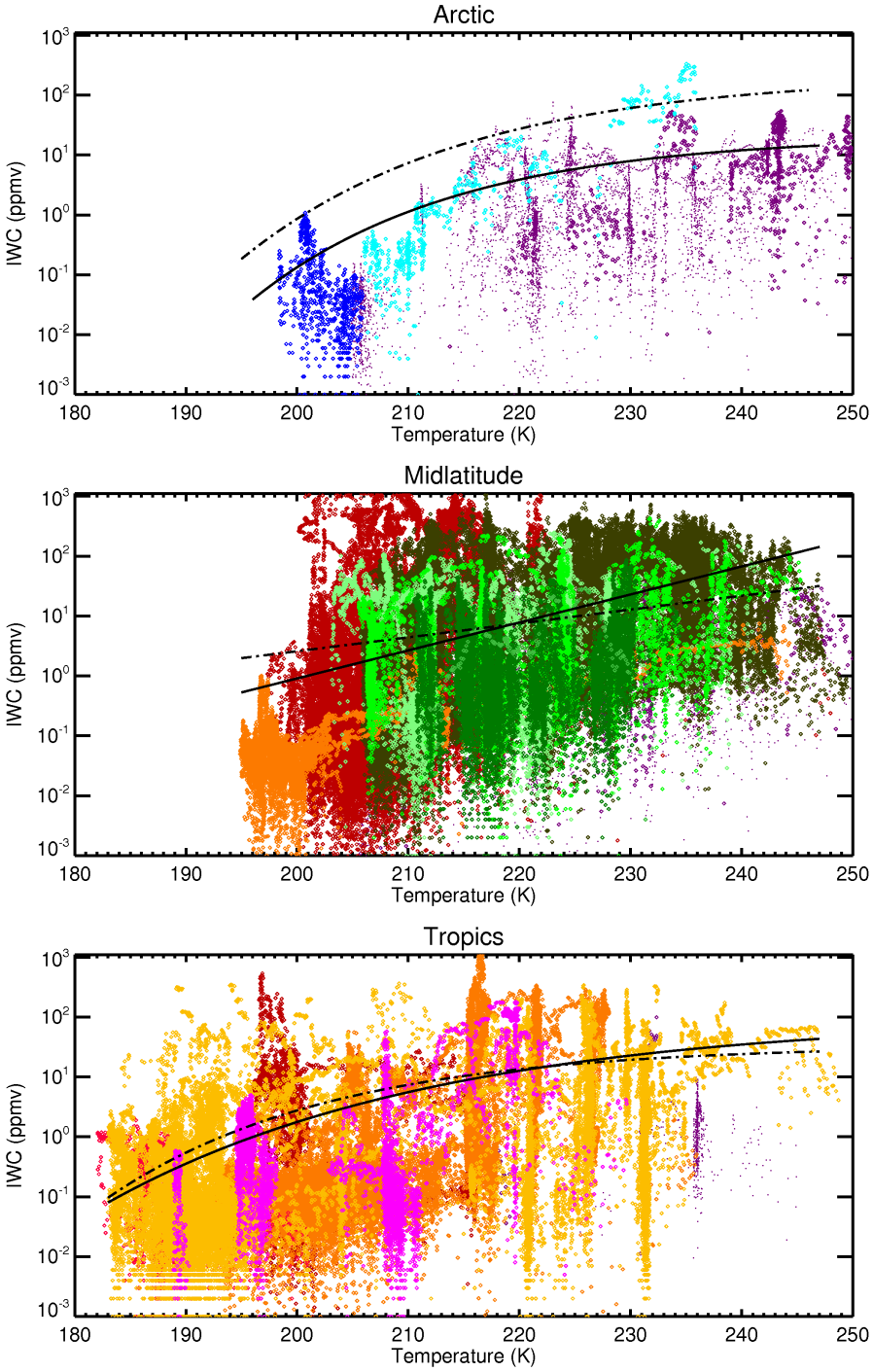

Figure 3.4. IWC as a function of temperature and geographic region. Color scheme as in Fig. 3.1. Data points represented as small dots are a combination of geographic locations and thus included in two plots (see text). The black line represents the median fit, while the dashed black line is the median fit from Schiller et al. (2008). It should be noted that the median fit lines from the Schiller climatology include convective data.

It can clearly be seen that new fit lines developed for the merged dataset compare well to those developed from the FISH observations by Schiller et al. For the tropical data, the new median fit line is very close to the old one, with the obvious differences occurring at the lower and higher temperatures where smaller and larger IWC values, respectively, are now more evenly represented. In the case of the midlatitudes, the difference between the new and old median fit lines is more significant. Once again, smaller IWC values are now influencing the median fit line more heavily in the lower temperature ranges, while the larger IWC values are doing the same at the higher temperature ranges. The new median fit line for the arctic data appears to have changed the most from the median fit line used by Schiller et al. For all temperatures the new median fit line is located at a smaller IWC, but the overall shape of the fit line has been preserved. This is most likely due to the differences in arctic datasets used for this analysis versus the data that were used by Schiller et al. since only a subset of those data are used in this analysis.

For all regions, the alterations in the fit lines could be a result of seasonal differences between the two original datasets. The observations from FISH resulted from experiments that took place in the boreal fall and winter months while the experiments that the CLH was a part of took place in the boreal spring and summer months. The possibility of a seasonal effect is not explored further in this paper.

3.3.2 New Statistical Analysis

Ice water content

In the introduction I noted work that has been done to parameterize IWC. Although the use of multiple variables helps to describe the range of IWC observed in nature, it does not fully capture the variability and is thus incomplete. Rather than attempting to incorporate multiple

variables in this work, I describe the IWC-temperature relationship through probability density functions (PDFs). These represent the distribution of IWC values for specific temperature bins without considering the mechanism(s) responsible for the variation.

The first step in my analysis is to develop PDFs from the full, merged dataset separated into 5-K temperature bins (Fig. 3.5). The full dataset was utilized because there is not sufficient data to accurately describe the behavior in each temperature bin for each geographic region. Note that the lowest temperature bin spans 180 – 194 K and the highest temperature bin spans 235 – 249 K. These bins are wider due to the limited amount of data that were collected at those temperatures. However, it is likely that the clouds in these bins share common development mechanisms. The 180 – 194 K temperature range is known to have cirrus formation mechanisms that are different from those seen in warmer regions of the troposphere (Krämer et al., 2009; Jensen et al., 2010; Spichtinger and Krämer, 2013). The 235 – 249 K temperature range, on the other hand, probably contains mixed-phase clouds that would alter the distribution of condensed water content with respect to temperature. It should be noted that the data used to develop the PDFs do not include samples taken in active tropical deep convection for the same reasons discussed previously. While tropical deep convection is important as a mechanism for cirrus formation, the temperature-IWC relationship that results is different enough from that of other cirrus formation mechanisms that I feel it should be analyzed separately.

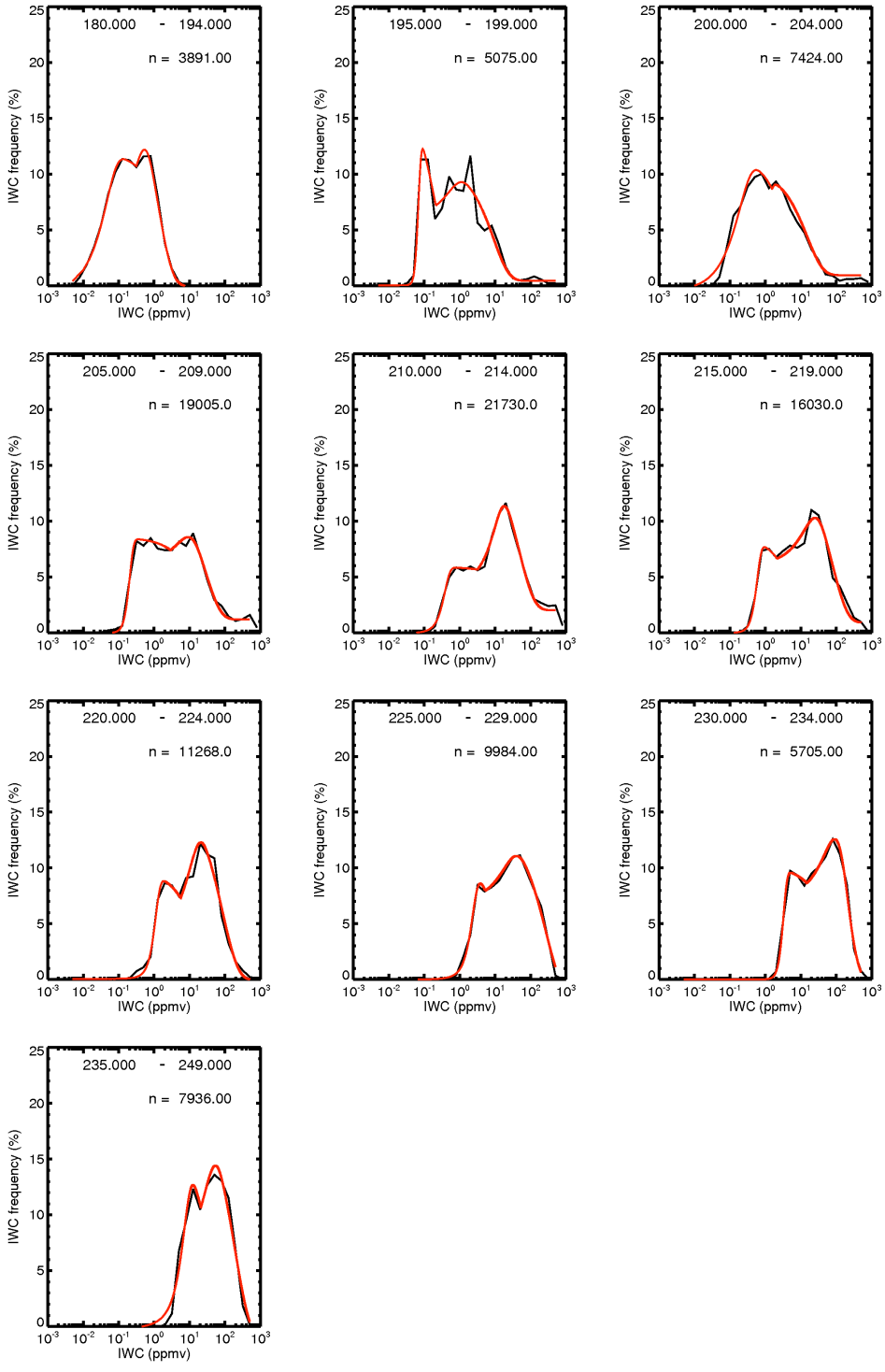

Figure 3.5. PDFs of IWC in various temperature ranges. The black lines are the PDF, the red lines are the curve fits.

As expected, the IWC distribution changes from bin to bin, with smaller IWC values dominating the distribution in the lower temperature bins and the largest IWC values dominating the distribution in the higher temperature bins. This is consistent with the known IWC-temperature relationship. The shape of the distribution is similar in each temperature bin, and it is bimodal in nature, except for the 195 K – 199 K bin, where the PDF shows several peaks. This difference is likely due to a smaller number of data points in the bin or potentially to the presence of multiple formation mechanisms exerting influence on the PDF. In general, the two peaks of the distribution shift monotonically in IWC value with temperature. As the temperature increases, the height of the first peak decreases, while the second peak shifts to larger values.

The PDF plots shown in Fig. 3.5 are ideal for capturing the IWC variability over small temperature ranges. Using the approximately Gaussian shape of the two modes in the PDFs, I have developed a fit function that describes IWC as a function of temperature, while also representing the variability of the IWC. It should be noted that this relationship is meant to describe the observations found in the statistical analysis of my data, not as a parameterization for use in modeling. I used a modified Gaussian fit developed in the data analysis software package OriginPro 8.1 (OriginLab, Northampton, MA) that was originally intended for use in chromatography. In the equation

$$f(x) = y_0 + \frac{A}{t_0}\exp\left[\frac{1}{2}\left(\frac{w}{t_0}\right)^2 - \frac{x - x_c}{t_0}\right]\int_{-\infty}^{z}\frac{1}{\sqrt{2\pi}}\exp\left(\frac{-y^2}{2}\right)dy \qquad (3.1)$$

where z is given as

$$z = \frac{x - x_c}{w} - \frac{w}{t_0} \qquad (3.2)$$

x and f(x) are the IWC (ppmv) and IWC frequency (%), respectively. The remaining coefficients (y, t, w, A, and z) are constants fit by the OriginPro program and do not hold any

physical meaning in terms of the contributing variables associated with IWC. They are purely used as descriptors of the curves fitting the PDFs. To accommodate the fact that the curves are bimodal, each PDF was treated as two Gaussian curves that overlap one another between peaks. The division between where one curve stopped and the other started was made on a case-by-case basis and was determined based on what appeared to provide the best fit. Figure 3.5 also illustrates the curves that were fit to each PDF. The coefficients for each curve and temperature bin can be found in Appendix A.

An additional depiction of the relationship observed in the PDFs is provided in Fig. 3.6 to show its representative nature. The two most frequently observed IWC values are plotted for each temperature bin, along with median fit functions to the entire dataset as determined here and in Schiller et al. (2008). It can easily be seen that there is a defined structure to the relationship between those IWC values and temperature and that it is similar in shape to the median fit. Also, the median fit lines fall directly between the two IWC values. In Schiller et al. (2008), a core region was defined where the frequency of occurrence was greater than 5%. The minimum and maximum values of that core region are illustrated in Fig. 3.6 by the dotted and dashed red lines, respectively. The peak IWC values for each temperature fall well within that core region, which lends confidence to the idea that these values are representative of a large portion of the data.

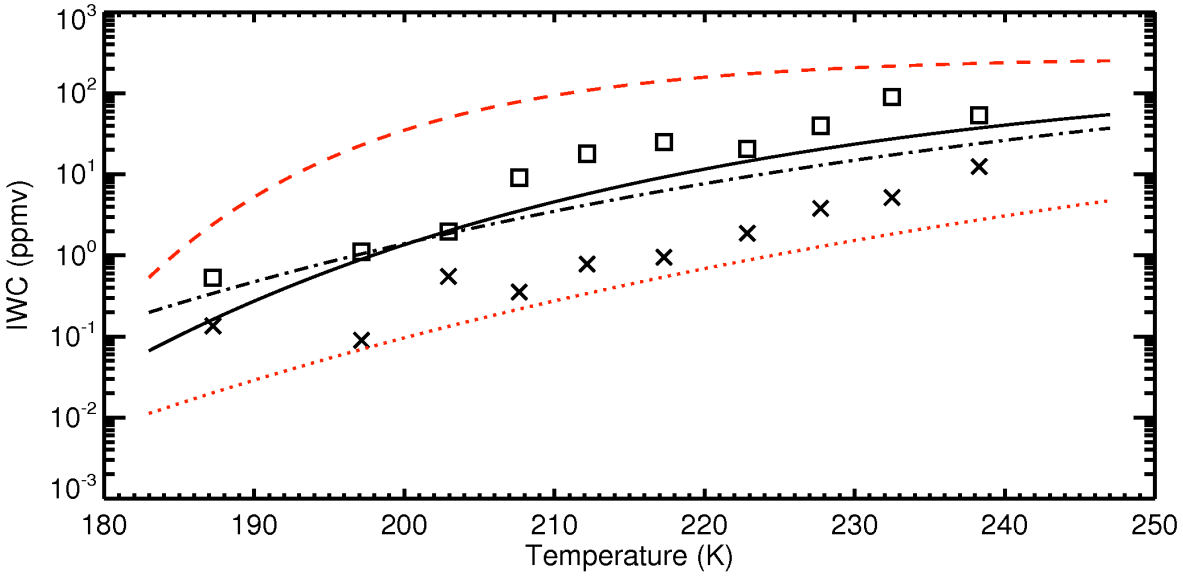

Figure 3.6. Peaks of the bimodal PDFs from Fig. 3.5. 'X' is the value of the first (lower IWC) peak, a square is the value of the second. The temperature at which they are plotted is the weighted mean temperature for each temperature bin. The black line represents the median fit line for the merged climatology, not including tropical deep convective data. The black dashed line is the median fit from Schiller et al. (2008) and includes convective data. The red dashed/dotted lines depict the maximum/minimum envelope of the most frequent (>5%) IWC as seen in Fig. 6 of Schiller et al. (2008).

Ice water content and crystal number

In order to interpret the meaning of the IWC-PDFs, PDFs where the data have been divided into three temperature ranges are looked at, as seen in Fig. 3.7a. The ranges used here correspond to the three temperature ranges used in Fig. 7a of Salzmann et al. (2010), which is reproduced here as Fig. 3.7b. The PDF graphs show ice crystal numbers (Ni) observed using a Forward Scattering Spectrometer Probe (FSSP, see Krämer et al., 2009). Unlike the previous PDFs, these were constructed with all data including tropical deep convective data (but note that the PDFs excluding convective data, not shown here, are nearly identical).

Since the measurements from Krämer et al. (2009) are not corrected for artifacts produced by ice crystal shattering, possible shattering effects on the Ni-PDFs are discussed here.

For that purpose, cirrus ice crystal numbers that are corrected for shattering are compared to those shown in Fig. 3.7b. Figure 3.7c shows Ni-PDFs in two temperature ranges, which come from measurements taken by the CAPS probe (Cloud and Aerosol Particle Spectrometer, described in Chapter 2) onboard the British BAE-146 during the Combined Observation of the Atmospheric boundary Layer to study the Evolution of StratoCumulus (COALESC) campaign in 2011 over the UK. The CAPS data acquisition includes records of particle interarrival times so that a removal of artifacts from shattering is possible. In addition, shattering was reduced by improving the CAPS sampling characteristics (Meyer et al., 2013).

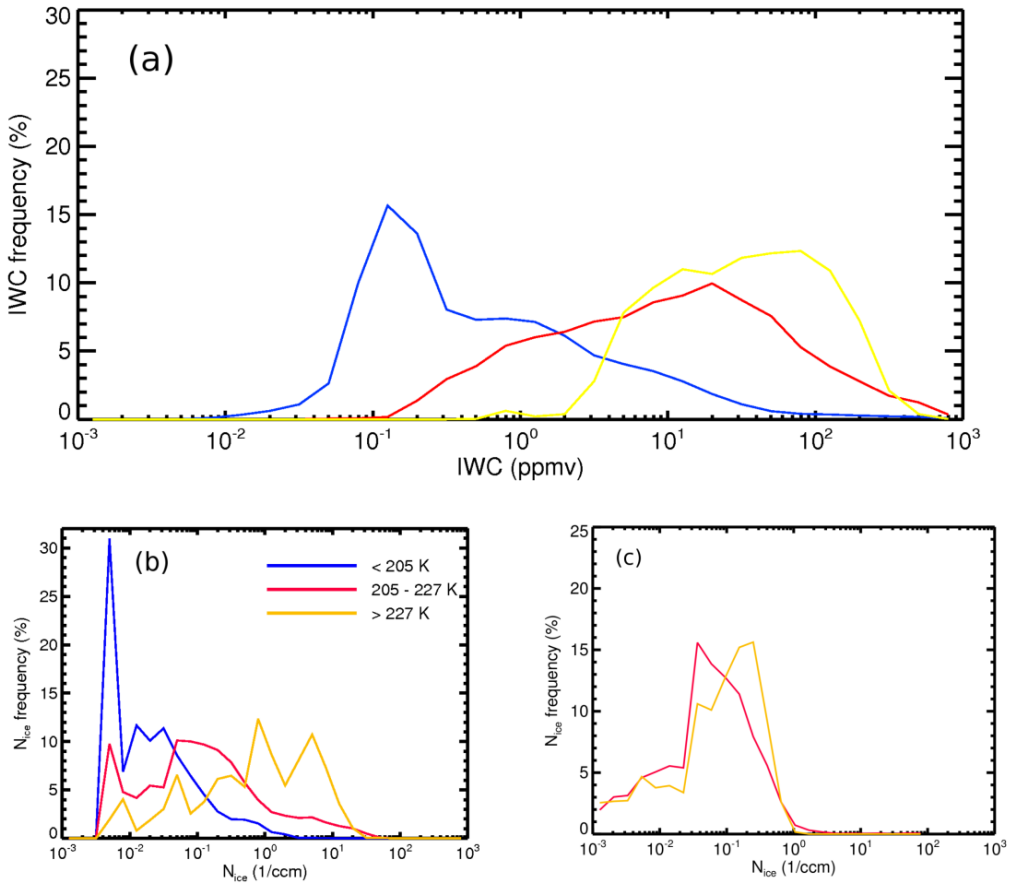

Figure 3.7. (a) Top: PDF of IWC; (b) Bottom-left: PDF of crystal number (FSSP); (c) Bottom-right: PDF of crystal number (CAPS). (b) is reproduced from Fig. 7a of Salzmann et al. (2010).

Inspecting the Ni-PDFs in panels b and c of Fig. 3.7 shows that in the lower temperature range (red curves) both PDFs are of a bimodal nature, though in the COALESC data set the peak at low Ni is much weaker than in the Krämer et al. (2009) dataset. In addition, a small amount of Ni concentrations larger than 1 cm^{-3} are visible in this dataset, which possibly originate from crystal shattering. The same conclusion holds for the higher temperature range (yellow curves), but as expected the contribution of Ni concentrations larger than 1 cm^{-3} is higher than at colder temperatures. No measurements for T < 205K were available from the COALESC observations, but it is likely that at the low temperatures shattering does not play an important role. In summary it can be seen that the general shape of the Ni-PDFs is bimodal, and also that the peaks at larger Ni concentrations shift to higher values with increasing temperature.

A comparison of the IWC-PDFs with the Ni-PDFs, for each of the three temperature ranges (blue: < 205 K, red: 205 – 227 K, yellow: > 227 K), shows that there is a similarity in the overall shape of the distributions, suggesting a connection. For example, and most noticeably, the narrow peak in ice number at approximately 0.005 cm^{-3} in the very low temperature range (blue curve), which is representative of conditions found at the tropical tropopause layer (TTL), coincides with a peak in IWC at approximately 0.1 ppmv, while a second broader peak appears at higher ice crystal numbers and IWCs. It is remarkable that the bimodal nature of the cirrus PDFs is found by two completely independent measurements. As a possible explanation of this structure of the ice crystal number frequencies, Spichtinger and Krämer (2013) propose, from extensive model simulations in comparison to the TTL cirrus observations of Krämer et al. (2009), that the first peak around 0.005 cm^{-3} is mainly caused by heterogeneous ice nucleation, while the higher ice crystal numbers stem from homogeneously formed cirrus clouds.

The remaining two temperature ranges are more difficult to interpret. It is clear, however, that there are two modes for each temperature range, both in IWC and Ni, thus providing me with good reason to speculate that they are linked to one another.

I summarize my findings with the following hypotheses: (i) the IWC is influenced by the ice crystal number, (ii) the IWC PDFs are observed to be bimodal over the complete cirrus temperature range, (iii) for cold TTL cirrus, it is highly likely that the mode with only a few ice crystals (low IWC) corresponds mainly to heterogeneous ice formation while the mode with a higher number of ice crystals (higher IWC) can be attributed to homogeneous ice formation. Extending the physical explanation of the two ice number/IWC modes from TTL cirrus to higher temperatures leads to the conclusion that both heterogeneously and homogeneously formed cirrus clouds are visible in the IWC PDFs as two modes of lower and higher IWC, where the lower and weaker Ni/IWC mode might represent heterogeneous freezing and the higher and stronger mode represents homogeneous freezing, as one would expect.. This might be a hint that heterogeneous freezing plays a larger role in cirrus modification than believed hitherto (Kärcher et al., 2009).

3.4 Conclusions

The importance of cirrus in the climate system is well documented, but the details are not yet well understood. The IWC of these clouds is also known to have a crucial role in that system through its effect on terrestrial and solar radiation, but it is difficult to parameterize owing to the large variability in IWC values possible for a given set of atmospheric conditions. Here, I have presented the extension of a cirrus IWC climatology originally developed by Schiller et al. This extension provides a highly comprehensive dataset in terms of covering the temperature, altitude,

and latitude ranges at which cirrus are observed and the IWC values that are known to be present in those clouds.

Previous work to create IWC parameterizations has been successful in exploiting the general relationship between IWC and temperature, but has been unable to capture the variability of IWC at a single temperature without the use of additional variables. Through the use of PDFs, I have been able to demonstrate and create a description of IWC in 5-K temperature bins that relies solely on the IWC-temperature relationship while still including the large range of IWC in a small temperature range.

The peak IWC values of the PDFs were shown to be consistent with the IWC-temperature relationship seen with the full, extended climatology and were easily bounded within a core region of the most frequent IWC values. It was also shown that the use of PDFs for describing the microphysical properties of ice clouds is both appropriate and useful. The comparison between IWC and Ni-PDFs indicate that the relationship between IWC and temperature is influenced by particle number. Further, I found hints that the general bimodal nature of the IWC PDFs might be caused by the two pathways for ice formation, namely heterogeneous and homogeneous freezing. The underlying processes that lead to a connection among Ni, IWC and the cirrus formation mechanism are the subject of Chapters 4 and 5.

Chapter 4 The Relationship of Ice Water Content and Crystal Number to Large-Scale Dynamics

4.1 Introduction

In Chapter 3, the relationship between IWC and Ni as a function of temperature was analyzed. Those results show that both the IWC and Ni distributions are bimodal across the full temperature range in which cirrus are typically observed. I hypothesized that the two observed modes are the result of homogeneous and heterogeneous nucleation, respectively. In order to more completely explore this result, it must first be recognized that the processes controlling cirrus formation are the result of dynamics at both the large and small scales. While the nucleation processes that take place on the small scale ultimately determine the microphysical properties of a cirrus cloud, considering the weather, synoptic conditions, and related large-scale dynamics can provide additional, significant information when it comes to understanding and parameterizing the processes occurring during and after cirrus cloud formation. Thus, the next two chapters focus on the dynamics at these two levels, beginning with the large scale.

In Chapter 1, I introduced the research carried out by Stone (1957) that contains the first documentation of the relationship between cirrus cloud occurrence and the jet stream, and subsequently with other weather related mechanisms as well - baroclinic fronts and lows, convection, and orographic lifting (Wylie, 2002). Starting with the results from Stone, their report determined that cirrus were most likely to be found on the northward-flowing side of Rossby wave troughs located between the trough axis and the ridge. More specifically, thick

cirrus clouds were observed on the southeastern side of where the strongest winds are found in the jet stream, termed the jet core, but is currently more commonly known as a jet streak. It was also noted that elsewhere along the jet stream cirrus clouds were less prevalent. Along the southward-flowing portion of a ridge, the cirrus clouds are thin, whereas the area around the trough yielded few, if any, clouds.

Capitalizing on the technological advancements made since Stone's work, Menzel et al. (1992) analyzed four years of satellite observations made by the GOES VAS (Geostationary Operational Environmental Satellites Visible-Infrared Spin Scan Radiometer [VISSR] Atmospheric Sounder) over the continental United States. They found that cirrus were more or less likely to exist depending on which quadrant around the core they examined. Briefly, convergent and divergent areas exist around the jet core due to the acceleration and deceleration of the winds entering and exiting the core (Shapiro and Kennedy, 1981). At the entrance to the core, the winds are accelerating, resulting in convergence on the northwest side and divergence on the southwest side. At the exit, the winds are decelerating, which results in convergence on the southeast side of the jet and divergence on the northeast side. As demonstrated in Fig. 1 from Menzel et al. (1992; reproduced here as Fig. 4.1), the likelihood of cirrus occurrence corresponds to the dynamics in each quadrant. On the accelerating side, not surprisingly, most of the cirrus is found where divergence is occurring, while the least occurs where convergence is occurring. Conversely, on the decelerating side, the cirrus was evenly distributed between the converging and diverging areas.

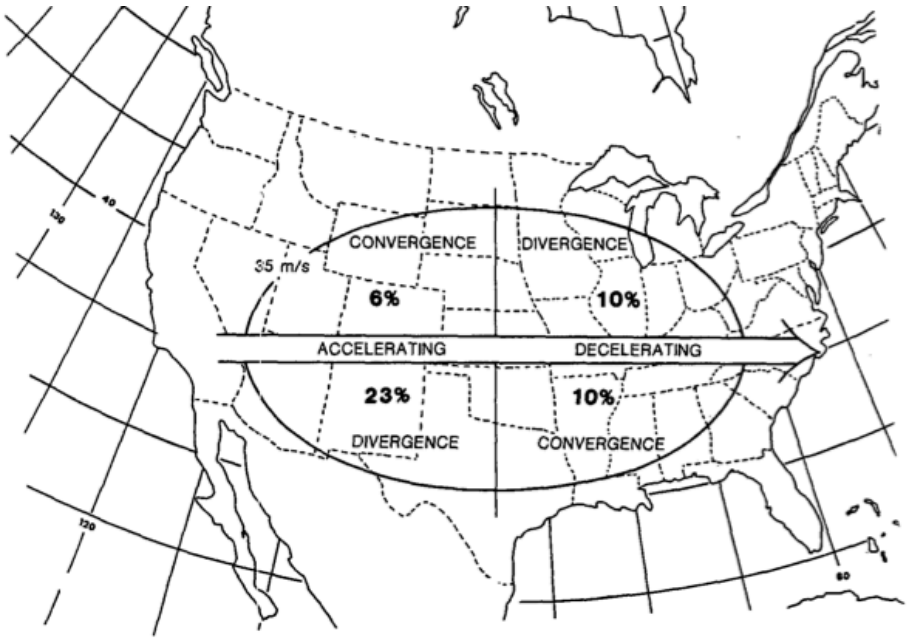

Figure 4.1. Illustration demonstrating the frequency of cirrus occurrence relative to jet streaks and the exit and entrance points of the jet. This figure is reproduced from Menzel et al. (1992).

Menzel et al.'s results confirm those from Stone (1957) and expand upon them with statistics that quantify the relationship of cirrus to two dynamical features - jet streams and convection associated with precipitation. In months where the jet stream winds are strong, typically during the winter, 40 – 60% of the cirrus clouds were found in one of the jet core quadrants. During times when the jet stream winds were weak, only 10 – 30% of the cirrus was associated with the jet stream. Menzel et al. also looked into the occurrence of cirrus clouds in relation to convective precipitation events. Using echoes from the National Weather Service's (NWS) radar summaries in comparison to the cirrus coverage, they determined that at least half of the cirrus that occurred in the summer months was due to these convective events. During the winter, when convection is less prevalent, only 22% of cirrus clouds were associated with these kinds of events.

Furthermore, Keyser and Shapiro (1986) had previously determined that the dynamics within the flow field can create variations of the vertical motions associated with the ageostrophic flow and, in conjunction with the available moisture in the upper troposphere, are the key to developing and maintaining midlatitude cirrus systems. Mace et al. (1995) used wind profiler data from the Wind Profiler Demonstration Network and radiosonde data from NWS to further explore and explain how kinematically derived ageostrophic vertical circulations evolve and how they relate to the resulting cloud field, as well as suggesting how to best parameterize these dynamics in global climate models (GCMs). A case study spanning 12 hours during the FIRE (First International Satellite Cloud Climatology Project [ISCCP]) Cirrus-II Intensive Field Observing Period in Coffeyville, Kansas demonstrated that trough amplification and a building ridge elsewhere led to the development and evolution of ageostrophic flow at the jet streak exit within their region of study over time. As a result, a cloud band located in the middle and upper troposphere was observed to form in conjunction with the increasing vertical motion brought on by the changes in ageostrophic flow. Also, the cloud band was successfully maintained throughout the observation period due to these same dynamics.

Not only are the statistics of the frequency of cirrus in relation to weather patterns known, but additional details on the relationship between large scale dynamics and microphysical properties have also been determined through various case studies. An early study by Heymsfield (1977) used 20 case studies between 1973 and 1975 to investigate four synoptic condition types: an overrunning warm front, an occluded warm front, a closed low aloft, and jet stream cirrus. Using aircraft instrumentation and Doppler radar, measurements such as the scale of these systems, vertical velocities, IWC, and particle concentration and size were made. Ultimately, Heymsfield demonstrated that temperature and vertical velocity are important drivers

behind cirrus ice crystal properties. In terms of vertical velocity, his results showed that, in warm frontal overrunning systems, the observed vertical velocities were typically around 10 cm s^{-1}, while in localized convective cells and convective jet stream elements, the vertical velocities were 50 cm s^{-1} or greater. It was also found that closed low pressure systems aloft were among the most convective with vertical velocities between 25 and 50 cm s^{-1}. As expected, the systems having higher vertical velocity values had larger water contents (liquid and ice) as well as greater ice crystal concentrations and a presence of specific ice crystal habits. Another noteworthy conclusion of this work is that within the convectively unstable layers where vertical velocity varied considerably, the microphysical properties did not display a variation and were found instead to be uniform.

Mace et al. (1995) point out that datasets composed of long-term observations would be particularly helpful for developing parameterizations to describe clouds and radiation. Studies such as those of Sassen and Campbell (2001) and Mace et al. (2006) took advantage of established ground-based remote sensing sites to create a database from which statistics could be derived. The study of Sassen and Campbell utilized data taken at the University of Utah Facility for Atmospheric Remote Sensing, which is part of the FIRE Extended Time Observations (ETO) program. They investigated the flow regimes that are common to the Salt Lake City, Utah area and noted the frequency of each. Five were found to be particularly predominant, including a ridge with a strong amplitude, a flat ridge, zonal jet stream flow, split jet stream flow associated with a low pressure system in the subtropical branch or cutoff from the main circulation, and a trough with the polar and subtropical jets in phase. They note that, while these results are likely to be site-specific, they establish details that may be important for comparing their results to similar studies in different geographic locations. The second part of this series of papers, from

Sassen and Benson (2001), goes on to discuss the observed microphysical properties of the cirrus clouds, but does not directly link them to the flow regime in which they were originally sampled.

Similarly, Mace et al. (2006) used data taken at the Atmospheric Radiation Measurement (ARM) Climate Research Facility (ACRF) in Oklahoma, in combination with the National Centers for Environmental Protection and the National Center for Atmospheric Research (NCEP-NCAR) reanalysis data, to investigate cirrus cloud properties and reconstruct the synoptic-scale conditions at the time of observation. They specifically looked at the large-scale ascent, relative humidity values at 300 hPa, the 500 hPa heights, absolute vorticity, and wind velocities in order to infer the structure of the synoptic environment. From their analysis, Mace et al. determined that cirrus clouds were present 25% of the time over the research site, and in agreement with the conclusions of other studies, they found cirrus cloud systems were more likely to coincide with periods of large-scale ascent. However, they also noted that mesoscale turbulence is enough to continue generating cirrus in an environment that is weakly descending, but that this cirrus is generally thin. They also noted that during the cold season, cirrus systems were most commonly found upstream of large-scale ridge axes, with thinner cirrus clouds closer to the ridge axis. As expected, warm-season cirrus was usually the result of detrainment from deep convection, but they found that large-scale ascent was still necessary to maintain these systems. In terms of the microphysical properties within the observed cirrus clouds, Mace et al.'s research indicates that the sensitivity to vertical motion is more pronounced in cold-season cirrus and less so in the cirrus produced by deep convection. In the cold season, IWC increases by nearly a factor of 2 between cirrus observed in ascending columns and cirrus observed in descending columns. This difference also exists in the warm season but was not as large. The

researchers infer that in the warm season, the moisture in those cases is detrained from deep convection, and therefore ascent anomalies will have less of an effect in this regard.

Each of the studies discussed here explored the notion that cirrus are generated by weather patterns and are supported by large-scale dynamics, both weak and strong features. Also, though the statistical likelihood of cirrus occurring in any location is unique to that site, it seems generally understood that the frequency of occurrence and the microphysical properties are largely the result of the synoptic environment. Using the in situ observations from two midlatitude airborne flight campaigns, the 2004 MidCiX campaign and the 2011 MACPEX campaign, these concepts can be studied further.

One intriguing feature of this analysis is that the observations in the MACPEX dataset are different from what has been observed in other, similar datasets such as MidCiX. Considering that MACPEX looks different from other cirrus datasets, this is a potentially good opportunity to explore how weather patterns affect cirrus microphysical properties. A comparison with MidCiX may help us to see these differences more clearly. It is also possible to investigate how different synoptic situations compare to one another as well as how the cirrus clouds are different from campaign to campaign. Section 4.2 describes the details of the MACPEX and MidCiX campaigns, including their similarities and differences. Section 4.3 uses case studies to demonstrate the effects of synoptic scale dynamics. Section 4.4 discusses the results of this analysis in more detail and includes possible explanations for the discrepancies in the theories presented here, including those observed in the vertical velocity distributions and the relationship between large-scale dynamics and Ni.

4.2 MACPEX and MidCiX

4.2.1 MACPEX

The Midlatitude Airborne Cirrus Properties Experiment (MACPEX) took place during the spring of 2011 (March – April) and was based out of Ellington Field in Houston, TX. The major focus of this flight campaign was to investigate the microphysical properties of midlatitude cirrus in order to better understand their influence on the radiative properties of this cloud type. Some of the primary science objectives include investigating the prevalence of small ice crystals (diameter < 50 μm), the involvement of other cirrus microphysical properties in cloud formation, the abundance of heterogeneous nuclei, and the evolution of microphysical properties throughout a cirrus cloud's lifecycle (www.espo.nasa.gov/macpex/). In addition to the in situ measurements collected by the aircraft, some flights were intended to coincide with NASA's Earth Observing System (EOS) A-Train satellite measurements for comparison and validation purposes. The flight domain covered parts of the southern half of the central United States including the area around the Department of Energy's Atmospheric Radiation Measurement (ARM) Climate Research Facility Southern Great Plains (DoE ARM SGP) site in Oklahoma.

A total of 14 flights were made with over 20 hours of in-cloud data collected. Only 10 flights are used here due to instrument- and aircraft-related circumstances, which determined the availability of data for a given flight. The aircraft used in this experiment was the NASA WB-57F, which was outfitted with a total of 24 instruments: nine water instruments (includes those that measure water vapor only or total water), seven particle probes, four aerosol/IN composition instruments, three instruments making measurements related to chemistry, and the MMS (see Chapter 2 for instrument description).

For the purposes of the analysis presented in this chapter, the data from three instruments are utilized: total water measurements from the CLH, which were used to calculate IWC, ice crystal concentration from the 2D-S probe, and atmospheric state parameter measurements from the MMS. Details concerning each of these instruments can be found in Chapter 2.

4.2.2 MidCiX

The MidCiX (Midlatitude Cirrus Experiment) campaign was first introduced in Chapter 3. Similar to the MACPEX campaign, MidCiX also took place during the spring, used the NASA WB-57F aircraft, flew in the same general regions of the United States, involved a similar instrument payload aboard the aircraft, and was carried out with the same general science questions and goals in mind. Taking place in 2004, a total of nine flights were made but only the seven that contain the full dataset necessary for this analysis are used here. The instrument payload included five water instruments (measuring total water or water vapor), four ice particle probes, and two other instruments measuring additional variables. The CLH and MMS were aboard the aircraft in MidCiX and provided the IWC and atmospheric measurements, respectively. The ice crystal concentration measurements are from the observations of the CAPS instrument, which is also described in Chapter 2. Additional information concerning MidCiX can be found in Table 3.1 in Chapter 3.

4.2.3 Comparison of MACPEX and MidCiX

Due to the similarities of payload, season, and mission objectives between MACPEX and MidCiX, a comparison between data from the two would be expected to produce similar relationships. Figure 4.2 illustrates the latitudes and altitudes sampled during each campaign. Based on the information shown here and the results of Chapter 3, it seems likely that the two campaigns would produce similar datasets, but it has already been noted that they did not.

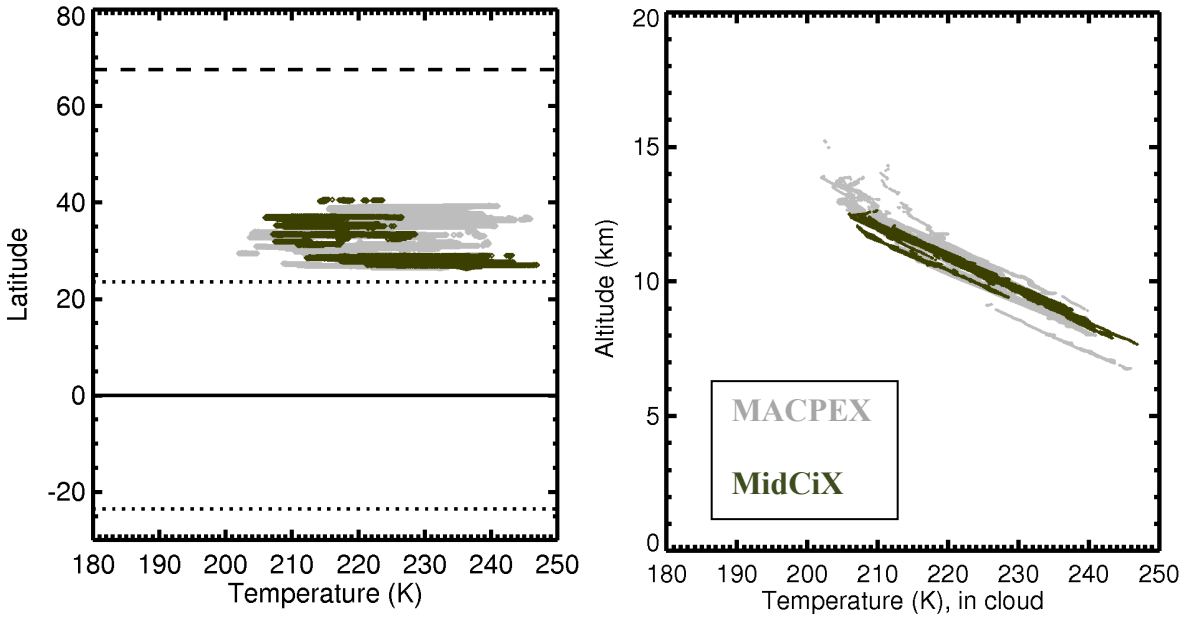

Figure 4.2. Left panel: Temperatures observed at various latitudes. Right panel: Temperatures observed over the sampled altitude range.

IWC-Temperature Relationships

The analysis work shown in Chapter 3 presented the IWC-temperature relationship through the use of probability distribution functions (PDFs). Presenting the dataset in this manner allowed the relationship as well as the variation and distribution of observations to be depicted. Here, a similar method is used to illustrate the results of the measurements taken during MACPEX.

In Figure 4.3a, the observed IWC for all 10 MACPEX flights is represented as a function of temperature. The data were grouped into 1-K temperature bins and divided into equal IWC bins. Each bin combination is then colored by the frequency of that observation with the darker yellows indicating a more frequent observation. Generally, the observed IWC-temperature relationship is consistent with the relationship discussed in Chapter 3: as temperature increases, IWC increases too. As in Figure 3.3, the black solid, dashed and dotted lines represent median,

maximum, and minimum IWC. However, looking more closely at the frequency as represented by color reveals that the most frequent observations do not agree completely with that relationship. Between about 210 – 220 K, the most frequent IWC observations are above the median value. A core region representing where IWC-temperature pairs represent > 5% of the frequency of observations as described by Schiller et al. (2008), is given by the red dashed/dotted lines. The high IWC measurements mostly fall within this core region, but between about 214 – 220 K, the most frequent observations are on or outside the maximum boundary.

The observed IWC from MidCiX is shown in Fig. 4.3b and the Krämer et al. (2009) climatology is shown in Fig. 4.3c for further comparison. The Krämer et al. climatology is the result of combining the data obtained by the FISH instrument during several different European campaigns. Though the dataset is comprised mostly of midlatitude measurements, samples from the Arctic and tropics are also included. Thus, it is a large and useful dataset for providing some context about the typical distribution of midlatitude microphysical properties. While the additional two datasets show the same general IWC-temperature distribution, a comparison of the three datasets together highlights that the IWC values in the lower temperature range as observed during MACPEX are larger than what is expected. The IWC distribution in the Krämer et al. data is more uniform across all temperatures. The MidCiX dataset is also more uniform in the higher temperature range, but contains a “high IWC” feature in the 210 – 220 K range similar to that seen in MACPEX. However, this feature does not appear to be as strong or as large in terms of frequency and IWC, respectively, in MidCiX as in MACPEX.

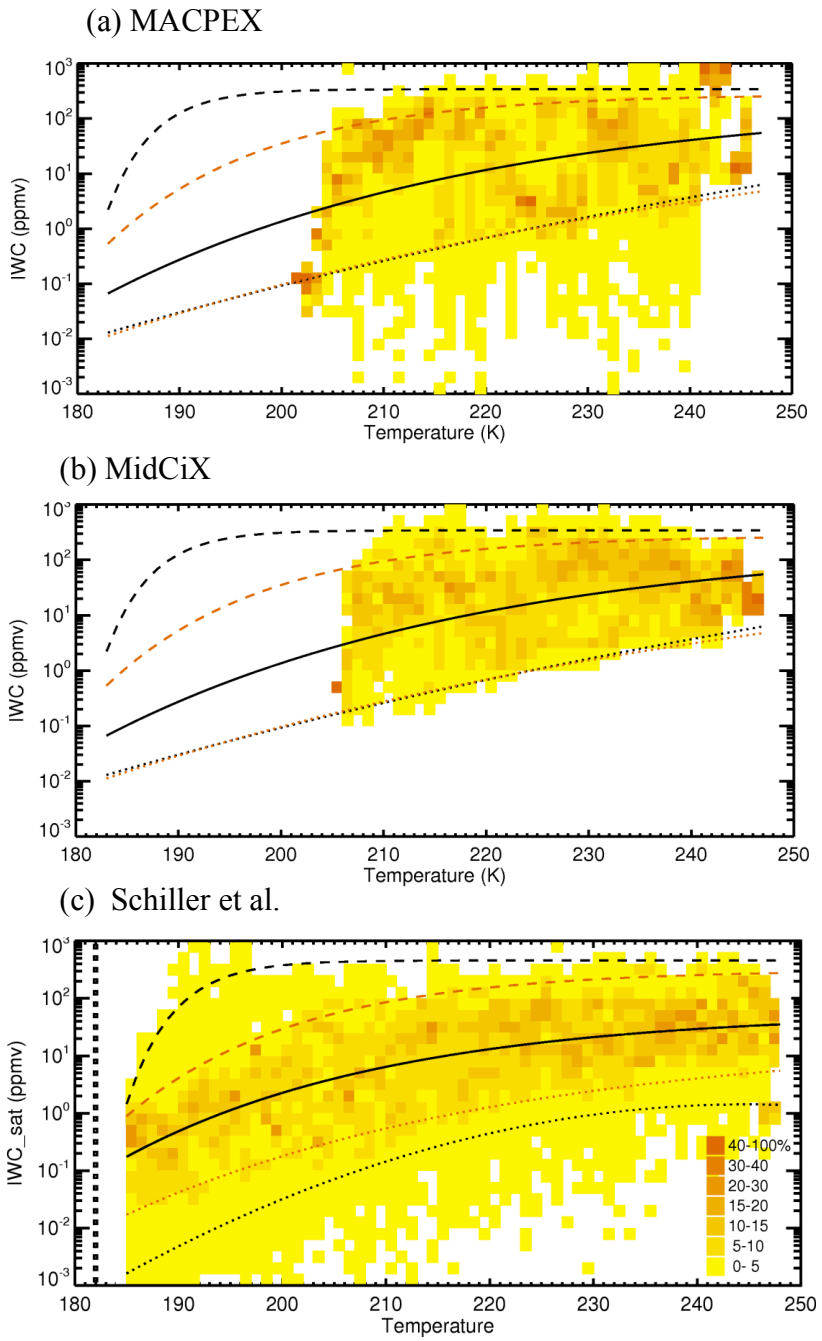

Figure 4.3a – c. (a) MACPEX; (b) MidCiX; (c) data from Schiller et al. IWC as a function of temperature and frequency of observation. The colorbar shown in (c) is consistent for all panels in this figure. The black solid, dashed and dotted lines represent median, maximum, and minimum IWC, respectively. The median line in (c) is from Schiller et al. (2008). The median lines in (a) and (b) are from the analysis in Chapter 3. The red dashed and dotted lines denote a core region demonstrating where IWC-temperature pairs represent the most frequent (> 5%) observations as described by Schiller et al. (2008).

Differences in Weather

A closer look at the flights during the two campaigns reveals that they did not sample cirrus clouds from the same distribution of weather patterns. The timing of these experiments is interesting given that they occur during midspring when the midlatitude storm track is weakening and convective events become more prevalent (Mace et al., 2006). Except for two cases in MACPEX, the synoptic conditions for each science flight were obvious from the project scientists' daily flight reports. During MACPEX, five cirrus systems were sampled that were associated with convective outflow, while three other flights were made to collect data from cirrus connected to the subtropical jet stream. In MidCiX, the distribution of cases is more varied. There is one flight exploring cirrus resulting from convection, one from the polar jet stream, one from the subtropical jet stream, three flights investigating cirrus associated with cutoff subtropical low pressure systems, and one flight looking at mountain wave cirrus clouds. This information is summarized in Table 4.1. Given the different range of synoptic cases sampled, it seems reasonable to infer that some of the differences in the IWC-Temperature relationships in the two aircraft campaigns could be explained by these different environments.

Additionally, it is worth noting that the data used by Schiller et al. is primarily from observations made in Europe. European dynamics are largely dominated by frontal systems, whereas convective events, like those commonly found in the U.S., are unusual. Therefore, it is not surprising that the IWC values from the Schiller et al. observations are low, given that they are generally the result of lower vertical velocity dynamics. This is expanded upon further in Chapter 5.

Table 4.1. Description of Synoptic Conditions Sampled During Each Flight

Campaign	Flight date	Synoptic Case
MACPEX	7 April 2011	Convective Outflow
	11 April 2011	Convective Outflow
	13 April 2011	Subtropical Jet Stream
	14 April 2011	Subtropical Jet Stream
	16 April 2011	Subtropical Jet Stream
	21 April 2011	Convective Outflow
	23 April 2011	Convective Outflow
	25 April 2011	Convective Outflow
MidCiX	19 April 2004	Subtropical Jet Stream
	22 April 2004	Cutoff Low Pressure System
	27 April 2004	Cutoff Low Pressure System
	30 April 2004	Convective Outflow
	2 May 2004	Polar Jet Stream
	5 May 2004	Mountain Wave
	6 May 2004	Cutoff Low Pressure System

Table 4.1. The synoptic case for each of the flights listed here could be clearly determined from daily flight reports. Flights for which the synoptic case was not clear were not included.

4.3 Cirrus Cloud Case Studies

4.3.1 Subtropical Jet Stream

Previous research has illuminated the fact that cirrus clouds are very often found to be associated with either the polar or subtropical jet stream. In this section of the analysis, I will focus on cirrus resulting from the subtropical jet stream since it appears in both campaigns. Given that the majority of the flights occurred over the southern part of the United States, it is

not surprising that the subtropical jet stream would be encountered. Observations from three cases - 19 April 2004 and 13 and 16 April, 2011 - are shown here.

Figure 4.4a-c shows the IWC observations from the CLH instrument as a function of temperature and includes information on the frequency of the observation (in the same format used in Fig. 4.3). Once again, the fit lines can be used as guidelines for comparing the plots. Starting with the flight from MidCiX on 19 April 2004 (Fig. 4.4a), the high frequency measurements are distributed evenly between the median and maximum fit lines. It should be noted that the data at temperatures greater than approximately 215 K are sparse for this flight and therefore not representative, despite being coded as high frequency. The two flights from MACPEX show different behavior from those observed in MidCiX and also from each other (Figs. 4.4b and c). The flight on 13 April yielded higher IWC values (close to the maximum core fit line) at high frequencies for most of the temperature range sampled. On the other hand, the 16 April flight mostly returned high frequency observations at the minimum fit line.

As suggested by the results in Chapter 3, it is also important to look at the ice crystals themselves for clues as to why the IWC observations are configured in a particular distribution pattern. Comparing the ice crystal concentrations also reveals that there are differences between the two campaigns. Ni fit lines from Krämer et al. (2009) demonstrate the maximum, middle, and minimum values and can be used as reference points to compare the different cases. Shown in Fig. 4.4d, the Ni observations during the 19 April MidCiX flight are generally around and above the middle fit line. In this case, the Ni measurements are consistent with the information provided by the IWC distributions. The two MACPEX cases, seen in Figs. 4.4e and f, both show that the observed Ni were generally below the middle line, but the results in Fig. 4.4e are at slightly larger Ni values than those shown in Fig. 4.4f. Given the difference in IWC between the

two MACPEX flights, this is expected. However, it is interesting that this relationship does not exist when comparing the MidCiX case to the 13 April MACPEX case, since there is a difference in the IWC values there as well.

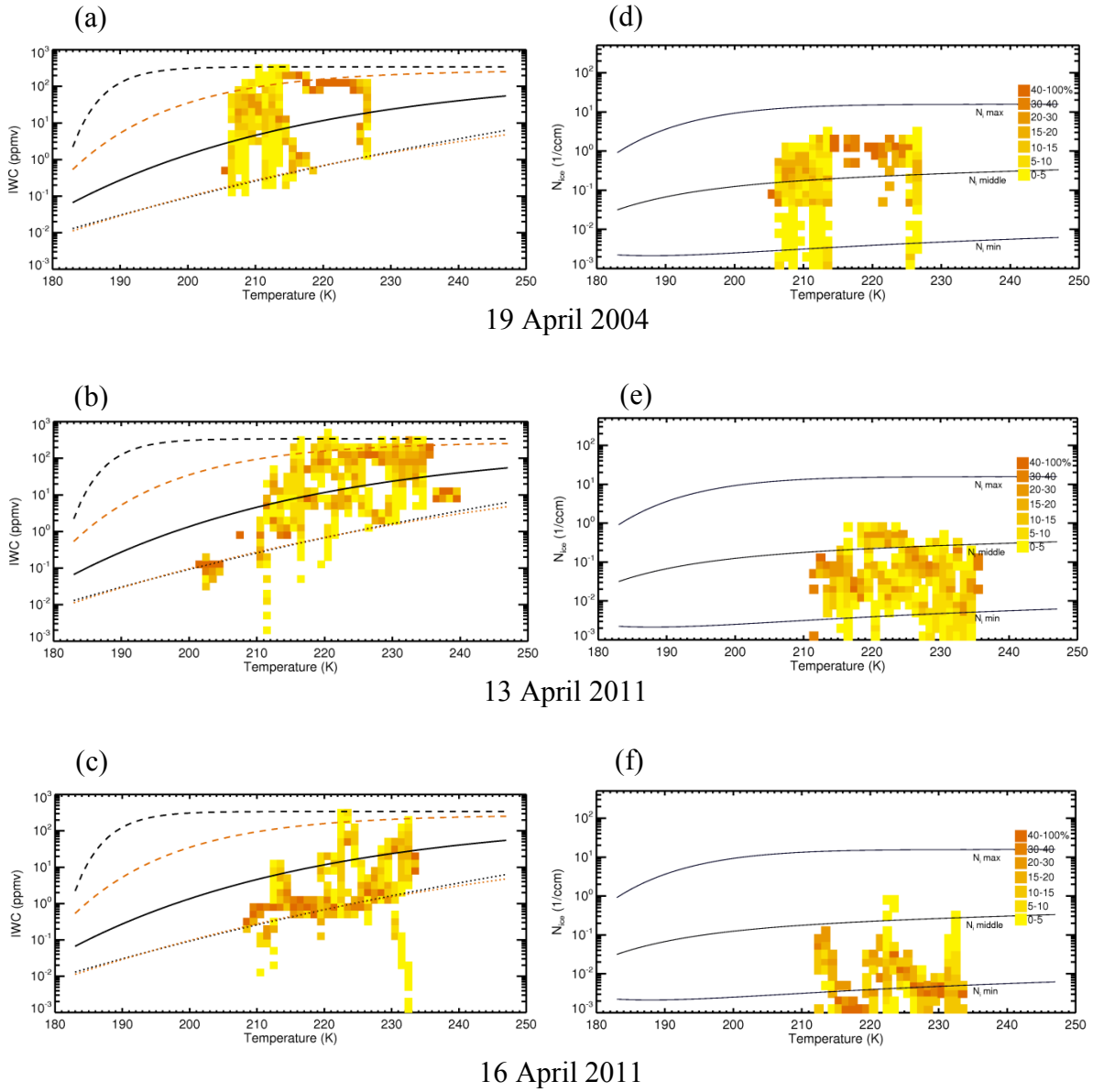

Figure 4.4a – f. Subtropical jet stream cirrus cases. Left column: IWC as a function of temperature and frequency of observation. Right column: Ni as a function of temperature and frequency of observation for ice crystals > 15μm in diameter. The colorbars seen in the Ni plots are consistent for all panels in this figure. The fit lines in the IWC plots are consistent with those seen in Fig. 4.3. The fit lines in the Ni plots come from the analysis of Krämer et al. (2009).

4.3.2 Cirrus from Convective Outflow

The second mechanism common to both the MidCiX and MACPEX campaigns is cirrus production through convection. This mechanism was frequently noted in the Introduction of this chapter to produce cirrus cloud systems. There is a single convective case from MidCiX, on 30 April 2004 and, as noted previously, there are five convective cases from the MACPEX dataset, but only two of them are shown here. These two were selected to demonstrate the differences between aged anvil cirrus, seen in the 7 April 2011 case, and fresh convection, seen in the 23 April 2011 case.

The IWC distribution for the MidCiX case shows that the high frequency measurements are positioned directly between the median and maximum fit lines (see Fig. 4.5a). For the two MACPEX cases, respectively, the aged outflow case (Fig. 4.5b) is represented by an IWC distribution where the higher frequency measurements are largely below the median and near the minimum line. In general, however, there is a large variation of IWC values covered. The fresh anvil cirrus (Fig. 4.5c) on the other hand is represented by high frequency IWC values at the maximum core value fit line and an IWC distribution with less variation.

The Ni observations in Fig. 4.5d – f show that the ice crystals sampled in the MidCiX case are just above the middle values and appear to follow the Ni-temperature relationship indicated by the minimum/middle/maximum lines. Though the two MACPEX cases were observed at different temperature ranges, the Ni distributions follow the same relationship just below the middle fit line. This is an interesting and potentially useful result considering the differences in the IWC measurements from these two flights.

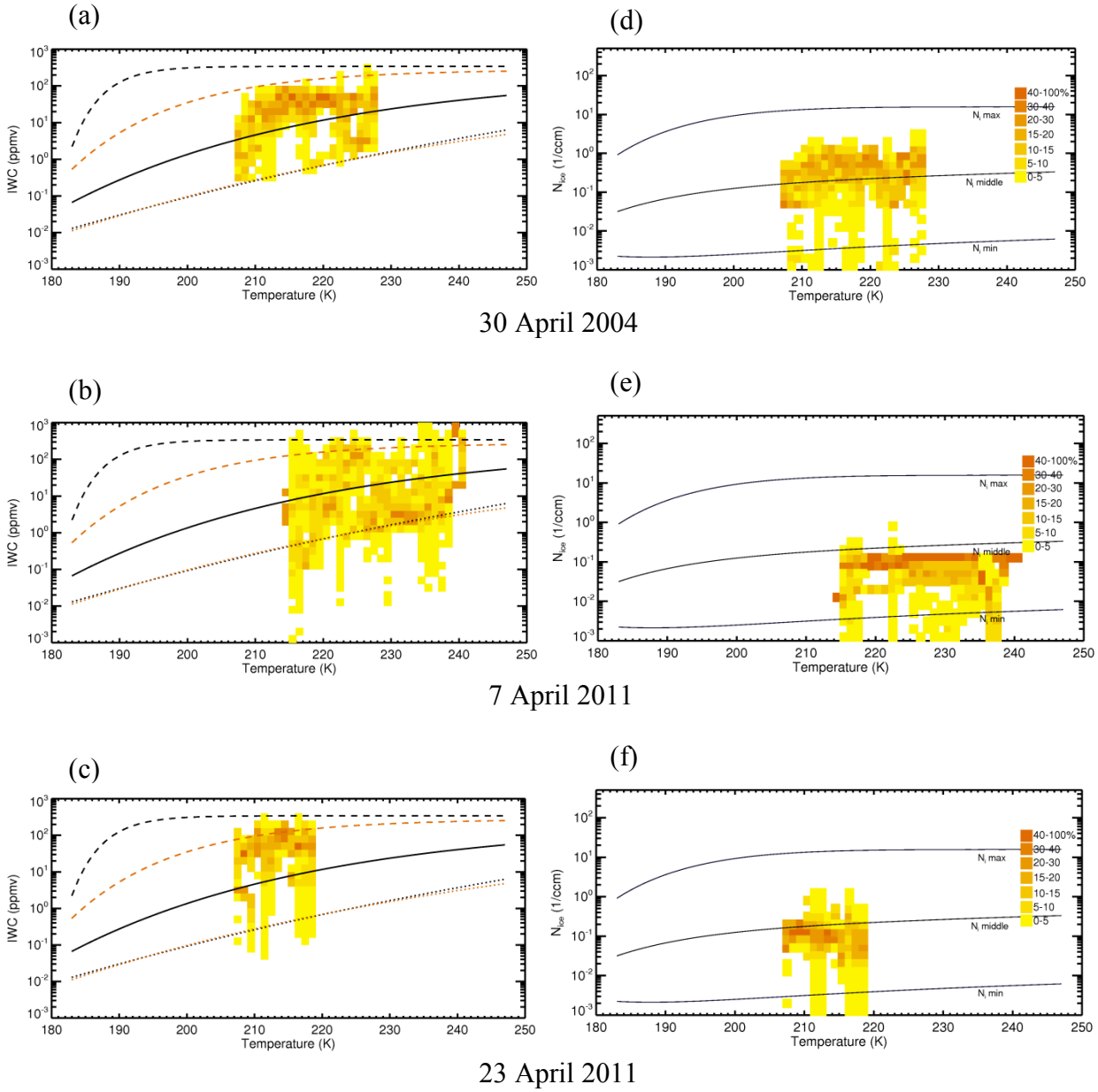

Figure 4.5a – f. Convective cirrus cases. Left column: IWC as a function of temperature and frequency of observation. Right column: Ni as a function of temperature and frequency of observation for ice crystals > 15μm in diameter. The colorbars seen in the Ni plots are consistent for all panels in this figure. All fit lines are the same as those seen in Figure 4.4.

4.3.3 Cutoff Low Pressure System

Though it is not mentioned directly in most of the literature as being a primary mechanism for cirrus formation, the closed-off low-pressure system is interesting to look at nevertheless. For instance, as noted in Section 4.1, the vertical velocities found in these systems tend to be high. Also, since it was more prevalent than any other mechanism during MidCiX, it is important that it is included in this analysis to properly represent the MidCiX dataset. The two cases shown here took place on 22 and 27 April 2004.

In the case of the 22 April flight shown in Fig. 4.6a, the IWC distribution clearly displays the expected IWC-temperature relationship - increasing IWC as temperature increases. The distribution of high frequency measurements are mostly around the median fit line. The case on 6 May (not shown here), displayed the same distribution but at lower temperatures. The 27 April case (Fig. 4.6b) displays high frequency observations that are above the median fit line and either at or above the maximum core boundary.

The Ni observations in each case are reflective of the IWC observations and can be seen in Figures 4.6c and d. The Ni distribution for the 22 April case is around the middle Ni line while the distribution for the 27 April case is above the middle line for most of the temperature range. However, the high frequency observations in the 27 April case decrease with temperature instead of increasing with temperature as the fit lines suggest.

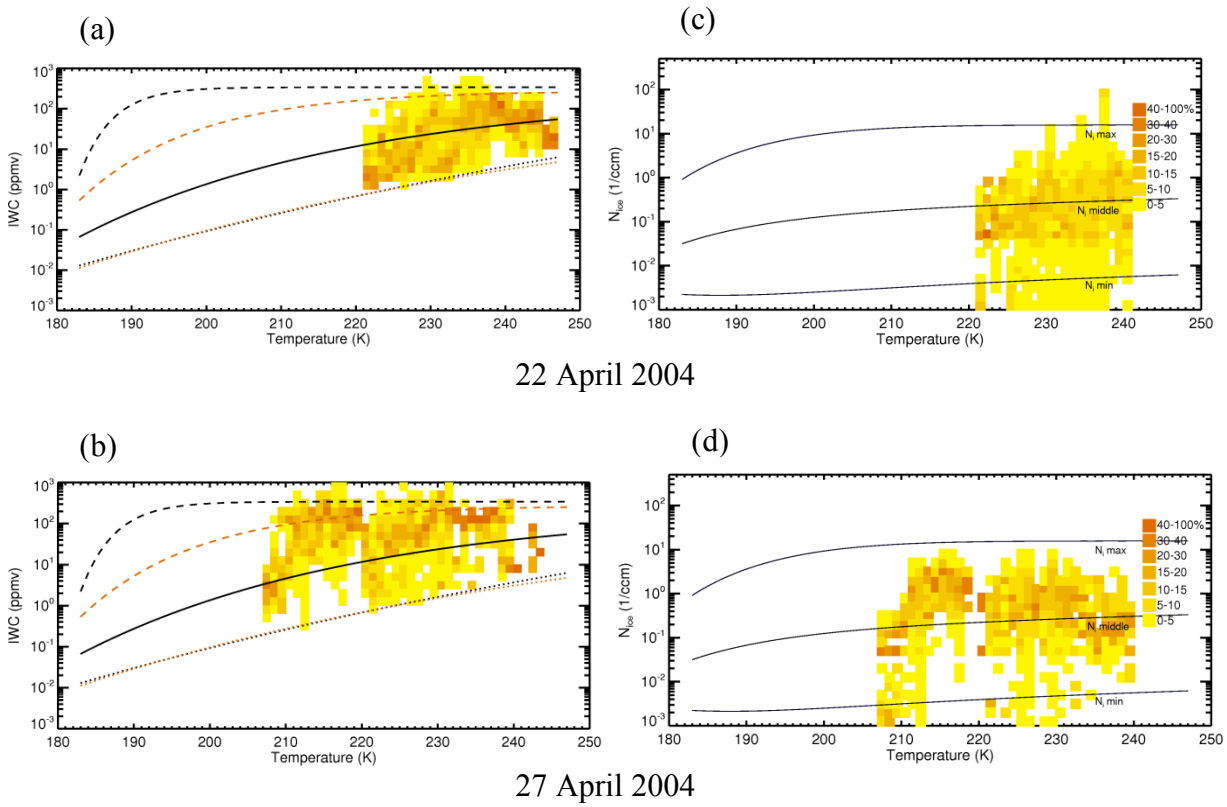

Figure 4.6a – d. Cutoff low pressure system cirrus case. Left column: IWC as a function of temperature and frequency of observation. Right column: Ni as a function of temperature and frequency of observation for ice crystals > 15μm in diameter. The colorbars seen in the Ni plots are consistent for all panels in this figure. All fit lines are the same as those seen in Figures 4.4 and 4.5.

Some of the relationships between IWC, Ni, and the synoptic conditions that were demonstrated in this section are consistent with what was expected – mechanisms known to involve strong uplift display high IWC and high Ni values and vice versa. However, observations from some flights, such as the 7 April 2011 flight from MACPEX, did not exhibit these characteristics, indicating that the relationships depend on more than vertical velocity. The next section (Section 4.4) refines this analysis further by including more specific details on the larger-scale dynamics. Additionally, for the reader's reference, Table 4.2 includes a qualitative and quantitative summary of the results from Section 4.3.

Table 4.2. Summary of Results Presented in Section 4.3.

Synoptic Case	Campaign	Flight date	IWC Observations (ppmv)	Ni Observations (cm^{-3})
Subtropical Jet Stream	MidCiX	19 April 2004	3 – 50 (median – maximum)	0.05 – 1 (middle)
	MACPEX	13 April 2011	20 – 200 (maximum)	0.05 – 0.5 (below middle)
		16 April 2011	0.4 – 2 (minimum)	0.001 – 0.03 (minimum)
Convective Outflow	MidCiX	30 April 2004	20 – 100 (above median)	0.04 – 1 (above middle)
	MACPEX	7 April 2011	2 – 20 (minimum – median)	0.02 – 0.2 (below middle)
		23 April 2011	30 – 200 (maximum)	0.03 – 0.2 (below middle)
Cutoff Low Pressure System	MidCiX	22 April 2004	2 – 200 (median – maximum)	0.04 – 1 (middle)
		27 April 2004	20 – 200 (median – maximum)	0.1 – 3 (above middle)

Table 4.2. The qualitative descriptions of each IWC and Ni distribution are based on the placement of the highest frequency of measurements relative to the fit lines in their respective figures. The quantitative descriptions are rough estimates of the range of values covered by the higher frequency observations. Ni observations are for ice crystals > 15μm in diameter.

4.4 The Large Scale Influence

The observations from each of the cases presented here make it clear that there are observable differences in IWC and Ni between synoptic situations and also within synoptic types, confirming that the synoptic-scale dynamics have some influence on the resulting microphysical properties. Given the size and duration of the datasets mentioned here, it would be misleading to offer any statistics concerning the frequency of cirrus clouds and the related synoptic conditions that produced those clouds. A dataset obtained on a longer timescale would be necessary to complete such a task. However, it can be pointed out that there is a difference between the types of synoptic conditions sampled between the MidCiX and MACPEX

campaigns. Though cirrus in similar synoptic types were sampled during each experiment, the MACPEX campaign is more representative of cirrus clouds resulting from convective systems whereas the MidCiX dataset is comprised of a mixture of cases with low pressure systems being the most represented case. As noted previously, the fact that these measurements took place during the springtime means that it is reasonable to assume that any and all of the synoptic cases may be observed, but that depending on the dynamics of the atmosphere that year, one case type may be more dominant than the others. It appears that during MidCiX the midlatitude storm tracks were still in place, but that during MACPEX they had weakened and convective storms were becoming more prevalent.

The body of literature discussed in Sect. 4.1 indicated that though jet stream cirrus clouds are extensively observed, they can contain some of the weakest uplift dynamics, particularly among the meteorological case types analyzed here. Thus, it would be reasonable to expect that the IWC values observed in these cases would be smaller than those observed in the more convective cases. However, the results of the analysis show that this is not necessarily the case.

There are also flights that produced very different looking results between synoptic cases and within synoptic case types. A closer look at the details of the synoptic conditions present during each flight may provide some answers as to why that is. Maps produced from archived meteorological data using the tools provided by the Plymouth State Weather Center (http://vortex.plymouth.edu/u-make.html) provide clues as to what conditions may have been like in the vicinity of the sampled clouds. This same archive also hosts infrared satellite images from the GOES satellites that can provide some confirmation as to the presence of the cirrus and the location of the associated weather system.

Starting with the subtropical jet stream cases (Section 4.3.1), it is very clear that the location of the cirrus relative to the jet stream is extremely important for determining the IWC values observed in the cirrus clouds. During the 19 April flight case, the cirrus that was sampled was located around the SGP ARM site near Norman, Oklahoma. Around the time of the measurements, the 300 mb map of geopotential heights and wind velocities, shown in Fig. 4.7a, indicates a strong jet streak located to the northeast, putting the site at the lower left entrance of the jet, which is an area of upper level divergence. Thus, it could be concluded that this area is particularly good for the uplift contributing to water transport and air parcel cooling needed for cirrus development, which is consistent with the median value IWC and Ni distributions. The 13 April MACPEX flight took place in west Texas just south of the jet core maximum as seen on the 300 mb map (Fig. 4.7b), also placing the area of observation in the lower left quadrant. There is also evidence of a shortwave trough moving through the area that could potentially contribute additional uplift. The high IWC values are consistent with these conditions, but the Ni values are unexpectedly low. The 16 April MACPEX flight provides a different scenario. The flight took place on the Texas coastline along the Gulf of Mexico. It was noted in the flight reports that the cirrus clouds were thin and patchy, which is consistent with the observations of quite low IWC and Ni values. The 300 mb map in Fig. 4.7c reveals that around the time of the observations, the jet core was further to the north and the location of the observations was on the upstream side of a longwave trough, which is indicative of drying and descending air.

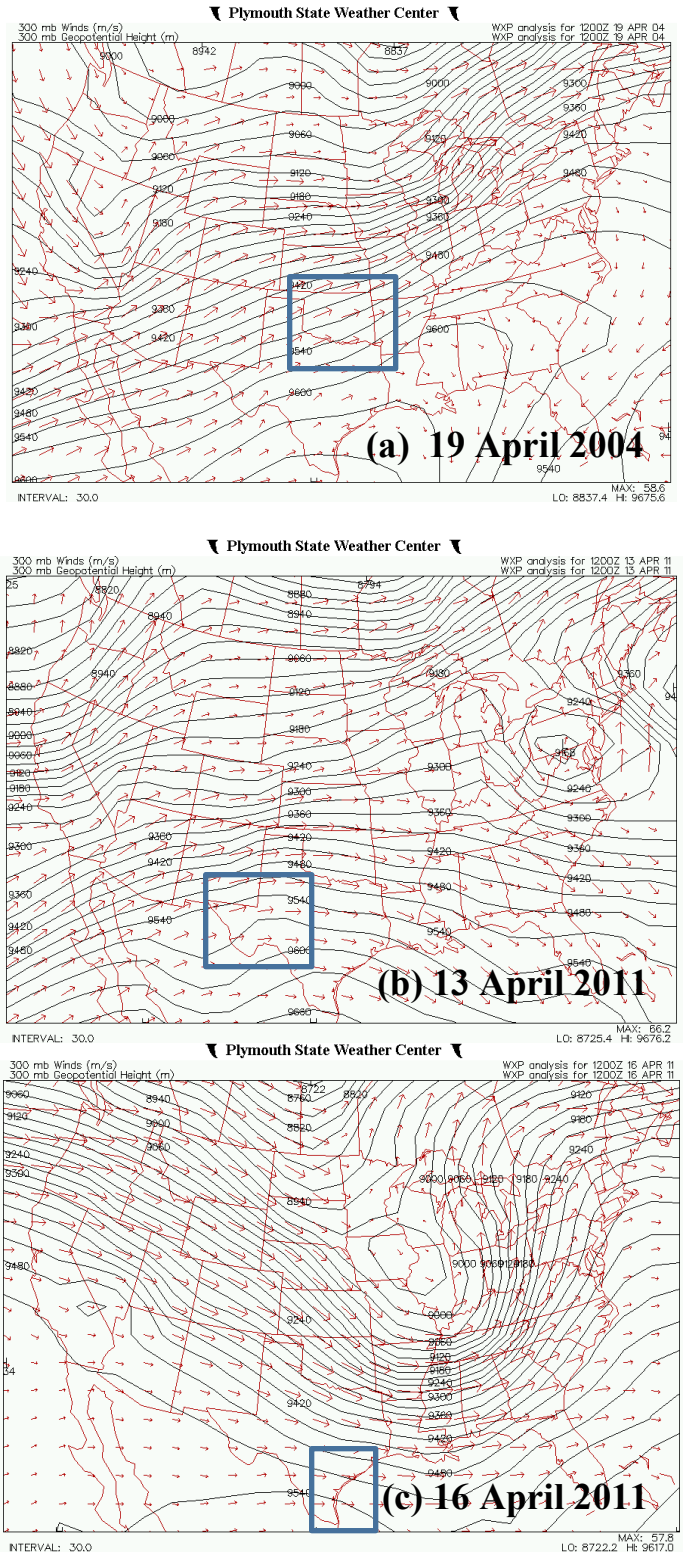

Figure 4.7a – c. Subtropical jet stream cirrus cases. 300mb maps of geopotential height and wind velocity at 12Z, before the flights. The blue boxes indicate the area of interest for each flight.

The convective cases presented in this analysis (Section 4.3.2) all differed from one another. The 7 April case from MACPEX demonstrated the results of what was noted to be an aged convective outflow in the Arkansas and Missouri area. Close to the time of the observations, the 300 mb weather map in Fig. 4.8a reveals that there is nothing synoptically significant happening in that area that would lead to ascending or descending air. The area of interest lies within the jet stream, but it is not clear if that feature provides any influence. From the satellite information (not shown here), it appears that after the convective event, the cirrus that was produced thinned and then disappeared. With that in mind, it seems likely that the clouds were sampled during a period of dissipation. The 30 April case from MidCiX yielded IWC measurements that were closer to median values. This cirrus system was also aged convective cirrus. The reason for the higher IWC values could be explained by the fact that the 300 mb weather map in Fig. 4.8b shows short wave disturbances moving through the area that may be providing the dynamics necessary to sustain the cirrus for a longer period of time. Lastly, the 23 April MACPEX case revealed very high IWC values when sampling new anvil cirrus outflow from a storm in the northeast part of Texas. At this time, the 300 mb weather map in Fig. 4.8c shows that several shortwave disturbances were present and unlike the other cases, surface level humidity values (not shown here) indicate that the area of interest was located along the dryline, which is a common feature associated with strong, convective storms.

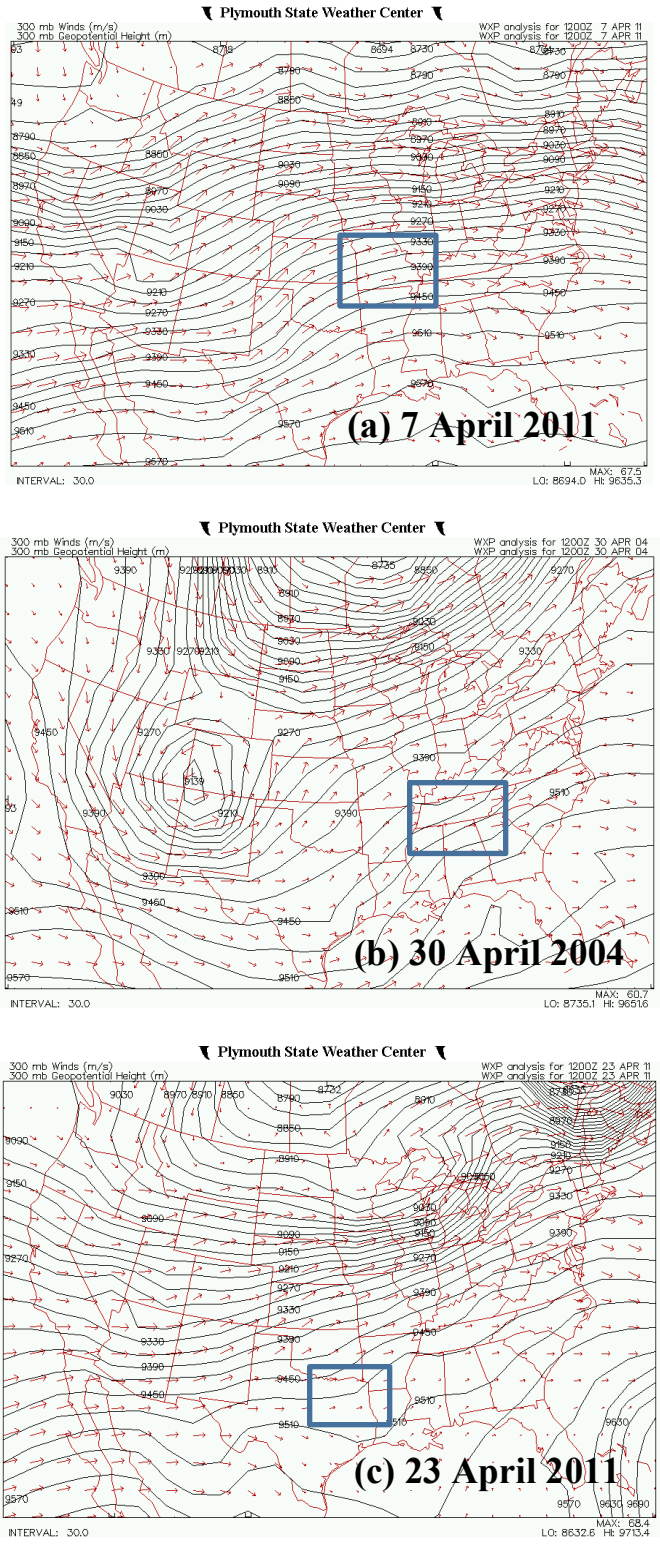

Figure 4.8a – c. Convective cirrus cases. 300mb maps of geopotential height and wind velocity at 12Z, before the flights. The blue boxes indicate the area of interest for each flight.

Though they are not shown here, it should be noted that the other convective cases observed during the MACPEX campaign are similar to those presented here. The flights on 21 and 25 of April are also fresh anvil cirrus cases and have IWC values that resemble the 23 April case. The flight on 11 April is combination of aged and new convective cirrus cloud systems and yields results that are between the median line and the maximum core value. Thus, it seems reasonable to conclude that the high IWC values observed in the overall MACPEX dataset are largely the result of the convective samples.

Another interesting feature of the convective cases from MACPEX is that the behavior observed in IWC values is not reflected in the Ni values. As noted in Sect. 4.3.2, despite the difference in the IWC distributions between the 7 and 23 April flights, the Ni observations are quite similar. In fact, all of the MACPEX convective flights yield lower-than-middle level Ni results. The next section includes a brief discussion of this point, but it is more thoroughly explored in the next chapter.

Lastly, the closed low pressure system cases that were observed also yielded different results that can be connected to the synoptic conditions in which they were observed. Both flights sampled cirrus resulting from closed low pressure systems located near the eastern Pacific and Mexico. It was noted in Sect. 4.1 that these systems can contain quite strong uplift mechanisms that produce vertical velocities equivalent to those observed in convective systems, so it is not surprising that the IWC observations are similar in magnitude to those observed in the convective cases. It also explains why the MidCiX dataset yields high IWC values despite being underrepresented by convective cases in comparison to MACPEX. The difference between these two flights comes from the location of the measurements relative to the low pressure

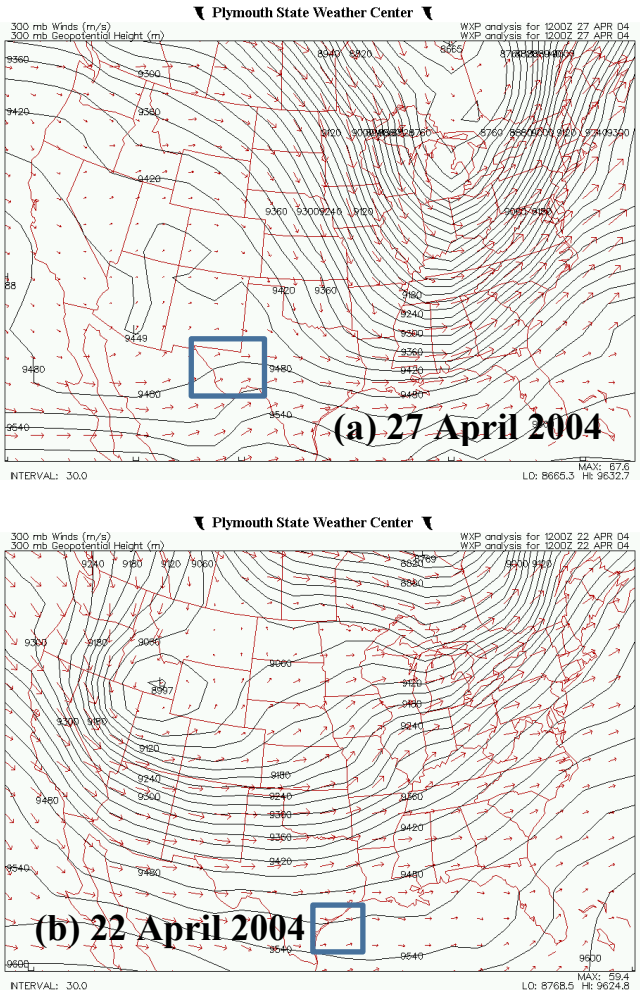

Figure 4.9a and b. Cutoff Low Pressure System. 300mb maps of geopotential height and wind velocity at 12Z, before the flights. The blue boxes indicate the area of interest for each flight.

system. In the 27 April case, which has the higher IWC values, the observations were made quite close to the system (see Fig. 4.9a for 300 mb map). In the flight report, this system was noted to be quite strong and the cirrus appeared thick. In comparison, the 22 April flight sampled the cirrus clouds in a location that was removed from the actual low pressure system, which was located in the eastern Pacific. A 12Z 300 mb map in Fig. 4.9b reveal that small disturbances moved through the area that may have sustained the cirrus. A third case, not shown here, was similarly observed at a location removed from the low pressure system and yielded

similar results. The Ni observations are a good reflection of the IWC observations in each of these cases.

4.4.1 Vertical Velocity

The discussion concerning the influence of synoptic scale conditions on the microphysical properties reveals that there is a connection between the two. It is clear that even within a single case type, differences in the conditions have an impact. They also provide some context in terms of an explanation as to why two seemingly similar datasets would present with differing results. However, it is clear that this qualitative explanation cannot explain the full picture alone.

One factor that is known to have an influence on the microphysical properties of cirrus clouds is the vertical velocity, which affects the nucleation mechanism responsible for producing the cirrus ice crystals (Jensen et al., 2013; Kärcher and Ström, 2003; Krämer et al., 2009; Spichtinger and Krämer, 2013; and references therein). Generally, the higher vertical velocities lead to larger IWC and Ni values. This concept is explained and explored in greater detail in Chapter 5. With this idea in mind, it is expected that the cases with higher vertical velocities would then show IWC and Ni values that are consistent with those conditions.

Figures 4.10a and b show the distributions of measured vertical velocity as a function of temperature and the frequency of those observations for MACPEX and MidCiX, respectively. As explained in Chapter 2, only level flight legs are used in analyses involving vertical velocity. By looking at the highest frequency measurements, the observations in MACPEX demonstrate that as temperature increases, so does vertical velocity for temperatures greater than ~ 220 K. Thus, if temperature is used as a gauge to measure altitude, higher vertical velocities are found at low altitudes and vice versa. The exception to this rule can be seen at approximately 210K

where high vertical velocity values were frequently observed. This could be attributed to waves at high altitudes, but is more likely to be the result of convection. Given the tower-like structure of convective storms and the very high vertical velocities, this result is not surprising. Due to the fact that only a subset of data can be used for this portion of the analysis, the MidCiX dataset became more sparsely populated after applying the procedure for isolating level flight legs of appropriate duration and the vertical velocity relationship to temperature/altitude cannot be visualized.

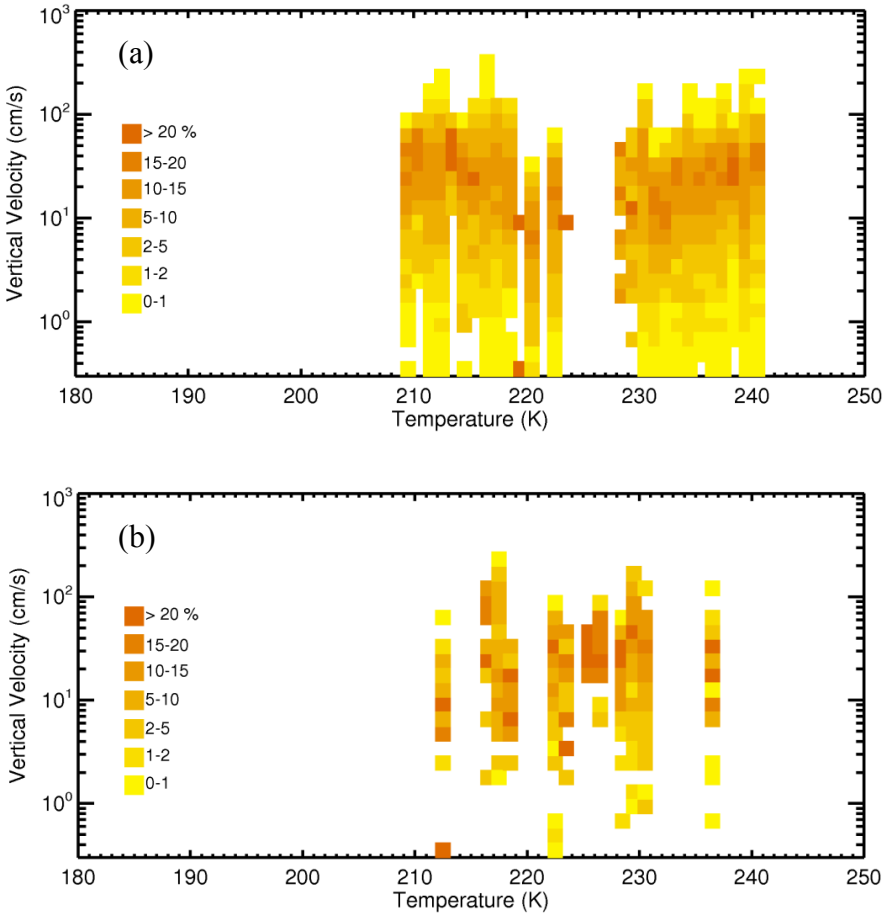

Figure 4.10a and b. Vertical velocity as a function of temperature and frequency of observation. Top panel: MACPEX. Bottom panel: MidCiX.

Another conclusion that can be drawn from these plots is the correlation between the high vertical velocities and the high IWC values. This is evident when comparing Fig. 4.10 (a and b) to Fig. 4.3 (a and b) for both campaigns.

Figure 4.11 shows a PDF of the vertical velocity distribution for each campaign. Generally, the two distributions are not that dissimilar from one another and both peak around the same vertical velocity value of 30 cm s^{-1}. Interestingly, the distribution from the MidCiX observations is broader with an obvious tail and a second, smaller peak around 120 cm s^{-1}. This feature does not exist in the MACPEX dataset. Given the prevalence of convective events in the MACPEX dataset, it seems reasonable to expect that the higher vertical velocity values would have been sampled in that campaign instead of MidCiX.

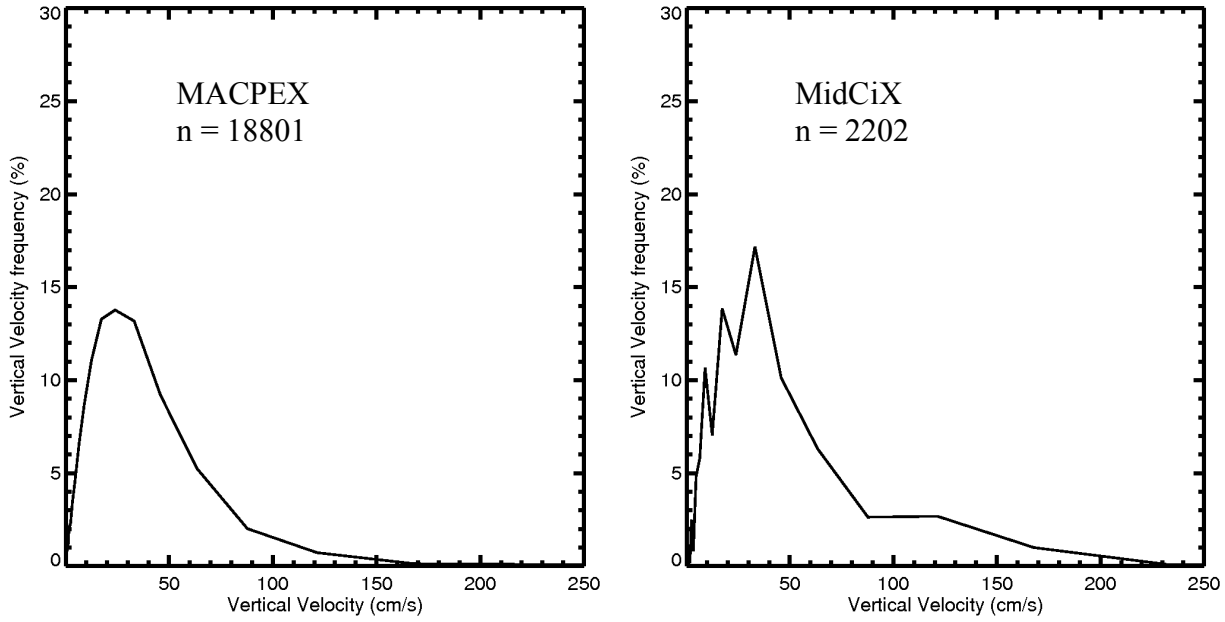

Figure 4.11. Frequency of vertical velocity observation as a function of vertical velocity. Left panel: MACPEX. Right panel: MidCiX.

By breaking down the vertical velocity distributions into the flight cases analyzed here, it can be determined which cases contributed the largest vertical velocity values and continue to explore how the conditions in each case are reflected by the observed IWC and Ni values. Figure 4.12a - h presents the results from the each of the flights. The top row of figures (Fig. 4.12a – c) represents the results from the subtropical jet stream cases. The 19 April MidCiX case and the 13 April MACPEX case have similar looking distributions in terms of the peak location near 30 cm s^{-1} and the fact that both have a tail extending past 100 cm s^{-1}. The tail on the 13 April case extends out to ~170 cm s^{-1}. The 16 April MACPEX case yields a much narrower distribution with a lower peak closer to 20 cm s^{-1}. These results are consistent with the observed IWC values and demonstrates that the higher vertical velocity values correspond to the higher IWC values.

The middle row of plots (Fig. 4.12d – f) represents the results from the cirrus clouds produced by convective systems. In comparison to the subtropical jet stream vertical velocities, the peak values and the broadness of the distributions are not much different. The broadest distribution comes from the MACPEX flight observing fresh anvil outflow on 23 April. Since the other two flight cases sampled aged outflow, it is reasonable that the large vertical velocities that originally produced those cirrus clouds are no longer present. Also, in all cases, it is a normal practice to avoid the most convective regions in these systems for flight safety reasons. Thus, the highest vertical velocities in these systems may not be directly observed even though their effects, such as the high IWC values, can be observed, as seen in the 23 April case. The important part is that convection initially supplied the large amounts of moisture and the rapid cooling that are required for cirrus formation, as described by Mace et al. (2006). The vertical

velocities observed outside the core or after the event has finished can aid in sustaining the cirrus clouds.

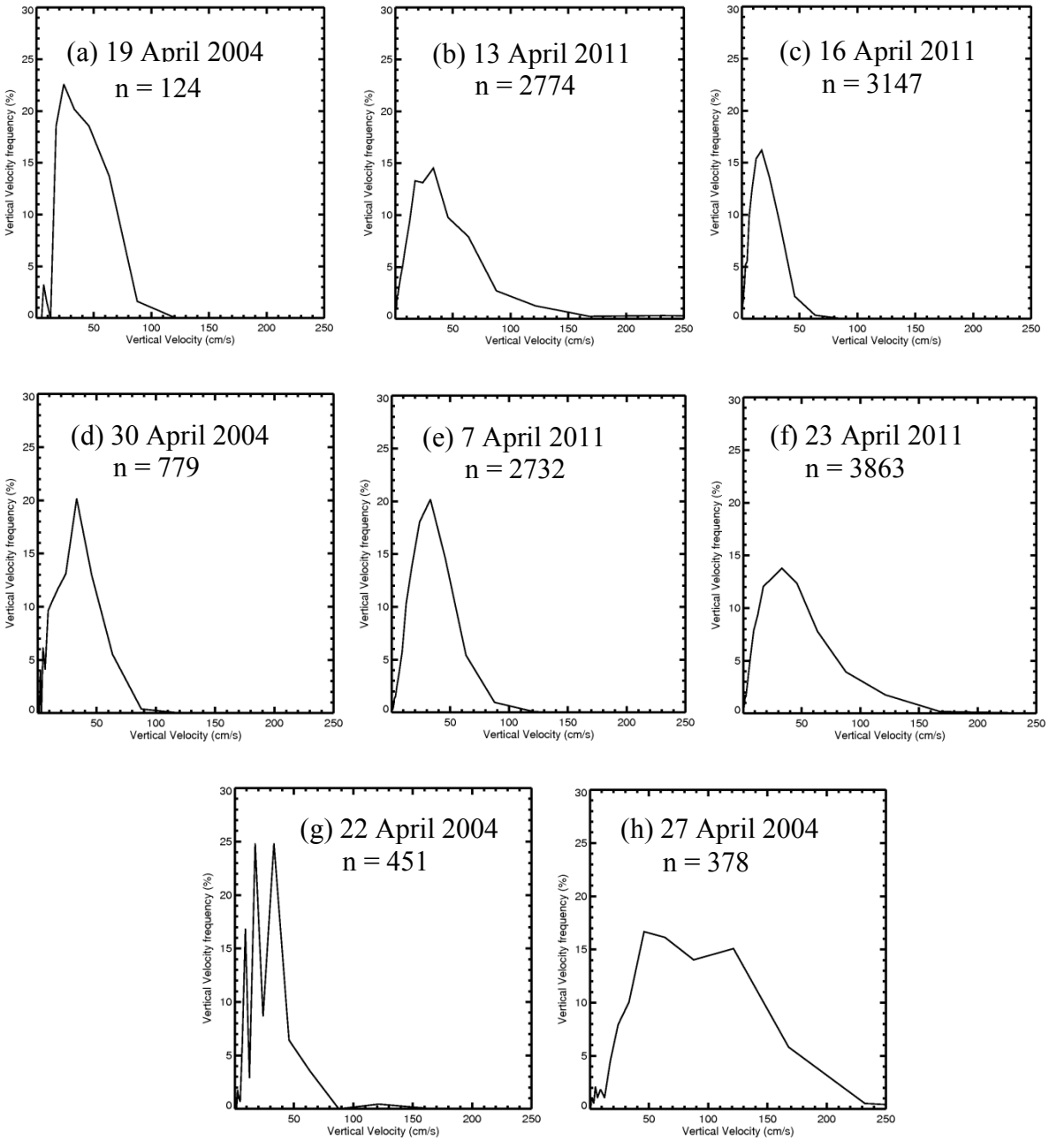

Figure 4.12a – h. PDF of vertical velocity frequency as a function of vertical velocity. Top row: subtropical jet stream cirrus cases. Middle row: Convective cirrus cases. Bottom row: Cutoff low pressure system cirrus cases.

The last row of plots (Fig. 4.12g and h) shows the two MidCiX cases that represent the cutoff low pressure systems. As reported throughout this chapter, this synoptic situation is capable of producing vertical velocity values that are on the same order of magnitude as the convective systems. The first case on 22 April was more removed from the low pressure system, thus it seems reasonable that the observations are similar in nature to those seen in other cases, with a peak value around 30 cm s^{-1}. The second case from 27 April produces results that are quite different from any others presented in this analysis. The distribution has two large peaks at approximately 50 cm s^{-1} and 120 cm s^{-1} as well as a tail extending out to 230 cm s^{-1}. This is by far the broadest of the distributions. It is also worth noting that the highest IWC and Ni observed during MidCiX were observed during this flight. This case provides an excellent example of the relationship between vertical velocity and IWC and Ni.

4.4.2 The Relationship Between Vertical Velocity and Ni

Up to this point, the Ni observations have only been briefly explored. However, throughout the chapter, it has been noted several times that while the Ni observations from the MidCiX campaign are generally a reflection of the IWC observations, the Ni observations from MACPEX do not uphold that same relationship. Instead, in comparison to the MidCiX observations and regardless of the IWC and vertical velocity observations, the Ni observations from MACPEX are almost consistently lower. Thus, given the link between vertical velocity and the nucleation mechanisms at the small scale, it is important to explore that relationship next in order to get a more complete picture. It is clear that it is not enough to assume that high vertical velocities will always result in high IWC and high Ni, and it is too simplistic to tie high IWC and high Ni together. In Chapter 5, these issues are taken into consideration and the results are more fully explored.

4.5 Conclusions

The goal of this chapter is to demonstrate and explore the relationship between large scale dynamics and the microphysical properties of cirrus clouds. This was done using the in situ measurements from two midlatitude airborne campaigns, MACPEX and MidCiX. An intriguing piece to this analysis is that the results from MACPEX differ from those observed in similar campaigns, which was shown in the comparison to the climatology from Krämer et al. and the MidCiX dataset. The similarities between the MACPEX and MidCiX dataset extend as far as the base location, time of year, aircraft, and instrumentation. Thus, it is surprising that they would yield such different results. Using what is known about the synoptic influences on cirrus clouds, I examined these differences more thoroughly.

Beyond the differences revealed by comparing MACPEX and MidCiX, the conclusion from this analysis has three parts. The first part concerns the connection between synoptic scale conditions and the resulting IWC and Ni observations. Consistent with previous results, it is clear that, while differences are likely to exist between synoptic case types, more detailed analysis of the synoptic conditions for each flight provided additional information to show that other disturbances, distance, and time are also influencing the observations. In relation to this point, an analysis of the vertical velocity observations showed that while the distributions between campaigns, case types, and flights may be similar, the microphysical properties may not be. Thus, the second part of the conclusion explains that the relationship between vertical velocity and IWC can be demonstrated. Generally, as vertical velocity increases, so does IWC. However, the differences in vertical velocity between campaigns and also between flights are not enough to explain some of the differences between the observed IWC values. In some cases, particularly the convective ones, this could simply be due to the fact that both time and distance

from active uplift have altered the synoptic conditions, but the results of the initial conditions may still be present.

The final part of the conclusion concerns the relationship between the large scale dynamics and Ni. As evidenced throughout the chapter, the relationship between the dynamics and IWC was demonstrable. The relationship between the large scale dynamics and Ni, however, is more complicated. In the case of the MidCiX results, the Ni observations are generally a reflection of the IWC observations. In other words, when the IWC values are high, the Ni values are high too. This is not the case in the MACPEX observations. Instead, the Ni observations are generally low regardless of the IWC observations. This fact did not change much between synoptic cases or as a function of vertical velocity. Generally, low Ni values are indicative of heterogeneous nucleation resulting from lower vertical velocities. They are also typically associated with low IWC values. Thus, by looking at the smaller scale and at nucleation dynamics, a more thorough and correct conclusion may be determined. At this point, it is only fair to say that while vertical velocity and synoptic dynamics have an influence, they cannot provide a complete picture.

Chapter 5 The Influence of Vertical Velocity and Ice Nuclei on Cirrus Microphysical Properties

5.1 Introduction

The previous chapter began an investigation into the relationship between large scale dynamics and microphysical properties. It was established that the distribution of IWC changes with synoptic conditions, including the strength of the vertical velocity. It was noted throughout the chapter that there was some evidence in the observations that Ni had a similar relationship, but this was more difficult to visualize. Also, the differences between the MACPEX and MidCiX datasets in terms of their Ni observations could not be completely explained by large scale dynamics alone.

As Section 4.1 and the following literature review show, the processes that lead up to and occur during ice nucleation have been extensively studied. Recent studies conclude that not only is vertical velocity important in forming and maintaining cirrus clouds, but it is also the most important factor controlling the mechanism(s) by which these ice clouds form. It has been shown that vertical velocity is highly influential in determining whether homogeneous freezing will occur, and is therefore a major component in determining the dominance of either homogeneous or heterogeneous ice nucleation. In any event, both mechanisms should be considered in any analysis of microphysical properties.

Kärcher and Ström (2003) discuss the importance of vertical velocity and atmospheric waves in homogeneous nucleation. Using observations from the midlatitude aircraft campaign

INCA (Interhemispheric Differences in Cirrus Properties from Anthropogenic Emissions), they compared ice crystal concentrations in cirrus clouds in both the northern and southern hemispheres. Their results show that large upward vertical velocities are often associated with large ice crystal concentrations, which is the result of homogeneous freezing. For young cirrus, vertical velocities of 10 – 100 cm s^{-1} were found to produce large ice crystal number densities (0.1 – 10 cm^{-3}), while a second mode of larger, but fewer, crystals (< 0.1 cm^{-3}) was associated with lower vertical velocities. However, Kärcher and Ström performed further modeling analysis, which showed that additional processes should also be considered. For example, in order to reproduce the lower ice crystal concentrations observed in the particle distribution, sedimentation and heterogeneous freezing must be considered in addition to homogeneous freezing, particularly for regions of lower updraft speeds.

The modeling study of Spichtinger and Krämer (2013) echoes the conclusions reached by Kärcher and Ström. Their work focused on cirrus clouds and dynamics found at the tropical tropopause instead of in the midlatitudes. Briefly, their modeling scheme includes nucleation (homogeneous and heterogeneous), growth by diffusion, sedimentation, and evaporation processes. In addition, they compared their results to ice crystal concentration measurements reported in Krämer et al. (2009). A series of model simulations was run using both slow and fast updraft regimes ($\leq$ 1 cm s^{-1} and > 1 cm s^{-1}, respectively) and using high and low frequency gravity waves. Ultimately, the authors' goal was to uncover the mechanism responsible for producing the low ice crystal concentrations that had been observed in supersaturated conditions. Previous research had suggested that homogeneous nucleation was the dominant formation mechanism for these clouds, but could not explain the supersaturation anomaly. Their findings showed that a combination of slow and fast updrafts, as well as a combination of homogeneous

and heterogeneous nucleation processes, was needed to reproduce the observations, as shown in Fig. 5.1. Approximately 80% of the measured cirrus ice crystal population could be explained by homogeneous nucleation, while the other 20% required the combination of processes. The low Ni values were likely to be caused by heterogeneous nucleation alone, while secondary homogeneous nucleation events were shown to be responsible for producing the less frequent, but larger, ice crystal concentrations. Additionally, Spichtinger and Krämer found that, during homogeneous nucleation, high frequency short waves can stunt ice crystal nucleation, while low frequency waves can promote it. This study demonstrates the importance of dynamics in cirrus formation and how their variance can affect the contribution of the different nucleation mechanisms to observed quantities. While the specifics of these results are only applicable to tropical tropopause cirrus clouds and the supporting dynamics, the concepts remain pertinent to cirrus formation in general.

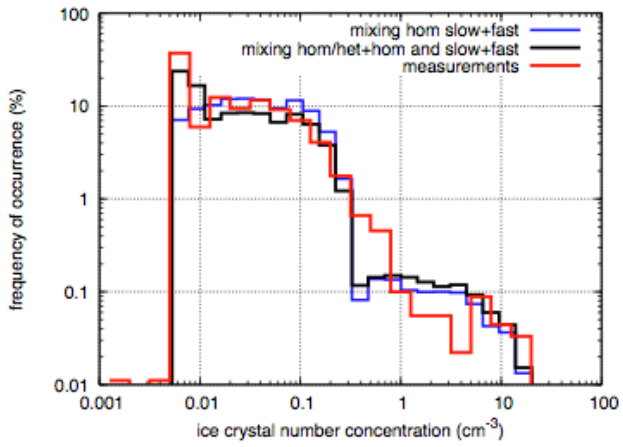

Figure 5.1. This figure demonstrates the results from Spichtinger and Krämer (2013; copied from Fig. 11), which shows that a combination of updraft speeds and nucleation mechanisms is necessary in order to reproduce the Ni distribution from observations.

In contrast to Spichtinger and Krämer, Brabec et al. (2012) did not require heterogeneous nucleation to produce agreement between their models and observations. Observations from the 2008 Lindenberg Upper-Air Methods Intercomparison (LUAMI) out of Lindenberg, Germany utilized measurements from a Cryogenic Frost point Hygrometer (CFH) and a backscatter sonde, the Compact Optical Backscatter and Aerosol Detector (COBALD), to examine high supersaturation in cirrus clouds and the underlying processes. Observations of an upper and lower layer of subvisible cirrus were made, both existing in supersaturations of 25 – 30 %. Using models, backtrajectories, and forecast fields, Brabec et al. simulated those observations and found that homogeneous nucleation in the presence of small-scale temperature fluctuations was sufficient to explain the measured particle distributions.

As an interesting aside, Brabec et al. cite the so-called "negative Twomey effect" (demonstrated in Fig. 5.2) as one reason for not including heterogeneous chemistry in their modeling scheme. The "negative Twomey effect" refers to the competition between homogeneous and heterogeneous nucleation that ultimately results in a decrease in the maximum possible Ni value (Kärcher and Lohmann, 2003). By including heterogeneous nucleation, the "negative Twomey effect" would have counteracted the small scale temperature fluctuations and the supersaturation would cease to exist. This competition effect is another extensively researched topic.

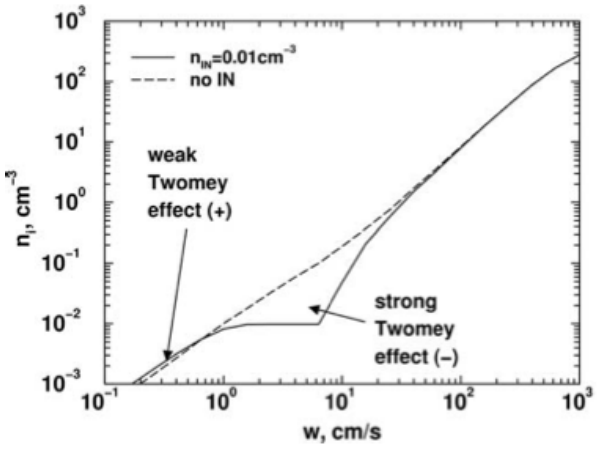

Figure 5.2. A graphical representation of the "negative Twomey effect" (copied from Fig. 9 of Kärcher and Lohmann, 2003).

Historically, it was generally understood and accepted that homogeneous nucleation was the more dominant mechanism for cirrus formation (e.g. Heymsfield and Sabin, 1989). The observations of orographic cirrus cloud formation in regimes with large vertical velocities (between 50 and 1000 cm s^{-1}) supported that conclusion. Also, it was thought that the ice nuclei (IN) that triggered heterogeneous freezing existed in the upper troposphere at concentrations less than those of their homogeneous counterparts. However, when Heymsfield et al. (1998) reported that midlatitude cirrus could be formed at RH_{ice} values too low for homogenous nucleation, based on aircraft observations, studies of the role of heterogeneous nucleation became more common.

Noting that the humidity regimes and observed Ni values were more consistent with heterogeneous freezing than with homogeneous freezing, analyses such as that of DeMott et al. (1997) investigated the potential for heterogeneous nucleation to occur and postulated the subsequent effects on ice cloud formation. Through numerical analysis, they found that the presence of IN may reduce Ni by up to a factor of 10 (given a liberal amount of IN; see Fig. 5.3)

and that different IN species are more adept at triggering heterogeneous nucleation than others. In relation to vertical velocity, their results showed that, for vertical motions less than 50 cm s^{-1}, heterogeneous freezing would lower the maximum Ni possible. For perspective, they note that for updrafts less than 20 cm s^{-1}, the range of max Ni can be between 10 – 2000 L^{-1} for homogeneous freezing alone. When heterogeneous freezing is included, that range shrinks to 1 – 500 L^{-1}. They also conclude that for every 1 IN in 100 CCN (cloud condensation nuclei) an influence could be observed until the 50 cm s^{-1} threshold at -50° C.

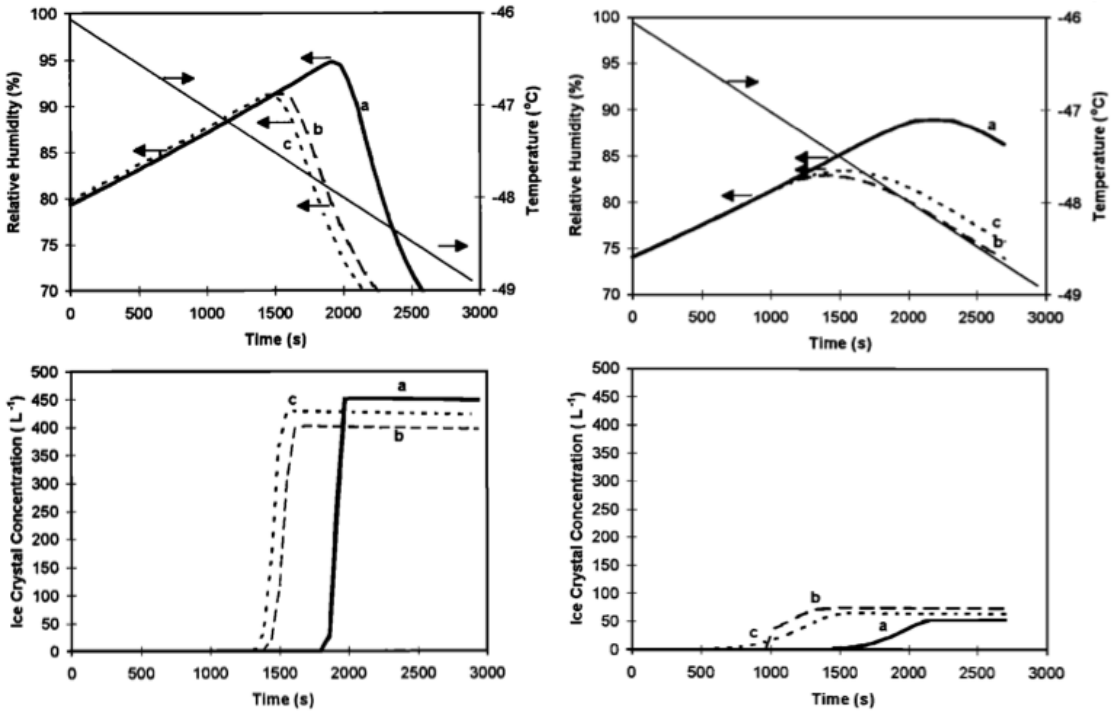

Figure 5.3. The panels on the left represent a simulation of RH_{ice}, temperature, and Ni over time when only homogeneous nucleation is allowed. The panels on the right represent the same simulation, but with heterogeneous nucleation included as well. The different lines for RH_{ice} and Ni indicate different CCN species. Both figures have been copied here from DeMott et al. (1997; left panels: Fig. 1, right panels: Fig. 4).

An additional study from DeMott et al. (1998) used airborne measurements from the SUCCESS (Subsonic aircraft Contrail and Cloud Effects Special Study) campaign to verify and expand upon the results in DeMott et al. (1997). The observations were made over the south-central Great Plains of the United States using the NASA DC-8 aircraft. An analysis of the orographically induced cirrus clouds in comparison to the results from a numerical model showed that heterogeneous IN and nucleation are indeed a part of orographic cirrus formation. However, the homogeneous events that took place later in cloud development lead to Ni values that masked the heterogeneous effect, which is in agreement with the conclusions of other, similar studies.

Outside of the orographic cirrus regime, the competition between homogeneous and heterogeneous nucleation is much more apparent. For example, in their effort to parameterize heterogeneous nucleation, Kärcher and Lohmann (2003) showed that, for very weak updrafts, the introduction of IN results in an increase in Ni. However, in synoptic-scale updrafts, weak turbulence or gravity waves, an increase in IN eventually lowers the resulting Ni. The reason that this occurs is that the initial heterogeneous event prevents the supersaturation from increasing to RH_{ice} levels that would allow homogeneous freezing to occur by taking up the available water vapor. If the vertical velocity increases past a certain point, then the supersaturation may presumably reach homogeneous freezing levels (as seen in Fig. 5.2). In essence, this situation becomes a competition between homogeneous and heterogeneous nucleation. Joos et al. (2013) have gone on to demonstrate this phenomenon in orographically induced cirrus clouds as well.

In addition to the fact the IN can ultimately limit homogenous nucleation, Barahona and Nenes (2009) found that setting a defined IN threshold value, which would lead to a defined Ni

limit, was sufficient to generate agreement between their parameterization of cirrus cloud formation and previous efforts. The limiting IN value increases with decreasing temperature and increasing vertical velocity, as expected. They go on to say that their result indicates that defining a homogeneous or heterogeneous dominant regime is therefore not necessary in parameterization. They also note that high IN values are rare in the upper troposphere where homogeneous freezing is thought to be the dominant freezing mechanism and where high vertical velocities and low temperature are also found. One complication associated with this study, and those like it, including those discussed here, is that a single, uniform population of IN species is often assumed. Further work is needed to assess the effects of multiple coexisting IN species.

In this final analysis chapter, the discussion that was started in Chapter 4 is expanded to include the effects of small-scale processes – homogeneous and heterogeneous nucleation – and the effects of IN on Ni observations. The differences in IWC and Ni measurements from MACPEX and MidCiX provide an interesting opportunity to acquire more information concerning how these cirrus formation processes work. Section 5.2 starts by recounting some of the results from Chapter 4 in regard to the expected and observed relationship between Ni and temperature. Next, that relationship is looked at again, but with the inclusion of vertical velocity and the effects of homogeneous nucleation in Section 5.3. The last piece of this analysis in Section 5.4 uses model simulations to demonstrate how heterogeneous nucleation has influenced the Ni observations from MACPEX and MidCiX. Additionally, it is shown that differences in IN are likely to be the most significant factor for determining why the cirrus clouds observed in MACPEX and MidCiX have different microphysical characteristics.

5.2 Ni Observations from MACPEX and MidCiX

In Chapter 4, the Ni observations from MACPEX and MidCiX were presented on a case by case basis. In Fig. 5.4, all observations from each campaign are presented as whole datasets. The ice crystal concentrations (for crystal diameters ≥ 15 μm) as observed by the 2D-S instrument during MACPEX are depicted in Fig. 5.4a. In the 210 – 220 K temperature range, Ni is not as large as anticipated considering the higher-than-expected IWC (see Fig. 4.3a for comparison). At lower temperatures larger Ni is observed than what was detected at high temperatures, but the values are not large enough to explain the observed high IWC. The minimum, middle, and maximum fit lines in this figure are derived from the work found in Krämer et al. (2009). It is clear from this distribution that Ni decreases with increasing temperature. Jensen et al. (2013) found this result as well and discuss that it is to be expected, given that the frequency of homogeneous freezing, and therefore high Ni values, also decreases with increasing temperature.

The Ni distribution from the observations of the CAPS instrument during MidCiX, seen in Fig. 5.4b, is largely uniform across all temperatures but is also more compatible with the IWC data (see Fig. 4.3b), if the theory that high IWC values and large Ni values are linked is applied. It should be noted that while the CAPS instrument has the ability to measure down to a diameter of 0.5 μm, only data with diameters ≥ 15 μm are used, for consistency with the MACPEX 2D-S measurements. The consequences of removing small particles from the dataset are discussed further in Sect. 5.3.2.

Thus far, any relationship between Ni and temperature has been difficult to pick out, particularly in the MACPEX dataset. It has clearly been demonstrated in the literature that vertical velocity is one of the most important variables determining the microphysical properties

of cirrus and it heavily influences the freezing mechanism as well. Given that a reasonably anticipated relationship between Ni and temperature has not emerged, I explore the possible role of vertical velocity in that relationship in the next section.

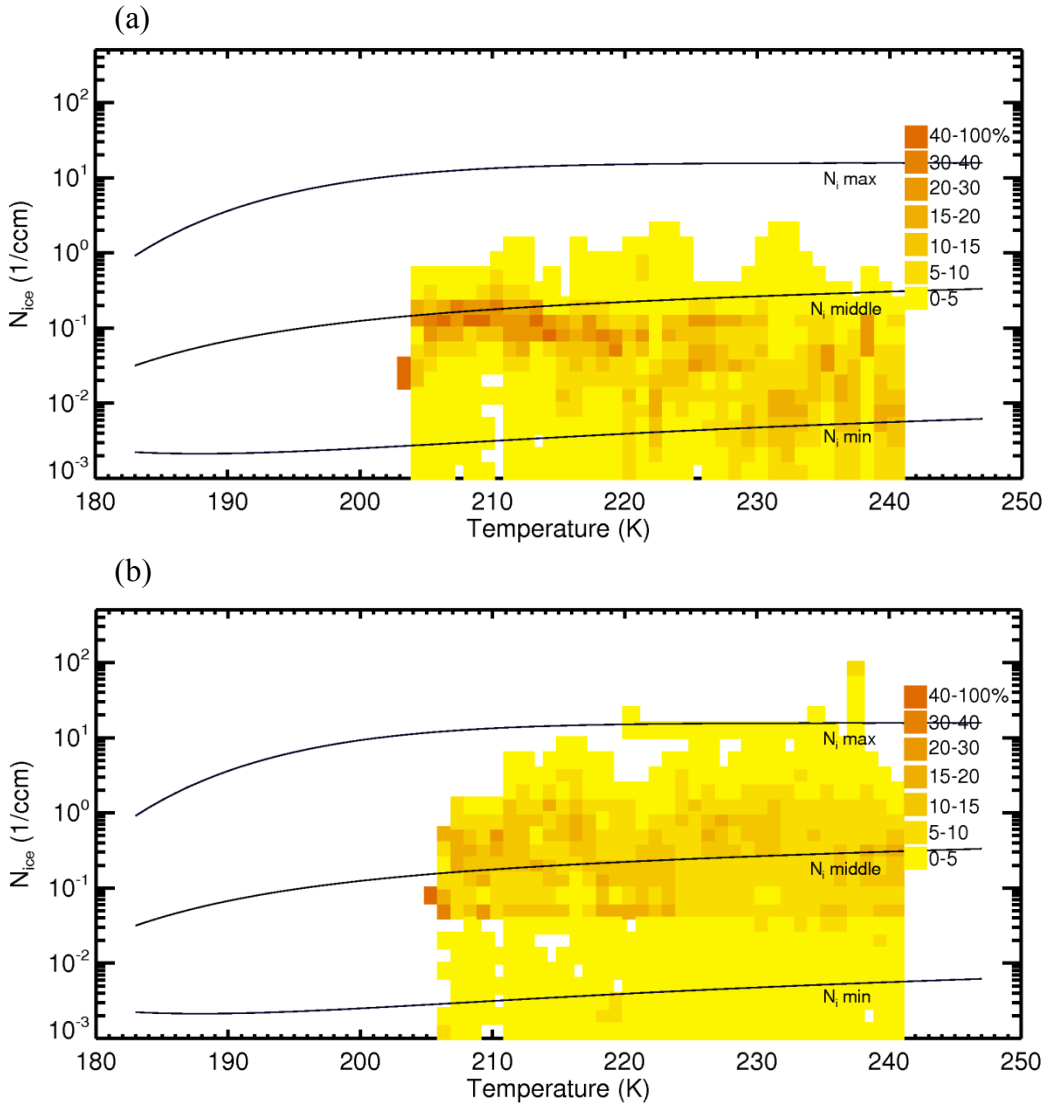

Figure 5.4. Ni (d ≥ 15 μm) as a function of temperature and frequency of observation. (a) MACPEX (b) MidCiX.

5.3 The Influence of Vertical Velocity on Homogeneous Freezing

5.3.1 As a Function of Temperature

In Krämer et al. (2009), calculations of ice crystal concentration are presented as a function of temperature for different vertical velocities (see the thick, solid lines in Fig. 5.5a, reproduced here from Fig. 9 in Krämer et al., 2009). The observations used by Krämer et al. all come from European flight campaigns that utilized the Forward Scattering Spectrometer Probe (FSSP) to measure the concentration of particles as small as 3 μm in diameter. Briefly, as described in Dye and Baumgardner (1984), the FSSP measures the size of an ice particle by collecting the light it scatters forward, within an angle of 4 – 12º, from a laser that crosses the sample volume. The scattering cross section is then converted into a size measurement using Mie-calculations. Different versions of the instrument are able to measure different size ranges. As noted in Krämer et al. (2009), the FSSP 100 and 300 were used to obtain measurements for their analysis, and those probes record particles in the size range of 1.5 – 15 μm and 0.3 – 20 μm, respectively. They also disclose that while shattering may have influenced their measurements, they do not believe it has a significant effect on the Ni-temperature relationship that they report.

The calculated lines in Fig. 5.5a show the relationship between Ni and temperature for homogeneous freezing only and are the results from a simple box model that incorporates ice microphysics from Spichtinger and Gierens (2009a) and nucleation rates from Koop et al. (2000). The results of these calculations illustrate how the homogeneous freezing mechanism can explain the observed ice crystal number distributions. In warm cirrus (> 205 K), a high frequency of large values of Ni and vertical velocities of 10 – 100 cm s^{-1} are indicative of homogeneous freezing. Cold cirrus (< 205 K), on the other hand, contains high frequencies of low Ni at vertical velocities of 1 cm s^{-1} and lower, which could be the result of homogeneous

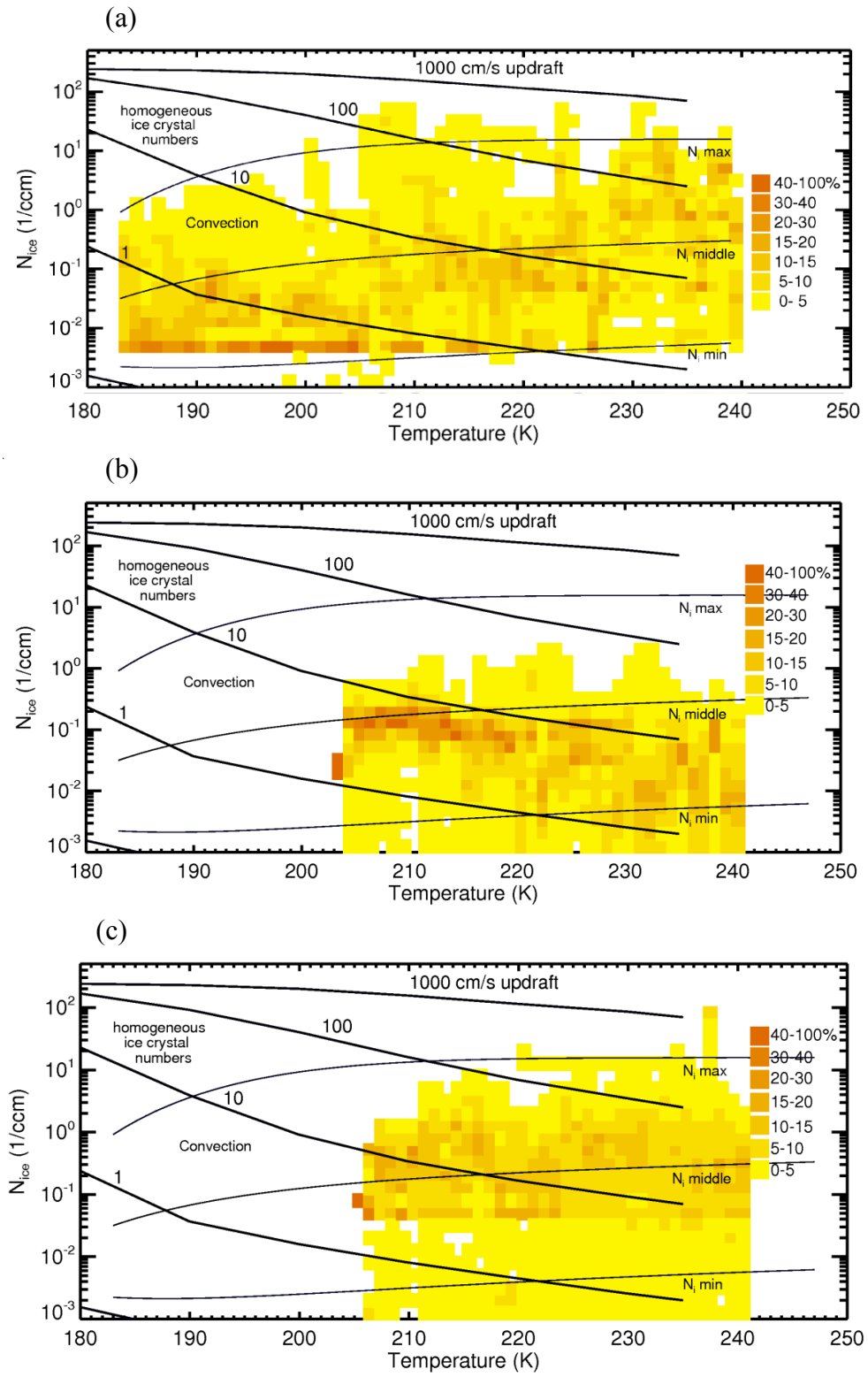

Figure 5.5a – c. Ni as a function of temperature and frequency of observation. Fit lines from Krämer et al. (2009) demonstrating Ni as a function of temperature and vertical velocity. (a) Copied from Fig. 9 of Krämer et al. (2009) (b) MACPEX (c) MidCiX.

freezing, heterogeneous freezing or the work of a nucleation suppression mechanism. It is likely to be some combination of the three possibilities as discussed by Spichtinger and Krämer (2013).

Figures 5.5b (MACPEX) and 5.5c (MidCiX) show the same Ni-temperature data from Fig. 5.4, but also include the model calculations seen in Fig. 5.5a. In comparison to one another, the datasets themselves appear to be quite different, particularly in the Ni-temperature relationships that they present. Also, the homogeneous freezing lines do not describe the distributions from MACPEX or MidCiX in the same way that they describe the data from Krämer et al. For example, the high frequency, large Ni values at warm temperatures and high vertical velocities are not observed in the MACPEX dataset. Also, the high frequency, small Ni values at low temperatures and low vertical velocities are not present in either MACPEX or MidCiX. While it is reasonable for some combination of temperatures and vertical velocities to produce any of the Ni distributions in Fig. 5.5, it does not appear that the theory supporting the observations in Krämer et al. (2009) is consistent with the observations from MACPEX and MidCiX.

One reason for this result could be due to the differences in dynamics between Europe and the U.S., which was first mentioned in Chapter 4. The bulk of the data used by Krämer et al. (2009) likely comes from frontal cirrus, which is characterized by lower vertical velocity values. Additionally, the higher vertical velocities observed at the higher temperatures are representative of orographic cirrus forced by mountains. In Chapter 4, it was shown that neither of these cases was significantly represented by either the MACPEX or MidCiX data. Also, in MACPEX, the prevalence of convection induced cirrus was shown, which is not likely to be observed in a European dataset.

5.3.2 As a Function of Vertical Velocity

Figure 5.6a and b shows a more direct representation of the relationship between ice crystal number and vertical velocity observed during MACPEX. The figure is similarly structured to those found in Sect. 4.3.1 in terms of displaying the frequency of observation (this time in blue), but Ni is now represented as a function of vertical velocity. The colored lines depict Ni as a function of vertical velocity resulting from homogeneous freezing at different temperatures between 200 and 230 K, based on the model of Koop et al. (2000). It should be noted that the chosen temperature range is largely representative of the temperature range observed in MACPEX and MidCiX.

Figure 5.6a displays the observations of Ni from MACPEX. The frequency distribution of Ni as a function of vertical velocity from MACPEX does not reveal any strong relationship. It is apparent, however, that the distribution is bimodal for each vertical velocity bin, which is evidenced by the dark blue color indicating a high frequency observation at each mode. The first peak is between 0.1 and 1 cm^{-3} and the second peak is between 0.01 and 0.1 cm^{-3}. Another noticeable feature is the discrepancy between the Ni-vertical velocity relationship and the calculated homogeneous freezing lines at different temperatures. These lines clearly depict a relationship in which Ni increases as vertical velocity increases. The observations from MACPEX show that at high (low) vertical velocities, Ni falls below (above) the model relationship.

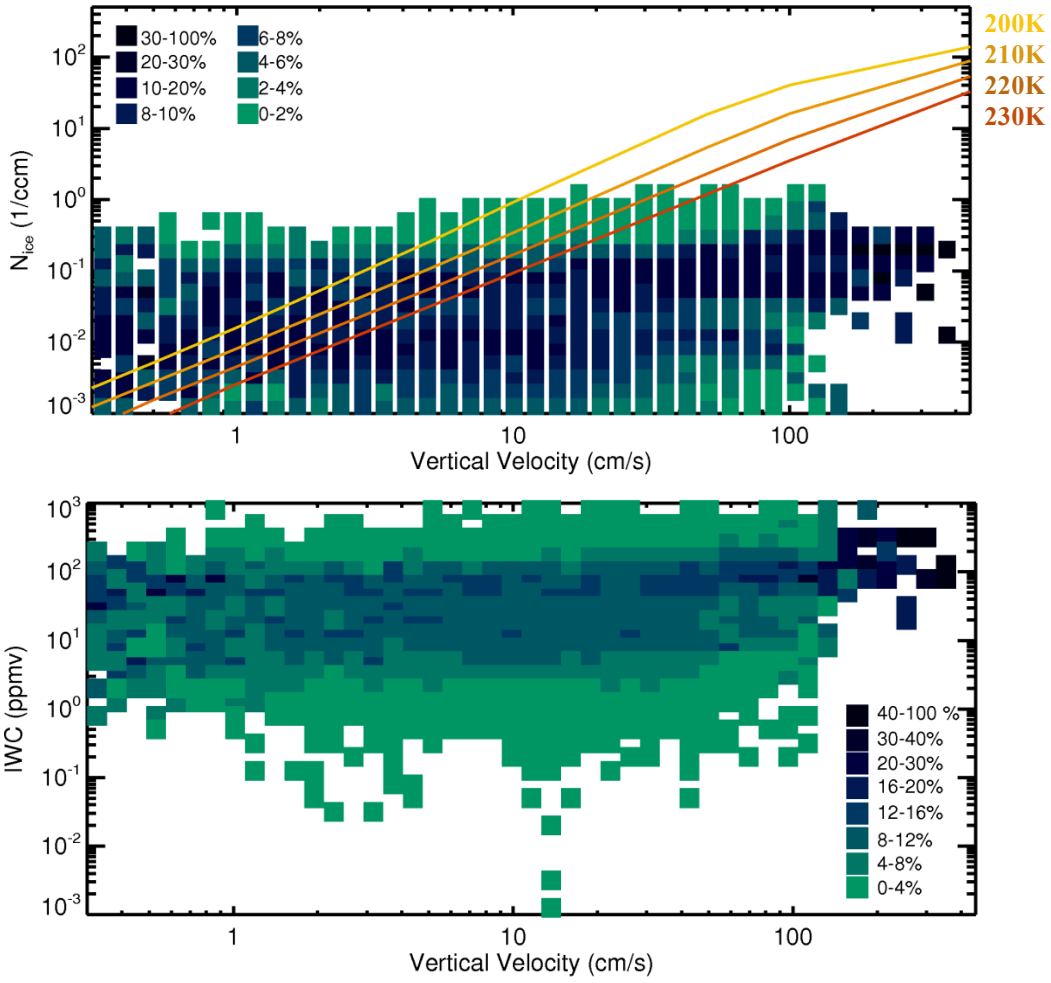

Figure 5.6. Observations from MACPEX of (a, top) Ni and (b, bottom) IWC as a function of vertical velocity and frequency of observation. (a) includes the homogeneous freezing fit lines seen in Fig. 5.5, except as a function of temperature.

Looking next at Figure 5.6b, it is also clear that there is not a strong relationship between IWC and vertical velocity either. Given the distribution of Ni with vertical velocity, this is not surprising.

On the other hand, the observations from MidCiX shown in Fig. 5.7a reveal different behavior. It can be seen that at vertical velocities below ~30 cm s^{-1}, there is not a strong indication of any relationship between Ni and vertical velocity. However, above ~30 cm s^{-1},

particle number increases with vertical velocity, which is consistent with the theoretical relationship described by the homogeneous freezing lines. Despite the presence of this relationship, the ice crystal numbers that were observed are lower than expected from theory, much like they were in the MACPEX observations.

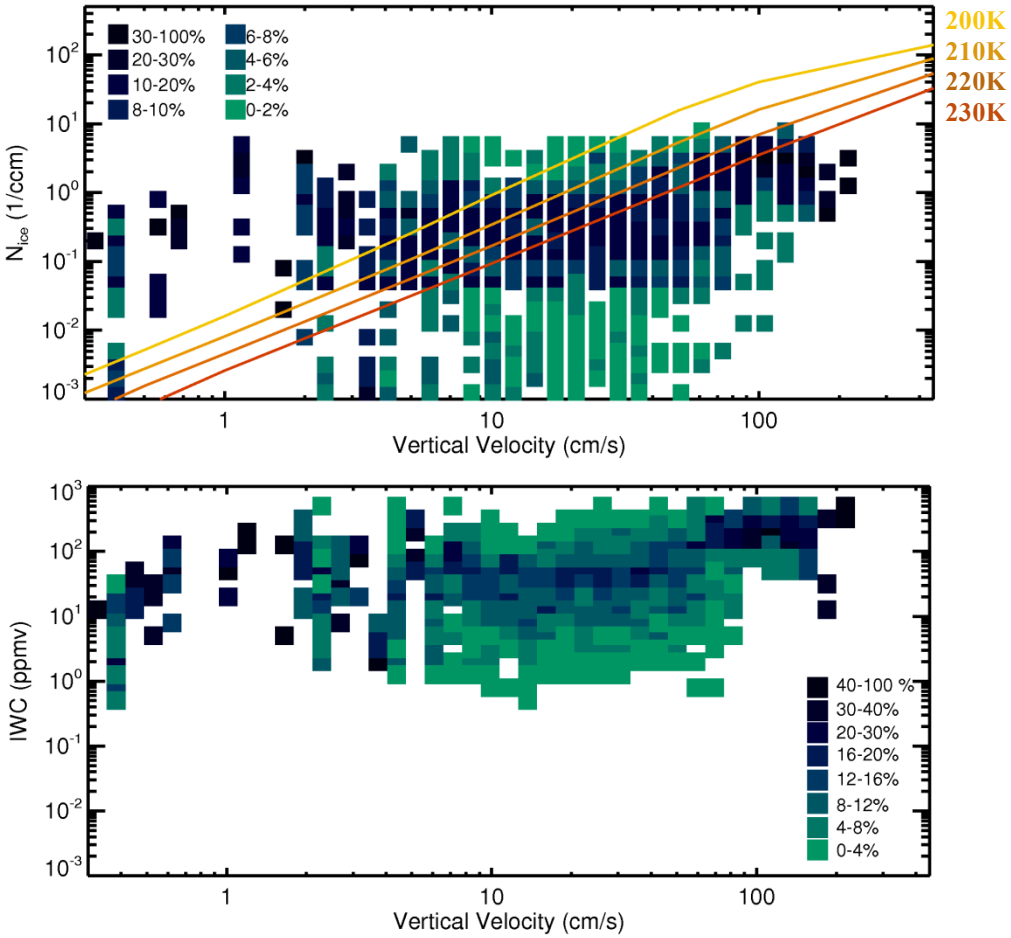

Figure 5.7. Observations from MidCiX of (a, top) Ni and (b, bottom) IWC as a function of vertical velocity and frequency of observation. (a) includes the homogeneous freezing fit lines seen in Fig. 5.5, except as a function of temperature.

Similar to what has been shown in Chapter 4, the IWC observations from MidCiX are consistent with the Ni measurements. Plotting the Ni and IWC observations as a function of

vertical velocity shows a similar pattern in both variables. At vertical velocities greater than ~ 30 cm s^{-1}, there is a distinct increase in IWC as vertical velocity increases (Fig. 5.7b).

Lack of Ice Crystal Observations < 15 μm

One issue that should be addressed here is the lack of small ice crystal observations and what effect that may have on visualizing the effects of homogeneous freezing on the Ni datasets from MACPEX and MidCiX. As explained in Chapter 2 (Sect. 2.3.2), it is not recommended that observations below diameter ~ 15 um from the 2D-S dataset are used and it is suggested that ice crystals smaller than this limit are not likely to significantly contribute to the overall Ni distribution. In comparison to the 2D-S, the CAPS instrument (also discussed in Chapter 2) used in MidCiX measured ice crystals as small as 5 μm. However, in order to make the 2DS and CAPS datasets more comparable, only values for diameters > 15 μm in the MidCiX dataset were included in this analysis.

In order to test the hypothesis that the presence of small particles in the analyzed dataset could have a significant influence on the results, data for particles with diameters between 5 and 15 μm were reintroduced to the MidCiX Ni dataset. The resulting Ni-vertical velocity relationship is shown in Fig. 5.8. Compared to Fig 5.7a, the addition of these small particles has led to an overall increase in ice crystal concentration. Also, at vertical velocities between 30-60 cm s^{-1}, Ni increases with vertical velocity and, more significantly, matches the theoretically determined homogeneous freezing lines. The fact that a large portion of the MidCiX data are between approximately 210 K and 230 K strengthens the argument that the inclusion of small particles has led to a better match since the homogeneous freezing lines seen in Fig. 5.8 are representative of that temperature range as well. Thus, it can be concluded that small crystals may be important for demonstrating Ni-vertical velocity relationship.

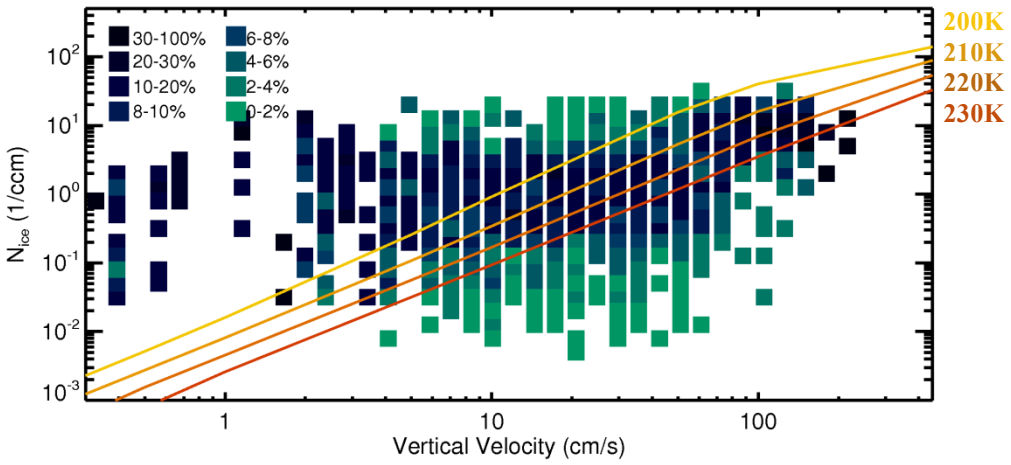

Figure 5.8. Observations from MidCiX of Ni ($d \geq 5\mu m$) as a function of vertical velocity and frequency of observation. This figure is the same as Fig. 5.7a, except that it includes ice crystals between 5 and 15 μm.

5.4 The Effects of Heterogeneous Ice Nuclei

As demonstrated by much of the previous work found in the literature, homogeneous freezing alone cannot explain the observed Ni results. This is also clearly true for the MACPEX and MidCiX observations. Thus, it is important to also explore the contribution of heterogeneous freezing to these measurements. Additionally, recent work has shown that heterogeneous freezing is tremendously important in the case of MACPEX.

5.4.1 Evidence of Heterogeneous Nucleation in MACPEX

Cziczo et al. (2013) report that mineral dust and metallic particles were the dominant materials found in ice crystals sampled during MACPEX. Mineral dust is known to be an efficient ice nucleus in heterogeneous nucleation while various metals have been found in mineral dust and are suspected to have some contribution (Lohmann, 2002). Cziczo et al. obtained their measurements using a Counterflow Virtual Impactor (CVI) inlet and the Particle

Analysis by Laser Mass Spectrometry (PALMS) instrument. Briefly, the CVI allows only large ice crystals (on the order of 10^1 - 10^2 μm) to be accepted for observation. The water is then evaporated in the warm, low humidity inlet leaving what Cziczo et al. refer to as an ice residual, which is the material that served as an ice nucleus during freezing. The ice residual enters the PALMS instrument where it is fragmented by a high energy laser. The resulting components are analyzed by mass spectrometry to reveal the chemical composition of the ice residual. Additional information on the PALMS can be found in Thomson et al. (2000).

Cziczo et al.'s analysis reveals that mineral dust was the dominant residual in 94% of cloud encounters over four aircraft campaigns taking place in different regions and at different times of year, including MACPEX. Contrary to what other studies have found, they go on to suggest that heterogeneous freezing is the dominant freezing mechanism throughout the region of their study.

Additionally, Cziczo et al. use relative humidity with respect to ice (RH_{ice}) calculated from water vapor measurements made by the Harvard Lyman-α water vapor instrument to supply further proof that heterogeneous freezing is the dominant nucleation mechanism (see Chapter 2 for information on this instrument). For MACPEX, they found that RH_{ice} rarely exceeded 120% outside of the cirrus clouds sampled. While this is an acceptable value for heterogeneous freezing to take place, it is far too low for homogeneous nucleation (Mangold et al., 2005; Möhler et al., 2005). This result was similar for the three other datasets used in their analysis. Conversely, RH_{ice} data from MidCiX were also analyzed and they found that the homogeneous freezing threshold (RH_{ice} ~155%) was reached occasionally, suggesting that homogeneous nucleation may have been possible. These observations can be seen in Fig. 5.9.

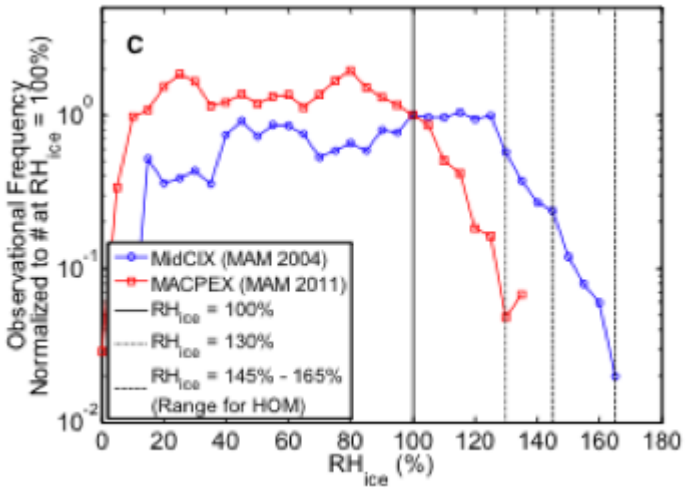

Figure 5.9. This figure shows the RH_{ice} values observed in MACPEX and MidCiX. This figure has been copied from Fig. S2 of Cziczo et al. (2013).

Jensen et al. (2013) also came to the same conclusion through the use of model simulations and airborne observations from MACPEX and the Small Particles In Cirrus (SPARTICUS) campaign. The ice crystal data in both cases come from the 2D-S instrument. Their model simulations include ice nucleation (both homogeneously and heterogeneously), growth via deposition, sublimation, sedimentation, and aggregation processes. Briefly, the simulations are driven by trajectories based on measured temperature and vertical wind profiles. They are also superimposed with temperature and vertical wind perturbations that are comparable with the conditions experienced in SPARTICUS and MACPEX. Along with demonstrating the importance of mesoscale waves in controlling the distribution of ice crystal concentrations, Jensen et al. also conclude that heterogeneous freezing is clearly a proficient competitor for homogeneous freezing. They found this to be true particularly for low ice crystal concentration regimes and at IN concentrations of 100 L^{-1}, though concentrations of 20 L^{-1} are

sufficient to observe an effect. They also assert that homogeneous freezing still occurs at low temperatures, but that those cases are rare.

5.4.2 MAID Model Comparison

In this section, I compare the MACPEX and MidCiX observations to results from the Model for Aerosol and Ice Dynamics (MAID), a box model that was developed specifically to simulate the ice nucleation processes that aerosols undergo in the upper troposphere (Bunz et al., 2008). It should be recognized that while this model represents a simplified version of what actually happens in the atmosphere, it is still a useful tool for obtaining a better understanding of the cirrus nucleation mechanisms.

The chemical and physical processes considered in this model include homogeneous freezing, ice formation activated by solid particles, growth, deposition, coagulation, and evaporation. The system of aerosols contained within the model is described using number density functions, which comprise the sizes and composition of the particles. Using specific and appropriate boundary conditions (e.g. temperature, H_2O_{gas}), the system is assumed to contain an aerosol composition that is homogeneously mixed. It should be noted that the heterogeneous ice nucleus species used in the model simulation shown below is mineral dust.

Both homogeneous freezing and heterogeneous freezing (via deposition or immersion) are included in the model. Homogeneous freezing is replicated using the parameterizations found in Koop et al. (2000) and Koop (2004). These parameterizations detail a homogeneous nucleation rate that is dependent on factors such as temperature and water activity and allows for nucleation to occur depending on the cooling rate of the air parcel and whether the saturation vapor pressure threshold specific to homogeneous nucleation has been reached. Heterogeneous

freezing is simulated using a parameterization from Kärcher and Lohmann (2003), which accounts for the lower saturation vapor pressure threshold that is required for this process.

In cases where heterogeneous freezing is allowed to occur, the overall process begins by defining the number density of heterogeneous ice nuclei and the heterogeneous freezing threshold, which has been determined by the experimental work found in Möhler et al. (2005). Ice particles are then allowed to nucleate until all of the ice nuclei have been consumed. At this point, one of two things may occur if the air parcel is cooled further. In the first scenario, water vapor deposition occurs on the existing crystals, and those crystals grow, but no new crystals form. Alternatively, the RH_{ice} may continue to increase until the homogeneous freezing threshold is reached, and Ni increases as new ice crystals form homogeneously on the liquid solution particles. The model also allows for sublimation of the ice crystals to occur if the ambient temperature is greater than the frostpoint temperature.

Fig. 5.10 demonstrates the work that has been done using this model as a means to better understand the relationship between vertical velocity, ice crystal concentration, and the two possible nucleation pathways available (Rolf et al., 2012). The figure shows the results of using two different starting ice nuclei number densities, 0.01 cm^{-3} and 0.1 cm^{-3}, indicated by the solid and dashed lines, respectively, and at three 10K temperature intervals between -56 and -36 °C (~217 – 237 K). It is assumed that all ice nuclei undergo heterogeneous nucleation forming an abundance of ice crystals that is equivalent to the starting ice nuclei number density. As vertical velocity is increased, the adiabatic cooling rate increases, resulting in an increase in RH_{ice}. However, up to a certain point, the RH_{ice} threshold remains below the homogeneous freezing threshold and no new crystals are created. Once that threshold is reached, at 10 cm s^{-1} and 50 cm s^{-1}, respectively, for 0.01 cm^{-3} and 0.1 cm^{-3} ice crystals, a secondary homogeneous freezing event

occurs. If the vertical velocity is increased further, RH_{ice} will continue to increase and allow for more particles to nucleate. As indicated by the figure, the number of crystals that will form is dependent on temperature.

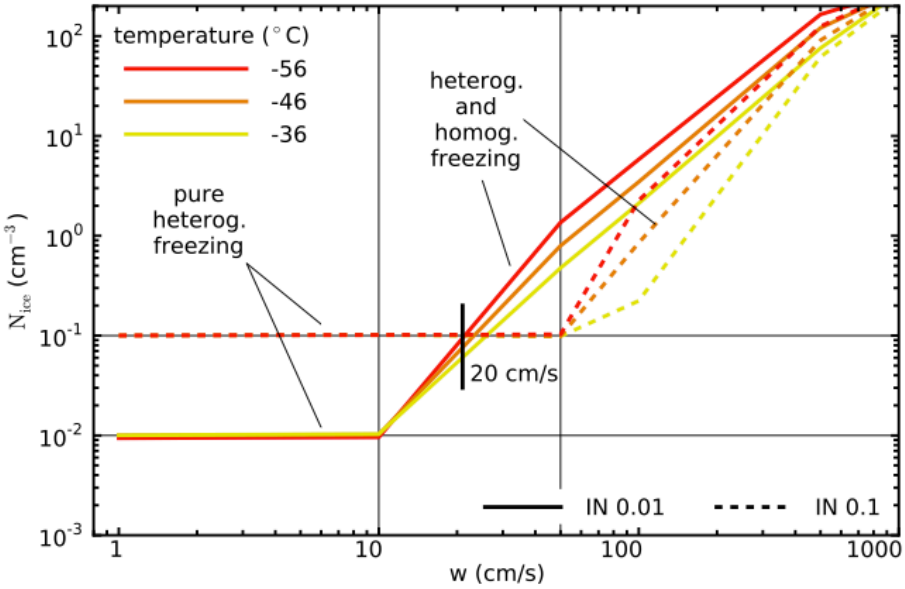

Figure 5.10. MAID model results demonstrating heterogeneous freezing and homogeneous freezing as a function of vertical velocity, temperature, and IN concentration. This figure is copied here from Fig. 7 from Rolf et al. (2012).

If the observations from MACPEX (Fig. 5.6a) are overlain with the results from the MAID model as shown in Fig. 5.11a, it can be inferred that the horizontal appearance of the distribution of Ni with respect to vertical velocity is due to the fact that heterogeneous freezing is the dominant mechanism creating the observed ice crystals. While homogeneous freezing cannot be completely ruled out as a formation mechanism, there are no obvious indications that it made a significant contribution. Considering the results reported by Cziczo et al. (2013) concerning the remarkable dominance of heterogeneous freezing materials in their observations during MACPEX and the observed RH_{ice} values from the Harvard water vapor instrument, it is

reasonable to conclude that heterogeneous freezing of a high concentration of IN likely explains the observed distribution.

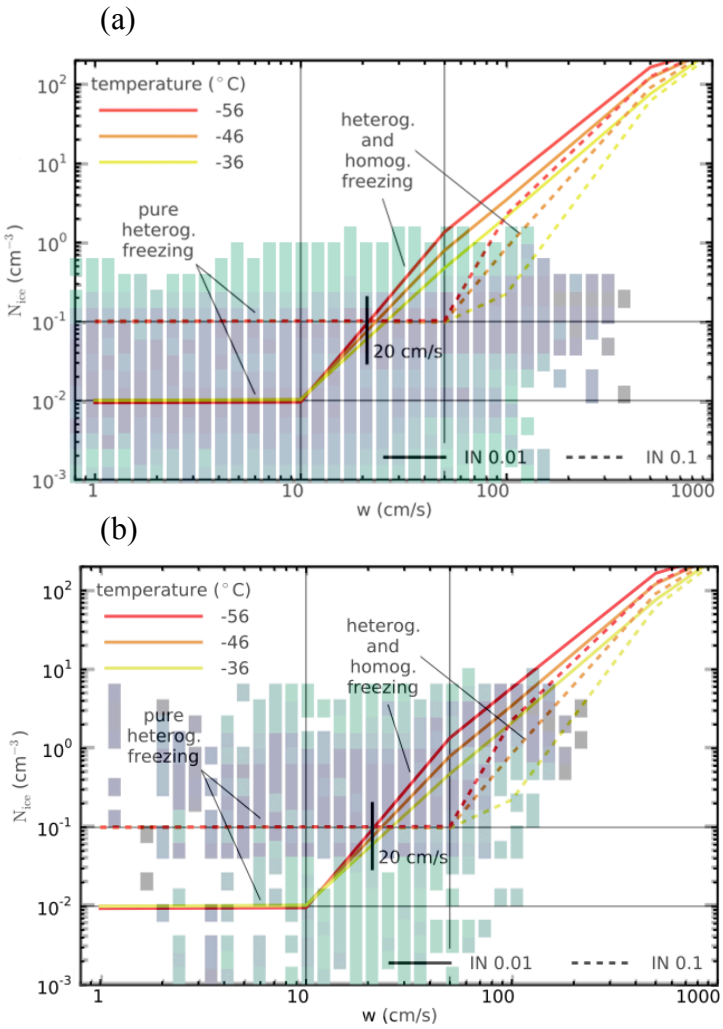

Figure 5.11. Comparison between MAID model results and (a) MACPEX observations and (b) MidCiX observations (d > 15 μm).

Additionally, the MAID model results are also combined with the MidCiX observations from Fig. 5.7a as seen in Fig. 5.11b. This figure reveals that the Ni distribution below ~ 30 cm s^{-1} is consistent with heterogeneous ice nucleation. Also, as discussed above, the distribution of Ni for vertical velocity values greater than ~30 cm s^{-1} is consistent with the homogeneous ice

nucleation events that can occur at high vertical velocities. The IWC distribution shown in Fig. 5.7b supplies further evidence that this is the case by also demonstrating the sudden increase in IWC at the same vertical velocity value of Ni increase.

5.4.3 Effects of Sedimentation

Another mechanism that may have influenced the observations and should be considered is the sedimentation of large ice crystals (see Chapter 1). Using the MAID model, the effects of sedimentation on ice crystal concentration have been simulated using the parameterization derived by Spichtinger and Gierens (2009a). In general, Fig. 5.12 is similar to Fig. 5.10, except that large ice crystals are allowed to sediment out of the box, thus reducing Ni below the starting ice nuclei concentration. Without the additional competition for water vapor from those ice crystals, RH_{ice} may increase more easily until the homogeneous freezing threshold is reached and new crystals can be formed. For weak vertical velocities, this Ni increase is quite small, but for stronger vertical velocities, the increase in Ni can be large. Similar to before, this mechanism has a temperature dependence. Also, the vertical velocity thresholds where a secondary homogeneous freezing event may occur are lower than for the scenario without sedimentation. Thus, the homogeneous freezing threshold may be reached at lower vertical velocities.

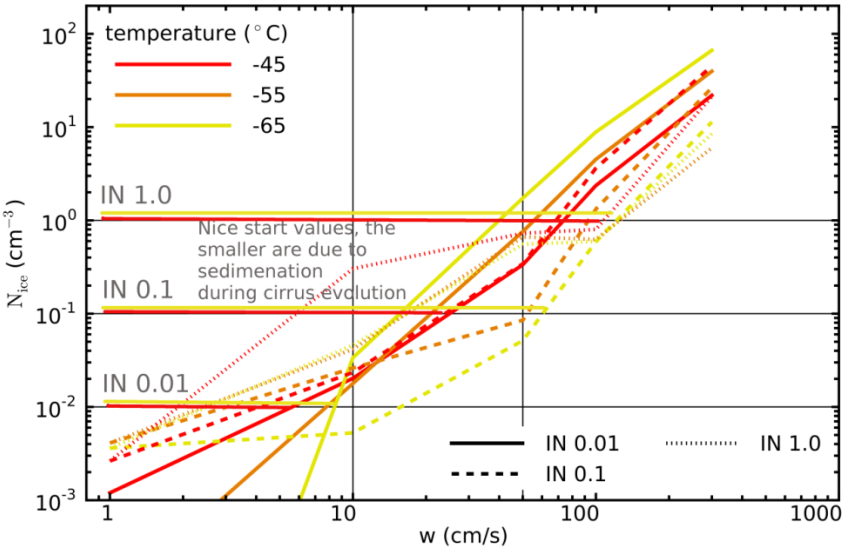

Figure 5.12. MAID model results including the effects of sedimentation. Ni is shown as a function of vertical velocity, temperature, and IN concentration.

While, the observations from the Harvard water vapor instrument in Cziczo et al. (2013) indicate that a successful homogeneous event in addition to the heterogeneous nucleation would be very unlikely in MACPEX, sedimentation may explain some of the very low Ni values that were observed. For the MidCiX observations, additional information would be necessary in order to better determine and visualize the relative importance of homogeneous and heterogeneous nucleation and sedimentation.

5.5 Conclusion

The results from Chapter 4 demonstrated that the observations from the MACPEX campaign are different from what has been previously observed. The analysis in that chapter showed that while large scale dynamics have an influence on the microphysical properties of cirrus clouds, there were observed features that could not be explained by variables such as vertical velocity alone. It is shown in the literature that vertical velocity has been found to play a

significant role in cirrus cloud formation due to the fact that it controls the cooling rate of an air parcel, and thus, the resulting RH_{ice} in the cloud. More significantly, the concentration of IN also plays an important role since the resulting ice crystal concentration ultimately influences the development of supersaturation by determining how much water vapor is available for deposition. The concentration of IN can lead to a competition between homogeneous and heterogeneous nucleation. Thus, it was imperative that these factors be included in the discussion of the differences between MACPEX and MidCiX.

The initial exploration involved the use of theoretical work detailing the homogeneous freezing mechanism, which is generally accepted as being the more dominant freezing pathway, particularly at cold temperatures. The results of this first analysis show that the observations in MACPEX are not consistent with this theory or even the expected Ni-vertical velocity relationship. This was also true for the MidCiX observations that were sampled at vertical velocities below ~30 cm s^{-1}. Above that threshold, the MidCiX observations were more consistent with homogeneous freezing.

The obvious next step to find a more conclusive answer was to look at heterogeneous freezing. This was made more important by the results from Cziczo et al. (2013) and Jensen et al. (2013) who show that heterogeneous freezing was very noticeably the dominant nucleation mechanism associated with the cirrus clouds sampled during MACPEX. Using the results from the MAID model, it was verified that the Ni and IWC distributions from the MACPEX observations could be explained by the heterogeneous freezing mechanism. It was noted by Jensen et al. (2013) that the MACPEX campaign took place during a season of particularly abundant biomass burning in the region of the United States sampled. This in turn produced an unusually high concentration of IN. With this in mind, the effects of IN on suppressing

homogeneous nucleation can be observed. Some of the high vertical velocity values and the high IWC indicate that homogeneous nucleation should have occurred, but the presence of unusually high IN concentration makes a strong case for why it did not. Instead, the abundance of heterogeneously formed ice crystals suppressed homogeneous nucleation, resulting in a lower than expected Ni concentration.

The conclusions from the MidCiX observations demonstrate a different scenario. The comparison to the MAID model results showed that for observations made at vertical velocities below ~30 cm s^{-1}, heterogeneous nucleation was the dominant nucleation mechanism. However, above that threshold value, a clear increase in Ni and IWC is observed that is consistent with secondary homogeneous nucleation events. This indicates that the IN present were neither abundant nor efficient enough to produce sufficient ice crystals to keep RH_{ice} below the homogeneous freezing threshold. Thus, when the vertical velocity threshold was reached, enabling an increase in RH_{ice} , homogeneous nucleation took place. RH_{ice} measurements from MidCiX are consistent with this scenario. The PALMS instrument was not a part of the MidCiX campaign so ice residual data are not available, but other data concerning the ice nuclei population are available from MidCiX that could be used to corroborate this assertion.

The final conclusion from this analysis pertains to fact that the differences between the MACPEX and MidCiX datasets are demonstrable for reasons relating to the small and large scale conditions in which the cirrus clouds were formed. The question remains whether one dataset is more representative of the "normal" state than the other. Jensen et al. (2013) conclude their analysis by asserting that heterogeneous nucleation is the dominant mechanism in the midlatitude cirrus formation regime. Cziczo et al. (2013) come to a similar conclusion. Conversely, the results from Krämer et al. (2009) strongly demonstrate a dominance of

homogeneous nucleation in midlatitude cirrus observed over Europe. This suggests that the dynamics or perhaps airmasses in the region that contribute to the available IN concentrations may be different. For instance, the prevalence of convective storms in Europe pales in comparison to what is observed in the United States. Similarly, it was noted that the dynamics observed in MidCiX were different from those sampled in MACPEX. A more thorough analysis of those dynamics, including the airmass contribution (e.g. continental versus marine) from back trajectories, may provide further evidence to support the observed and surmised IN concentrations associated with MACPEX and MidCiX, respectively. Thus, at this point, it seems wise to caution against using the MACPEX results as a representative dataset.

Chapter 6 Conclusions

6.1 Analysis Summary

The high degree of scientific uncertainty concerning the role of clouds in the radiation budget of the atmosphere has been made clear by publications, like the IPCC reports, that survey scientific research. The numerous and variable macrophysical and microphysical properties of clouds make parameterizations that accurately describe cloud formation processes, relationships between properties, and relationships to other atmospheric characteristics difficult to obtain. However, a high degree of understanding of the role of clouds and a significant level of fidelity in describing their properties is necessary to create GCMs (global climate models) that can more precisely project what climate change can and will look like. Those tools will then allow other sectors within society to develop the policies, technology, and ideas that can allow us to prevent, manage, and adapt to the current and predicted scenarios.

The analysis that I presented in this dissertation focused on obtaining a better understanding of the relationship between cirrus cloud properties and the large and small scale processes that determine those properties. Among them, IWC is important for calculating other microphysical properties, such as extinction and effective radius; however, we need to understand the relationship that it has to the atmospheric state and dynamical forcing before using it to estimate the radiative properties of cirrus clouds.

To address this, I have relied solely on in situ measurements from a number of airborne field campaigns, both of domestic origin and abroad. Due to the small temporal and spatial

scales on which these instruments measure, they are ideal for obtaining data that are comparable to the scales on which cirrus formation and maintenance processes operate. In Chapter 2, the instruments used to collect the atmospheric water data, ice crystal concentrations, and information associated with variables to characterize the atmospheric state were discussed. I demonstrated that the instruments that contributed data to my analysis were suited for cirrus research based on the measurement techniques that they employ. Also, based on the range of values that they measure for their variable of interest, they are able to provide a comprehensive picture of cirrus properties. This chapter also noted some of the challenges facing these instruments. For example, the measurements of atmospheric water have displayed a long-standing disagreement between instruments using the same measurement technique and among instruments utilizing different methods, the cause of which has yet to be determined. The issues relating to ice crystal measurements have largely focused on the potential for shattering large crystals, resulting in an overestimation of the number of small crystals that were observed. As noted in that chapter, an incorrect representation of the number of small crystals impacts the calculations used to determine a cloud's radiative forcing and the assumptions made about the processes leading to the formation of a cloud with that characteristic.

Once the measurements are in hand, the next question is how to use them. In Chapter 3, the first analysis that I discuss has two parts. The first part speaks to the importance of having a good dataset. By combining the observations from several U.S. and European airborne campaigns, I was able to develop a large dataset that contains comprehensive IWC measurements over the full range of values seen in cirrus clouds and also covering the temperatures, altitudes, and latitudes where cirrus clouds are commonly found. This work is an

extension of the climatology development started by Schiller et al. (2008) and has been published (Luebke et al., 2013).

The second part of Chapter 3 uses the combined dataset to explore a common relationship between cirrus microphysics and atmospheric conditions – the IWC-temperature relationship. It is already understood that as the temperature increases, the IWC of a cirrus cloud increases as well. However, it has long been observed that the IWC varies considerably for a given temperature. The existing parameterizations of this relationship are unable to capture this variability and are, therefore, inaccurate and of limited utility. Using probability distribution functions (PDFs), I demonstrated that descriptions of the IWC-temperature relationship could be developed while still maintaining a representation of the IWC variability.

Additionally, the visualization of the IWC-temperature relationship using PDFs brought to light other details about ice water content. In particular, the distribution of IWC in each 5-K temperature bin was noted to be bimodal. Though the influence of other factors, such as vertical velocity, had already been suggested in the literature, this observation was a strong indication that the impacts of two processes likely result in this IWC distribution. Ni observations from an external source exhibited the same bimodal distribution and could be tied to homogeneous and heterogeneous freezing mechanisms. This, in turn, led to a hypothesis concerning the additional factors determining the IWC-temperature relationship, which includes contributions from those two freezing pathways and the significance of Ni.

The next two chapters in this dissertation build upon the hypothesis put forth in Chapter 3 by further exploring the variables contributing to the IWC-temperature relationship. The broader domain of nucleation mechanisms and the resulting microphysical properties, namely Ni, are the cirrus formation processes. This encompasses a number of variables and dynamics such as

synoptic-scale uplift, vertical velocity, supersaturation development, and IN concentration. Starting with the role of dynamics on the larger scale, I investigated the effects that different synoptic patterns have on IWC and Ni. This was accomplished using two seemingly similar midlatitude in situ datasets from the MACPEX and MidCiX campaigns. Factors such as the time of year, the location of the measurements, and the majority of the instrumentation are consistent between the two campaigns, but the IWC- and Ni-temperature relationships are not similar. One of the differences between the two campaigns is the distribution and type of synoptic conditions in which the cirrus clouds were sampled. Briefly, the MACPEX dataset is more representative of cirrus resulting from convective outflow, whereas the MidCiX dataset contains a variety of cirrus types. Using a case study approach, I demonstrated that differences in IWC and Ni were observed between different synoptic cases, but that more details on the atmospheric conditions (e.g. the appearance of shortwave troughs and ridges or the location of the jet stream) were necessary for understanding differences in IWC between flights sampling the same synoptic case type. The most notable conclusion of this analysis is that, while the relationship between the large-scale dynamics and IWC was demonstrable, the relationship to Ni was not, particularly in the case of the MACPEX data.

The MidCiX IWC and Ni data follow the relationship discussed in Chapter 3 – more ice crystals mean a large IWC and vice versa. However, this relationship cannot be observed in the MACPEX data. Though there are many observations of large IWC, the Ni observations are consistently on the low side. Vertical velocity and general uplifting mechanisms are responsible for transport of water that ultimately lead to cloud formation, but they are also responsible for determining the conditions on the small-scale that are necessary for cirrus cloud formation – namely, the rate of cooling and therefore RH_{ice}. For years, the relative contributions of

homogeneous and heterogeneous nucleation in cirrus cloud formation have been hotly debated; the results of this analysis show that heterogeneous nucleation plays a dominant role. By comparing observations of Ni to model calculations, the cirrus sampled during MACPEX were determined to be the result of heterogeneous nucleation. Also, given the IN species and concentrations measured during MACPEX by Cziczo et al., it is likely that the abundance of heterogeneously nucleated crystals ultimately suppressed homogeneous nucleation by preventing supersaturation levels from reaching the threshold necessary for homogeneous nucleation to take place. The MidCiX Ni and IWC datasets, on the other hand, show that, while heterogeneous nucleation was a major factor, in cases where the vertical velocity was greater than ~ 30 cm s^{-1}, a noticeable increase in Ni and IWC took place, which is indicative of a secondary homogeneous nucleation event. While this cannot be confirmed without knowledge of the IN present during MidCiX, it seems reasonable to assume that the IN characteristics of MACPEX and MidCiX were different. If fewer or less-effective IN were present during MidCiX, the number of heterogeneously nucleated particles would be able keep the supersaturation levels low only up to a certain point. In this case, vertical velocity values greater than ~30 cm s^{-1} were the trigger.

6.2 Implications of the Work Presented Here

My analyses contribute to the understanding of cirrus clouds in three respects. Firstly, the development of the large IWC dataset presented in Chapter 3 provides an extensive dataset that can be useful for comparison and evaluation purposes in climate models. Additionally, while the relationships determined by that analysis are not appropriate for direct use in climate models, they can be used for the same evaluation purposes.

Secondly, the demonstration of the relationships between IWC and Ni to other factors has provided useful information concerning the relative dominance of those factors in characterizing

a cirrus cloud. In the order of the least amount of influence to the greatest are temperature, vertical velocity, and IN. However, it should be noted that an analysis including all of those factors illustrates a comprehensive picture of how the cirrus cloud was formed, developed, and sustained/dissipated. In the literature, the complexity of the processes and relationships is understood, but how to express that complexity on the proper scales is not. The work here suggests that for IWC, the processes and relationships involved may be more complex than can be demonstrated in a single parameterization.

Finally, the comparison between MACPEX and MidCiX raises an important issue. It is not clear whether the MACPEX results or the MidCiX results are reflective of what typically occurs in the midlatitudes or, for that matter, in the southern part of the central U.S. Therefore, labeling either of these datasets as "representative" would be misleading until what is "representative" can be defined. For instance, the dominance of heterogeneous nucleation and high IWC values in the MACPEX dataset is indicative of a dominance of large ice crystals. This in turn could be interpreted to mean that the cirrus observed in MACPEX are more suited to absorbing the outgoing terrestrial radiation, thus having a warming effect on the atmosphere. However, labeling all cirrus clouds based on this one dataset could lead to a misrepresentation of the role of cirrus clouds in the climate system. Thus, caution should be exercised in the use of a single dataset or a few datasets for evaluation purposes, as they may not represent what is typical for cirrus or even a specific subset of cirrus therein.

6.3 Future Work

While the work done here has made steps to more accurately describe cirrus clouds, there are other avenues to explore. For instance, on the large-scale, the results from Chapter 4 and 5 have introduced the importance of time and spatial scales as well as how the contribution of

different air masses with different characteristics can influence cirrus development and lifetime. The use of back trajectory analysis to visualize these variables may offer more information in regards to how the IN population, water vapor concentration, and the cloud itself have evolved up to the point of observation.

Conversely, on the small-scale, the ice crystals within a cirrus cloud can move vertically, thus changing characteristics such as Ni, IWC, and RH_{ice} at different levels throughout the cloud. Generally, the top of the cloud contains the "nucleation zone" where the smaller ice crystals reside, and the lower layers contain the larger crystals that have fallen as they grow. Numerical studies, such as Lin et al. (2005), have been able to simulate the processes in these layers, but it would be interesting to observe them individually in situ. Looking at the microphysical properties and dynamics existing in and impacting those layers may further refine the explanation of the relationships discussed in the analyses here.

The results in this dissertation have largely focused on the midlatitudes over the U.S. Therefore, it would be useful to expand this analysis to include datasets from different regions. Not only is it important to demonstrate the similarities and differences in the microphysical properties and atmospheric conditions between regions (tropics, midlatitudes, and arctic), but it may also be useful to demonstrate the differences that exist longitudinally. For example, the results in Chapters 4 and 5 brought attention to the fact that while the IWC values may be comparable, differences in the Ni observations between MACPEX/MidCiX and the data from Krämer et al. may be indicative of differences in dynamics, such as convection. To that end, would a cirrus cloud parameterization based on U.S. data be representative of European datasets too?

Regardless of the research pathway that I choose next, I will continue to utilize and add to the expanded IWC climatology to make further inquiries into the mechanisms responsible for determining IWC in order to enhance the understanding of the processes that form and maintain cirrus clouds and to improve the representation of clouds in global climate models.

References

Ansmann, A.: Molecular-Backscatter Lidar Profiling of the Volume-Scattering Coefficient in Cirrus, in: Cirrus, Lynch, D. K., Sassen, K., Starr, D. O'C., Stephens, G. (Eds.), Oxford University Press, New York, New York, 197 – 210, 2002.

Baker, B., Mo, Q., Lawson, R. P., O'Connor, D., and Korolev, A.: Drop size distributions and the lack of small drops in RICO rain shafts, J. Appl. Meteor. Climatol., 48, 616 – 623, 2009.

Barahona, D. and Nenes, A.: Parameterizing the competition between homogeneous and heterogeneous freezing in cirrus cloud formation – monodisperse ice nuclei, Atmos. Chem. Phys., 9, 369 – 381, 2009.

Baumgardner, D., Jonsson, H., Dawson, W., O'Connor, D., and Newton, R.: The cloud aerosol and precipitation spectrometer: a new instrument for cloud investigations, Atmos. Res., 59 – 60, 251 – 264, 2001.

Bertaux, J.-L. and Delannoy, A.: Vertical distribution of H_2O in the stratosphere as determined by UV fluorescence in-situ measurements, Geophys. Res. Lett., 5, 1017 – 1020, 1978.

Brabec, M., Wienhold, F. G., Luo, B. P., Vömel, H., Immler, F., Steiner, P., Hausammann, E., Weers, U., and Peter, T.: Particle backscatter and relative humidity measured across cirrus clouds and comparison with microphysical cirrus modelling, Atmos. Chem. Phys., 12, 9135 – 9148, doi:10.5194/acp-12-9135-2012, 2012.

Bunz, H., Benz, S., Gensch, I., and Krämer, M.: MAID: a model to simulate UT/LS aerosols and ice clouds, Environ. Res. Lett., 3, 035001, doi:10.1088/1748-9326/3/3/035001, 2008.

Cziczo, D. J., Froyd, K. D., Hoose, C., Jensen, E. J., Diao, M., Zondlo, M. A., Smith, J. B., Twohy, C. H., and Murphy, D. M.: Clarifying the Dominant Sources and Mechanisms of Cirrus Cloud Formation, Science, 340, 1320 – 1324, doi: 10.1126/science.1234145, 2013.

Davis, S. M., Hallar, A. G., and Avallone, L. M.: Measurement of Total Water with a Tunable Diode Laser Hygrometer: Inlet Analysis, Calibration Procedure, and Ice Water Content Determination, J. Atmos. Ocean. Tech., 24, 463 – 475, doi: 10.1175/JTECH1975.1, 2007a.

Davis, S. M., Avallone, L. M., Weinstock, E. M., Twohy, C. H., Smith, J. B., and Kok, G. L.: Comparisons of in situ measurements of cirrus cloud ice water content, J. Geophys. Res., 112, D10212, doi:10.1029/2006JD008214, 2007b.

DeMott, P. J., Rogers, D. C., Kreidenweis, S. M.: The susceptibility of ice formation in upper tropospheric clouds to insoluble aerosol components, J. Geophys. Res., 102, D16, 19575 – 19584, 1997.

DeMott, P. J., Rogers, D. C., Kreidenweis, S. M., Chen Y., Twohy, C. H., Baumgardner, D., Heymsfield, A. J., and Chan, K. R.: The role of heterogeneous freezing nucleation in upper tropospheric clouds: Inferences from SUCCESS, Geophys. Res. Lett., 25, 9, 1387 – 1390, 1998.

Dye, J. E. and Baumgardner, D.: Evaluation of the Forward Scattering Spectrometer Probe. Part I: Electronic and Optical Studies, J. Atmos. Ocean. Tech., 1, 329 – 344, 1984.

Engblom, W. and Ross, M.: Numerical Model of Airflow Induced Particle Enhancement for Instruments Carried by the WB-57F Aircraft, ATR-2004(5084)-1, El Segundo, CA, 2003.

Forster, P., Ramaswamy, V., Artaxo, P., Berntsen, T., Betts, R., Fahey, D. W., Haywood, J., Lean, J., Lowe, D. C., Myhre, G., Nganga, J., Prinn, R., Raga, G., Schulz, M., and Van Dorland, R.: Changes in Atmospheric Constituents and in Radiative Forcing. In: Climate Change 2007: The Physical Science Basis. Contribution of Working Group I to the Fourth Assessment Report of the Intergovernmental Panel on Climate Change [Solomon, S., Qin, D., Manning, M., Chen, Z., Marquis, M., Averyt, K. B., Tignor, M., and Miller, H. L. (eds.)], Cambridge University Press, Cambridge, United Kingdom and New York, NY, USA, 2007.

Gierens, K.: On the transition between heterogeneous and homogeneous freezing, Atmos. Chem. Phys., 3, 437 – 446, 2003.

Hallar, A. G., Avallone, L. M., Herman, R. L., Anderson, B. E., and Heymsfield, A. J.: Measurements of ice water content in tropopause region Arctic cirrus during the SAGE III Ozone Loss and Validation Experiment (SOLVE), J. Geophys. Res., 109, D17203, doi:10.1029/2003JD004348, 2004.

Heymsfield, A. J.: Precipitation development in stratiform ice clouds: A microphysical and dynamical study, J. Atmos. Sci., 34, 367 – 381, 1977.

Heymsfield, A. J. and Donner, L. J.: A Scheme for Parameterizing Ice-Cloud Water Content in General Circulation Models, J. Atmos. Sci., 47, 15, 1865 – 1877, 1990.

Heymsfield, A. J., Miloschevich, L. M., Twohy, C., Sachse, G., and Oltmans, S.: Upper tropospheric relative humidity observations and implications for cirrus ice nucleation, Geophys. Res. Lett., 25, 1343 – 1346, 1998.

Heymsfield, A. J. and Platt, C. M. R.: A Parameterization of the Particle Size Spectrum of Ice Clouds in Terms of the Ambient Temperature and the Ice Water Content, J. Atmos. Sci., 41, 5, 846 – 855, 1984.

Heymsfield, A. J. and Sabin, R. M.: Cirrus crystal nucleation by homogeneous freezing of solution droplets, J. Atmos. Sci., 46, 2252 – 2264, 1989.

Heymsfield, A. J., Winker, D., and van Zadelhoff, G. J.: Extinction-ice water content-effective radius algorithms for CALIPSO, Geophys. Res. Lett., 32, L10807, doi:10.1029/2005GL022742, 2005.

Hintsa, E. J., Weinstock, E. M., Anderson, J. G., May, R. D., and Hurst, D. F.: On the accuracy of in situ water vapor measurements in the troposphere and lower stratosphere with the Harvard Lyman-α hygrometer, J. Geophys. Res., 104, D7, 8183 – 8189, 1999.

Hoyle, C. R., Luo, B. P., and Peter, T.: The Origin of High Ice Crystal Number Densities in Cirrus Clouds, J. Atmos. Sci., 62, 2568 – 2579, 2005.

Jensen, E. J., Lawson, P., Baker, B., Pilson, B., Mo, Q., Heymsfiled, A. J., Bansemer, A., Bui, T. P., McGill, M., Hlavka, G., Heymsfield, G., Platnick, S., Arnold, G. T., and Tanelli, S.: On the importance of small ice crystals in tropical anvil cirrus, Atmos. Chem. Phys., 9, 5519 – 5537, 2009.

Jensen, E. J., Lawson, R. P., Bergman, J. W., Pfister, L., Bui, T. P., and Schmitt, C. G.: Physical processes controlling ice concentrations in synoptically forced midlatitude cirrus, J. Geophys. Res., 118, 1 – 13, doi:10.1002/jgrd.50421, 2013.

Jensen, E., Pfister, L., Bui, T., Lawson, P., and Baumgardner, D.: Ice nucleation and cloud microphysical properties in tropical tropopause layer cirrus. Atmos. Chem. Phys., 10, 1369-1384, 2010.

Jensen, E., Starr, D., and Toon, O. B.: Mission investigates tropical cirrus clouds, EOS, 85, 45 – 50, 2004.

Joos, H., Spichtinger, P., Reutter, P., Fusina, F.: Influence of heterogeneous freezing on the microphysical and radiative properties of orographic cirrus clouds, Atmos. Chem. Phys. Discuss., 13, 18069 – 18112, doi:10.5194/acpd-13-18069-2013, 2013.

Kärcher, B. and Lohmann, U.: A parameterization of cirrus cloud formation: Homogeneous freezing of supercooled aerosols, J. Geophys. Res., 107, D2, 4010, 10.1029/2001JD000470, 2002.

Kärcher, B. and Lohmann, U.: A parameterization of cirrus cloud formation: Heterogeneous freezing, J. Geophys. Res., 108, 4402, doi:10.1029/2002JD003220, 2003.

Kärcher, B. and Spichtinger, P.: Cloud-controlling Factors of Cirrus, Clouds in the Perturbed Climate System: Their Relationship to Energy Balance, Atmospheric Dynamics, and Precipitation (from the Strüngmann Forum Report), edited by: Heintzenberg, J. and Charlson, R. J., MIT Press, Cambridge, Massachusetts, 235 – 267, 2009.

Kärcher, B. and Ström, J.: The roles of dynamical variability and aerosols in cirrus cloud formation, Atmos. Chem. Phys., 3, 823 – 838, 2003.

Keyser, D. and Shapiro, M. A.: A review of the structure and dynamics of upper-level frontal zones, Mon. Wea. Rev., 114, 452 – 499, 1986.

Kinne, S. and Liou, K.-N: The Effects of the Nonsphericity and Size Distribution of Ice Crystals on the Radiative Properties of Cirrus Clouds, Atmos. Res., 24, 273 – 284, 1989.

Kley, D., Russell III, J. M., and Phillips, C. (Eds.), SPARC Assessment of Upper Tropospheric and Stratospheric Water Vapour, World Climate Research Programme, WCRP-113, 2000.

Kley, D. and Stone, E. J.: Measurement of water vapor in the stratosphere by photodissociation with Ly-α (1216 Å) light, Rev. Sci. Instrum., 29, 691 – 697, 1978.

Koop, T.: Homogeneous ice nucleation in water and aqueous solutions, Zeitschrift Fur Physikalische Chemie, 218, 1231–1258, doi:10.1524/zpch.218.11.1231.50812, 2004.

Koop, T., Luo, B., Tsias, A., and Peter, T.: Water activity as the determinant for homogeneous ice nucleation in aqueous solutions, Nature, 406, 611 – 614, 2000.

Korolev, A. V., Strapp, J. W., and Isaac, G. A.: Evaluation of the accuracy of PMS optical array probes, J. Atmos. Ocean. Tech., 15, 708 – 720, 1998.

Krämer, M. and Afchine, A.: Sampling characteristics of inlets operated at low U/U_0 ratios: new insights from computational fluid dynamics (CFX) modeling, J. Aerosol Sci., 35(6), 683 – 694, doi:10.1016/j.jaerosci.2003.11.011, 2004.

Krämer, M., Schiller, C., Afchine, A., Bauer, R., Gensch, I., Mangold, A., Schlicht, S., Spelten, N., Sitnikov, N., Borrmann, S., de Reus, M., and Spichtinger, P.: Ice supersaturations and cirrus cloud crystal numbers, Atmos. Chem. Phys., 9, 3505 - 3522, doi:10.5194/acp-9-3505-2009, 2009.

Lawson, R. P., O'Connor, D., Zmarzly, P., Weaver, K., Baker, B., Mo, Q., and Jonsson, H.: The 2D-S (Stereo) Probe: Design and Preliminary Tests of a New Airborne, High-Speed, High-Resolution Particle Imaging Probe, J. Atmos. Ocean. Tech., 23, 1462 – 1477, 2006.

Lin, R.-F., Starr, D. O, Reichardt, J., and DeMott, P. J.: Nucleation in synoptically forced cirrostratus, J. Geophys. Res., 110, D08208, doi:10.1029/2004JD005362, 2005.

Liou, K. N.: Review. Influence of Cirrus Clouds in Weather and Climate Processes: A Global Perspective, Mon. Weather Rev., 114, 1167 – 1199, 1986.

Liou, K. N., Gu, Y., Yue, Q., and McFarquhar, G.: On the correlation between ice water content and ice crystal size and its application to radiative transfer and general circulation models, Geophys. Res. Lett., 35, L13805, doi:10.1029/2008GL033918, 2008.

Lohmann, U.: A glaciation indirect effect caused by soot aerosols, Geophys. Res. Lett., 29, 4, 1052 – 1055, 10.1029/2001GL014357, 2002.

Lohmann, U. and Feichter, J.: Global indirect aerosol effects: a review, Atmos. Chem. Phys., 5, 715 – 737, 2005.

Luebke, A. E., Avallone, L. M., Schiller, C., Meyer, J., Rolf, C., and Krämer, M.: Ice Water Content of Arctic, Midlatitude, and Tropical Cirrus. Part II: Extension of the Database and New Statistical Analysis, Atmos. Chem. Phys., 13, 6447 – 6459, 2013.

Mace, G. G., Benson, S., and Vernon, E.: Cirrus Clouds and the Large-Scale Atmospheric State: Relationships Revealed by Six Years of Ground-Based Data, J. Climate, 19, 3257 – 3278, doi:10.1175/JCLI3786.1, 2006.

Mace, G. G., Clothiaux, E. E., and Ackerman, T. P.: The Composite Characteristics of Cirrus Clouds: Bulk Properties Revealed by One Year of Continuous Cloud Radar Data, J. Climate, 14, 2185 – 2203, 2001.

Mace, G. G., Starr, D. O'C., Ackerman, T. P., and Minnis, P.: Examinations of Coupling between and Upper-Tropospheric Cloud System and Synoptic Scale Dynamics Diagnosed from Wind Profiler and Radiosonde Data, J. Atmos. Sci., 52, 23, 4094 – 4127, 1995.

Mangold, A., Wagner, R., Saathoff, H., Schurath, U., Giesemann, C., Ebert, V., Krämer, M., and Möhler, O.: Experimental investigation of ice nucleation by different types of aerosols in the aerosol chamber AIDA: implications to microphysics of cirrus clouds, Meteorologische Zeitschrift, 14, 485–497, doi:10.1127/0941-2948/2005/0053, 2005.

Marchand, R., Beagley, N., Thompson, S. E., Ackerman, T. P, and Schultz, D. M.: A Bootstrap Technique for Testing the Relationship between Local-Scale Radar Observations of Cloud Occurrence and Large-Scale Atmospheric Fields, J. Atmos. Sci., 63, 2318 – 2830, 2006.

May, R. D.: Open-path, near-infrared tunable diode laser spectrometer for atmospheric measurements of H_2O, J. Geophys. Res., 103, D15, 19161 – 19172, doi: 10.1029/98JD01678, 1998.

McFarquhar, G. M. and Heymsfield, A.J.: Parameterization of Tropical Cirrus Ice Crystal Size Distributions and Implications for Radiative Transfer: Results from CEPEX, J. Atmos. Sci., 54, 2187 – 2200, 1997.

McFarquhar, G. M., Um, J., Freer, M., Baumgardner, D., Kok, G. L., and Mace, G.: The importance of small ice crystals to cirrus properties: Observations from the Tropical Warm Pool Internations cloud Experiment (TWP-ICE), Geophys. Res. Lett., 57, L13803, doi:10.1029/2007GL029865, 2007.

Menzel, W. P., Wylie, D. P., and Strabala, K. I.: Seasonal and diurnal changes in cirrus clouds as seen in four years of observations with the VAS, J. Appl. Meteor., 31, 370 – 385, 1992.

Meyer, J., Baumgardner, D., Schnaiter, M., Möhler, O., Benz, S., Abdelmonem, A., Schmitt, C., Newton, R., Afchine, A., and Krämer, M.: Size spectra of ice and drops in mixed phase clouds: measurements with the novel cloud instrument NIXE-CAPS at the AIDA Cloud Chamber, in preparation for Atmos. Chem. Phys., 2013.

Mioche, G., Josset, D., Gayet, J.-F., Pelon, J., Garnier, A., Minikin, A., and Schwarzenboeck, A.: Validation of the CALIPSO-CALIOP extinction coefficients from in situ observations in midlatitude cirrus clouds during the CIRCLE-2 experiment, J. Geophys. Res., 115, D00H25, doi:10.1029/2009JD012376, 2010.

Möhler, O., Buttner, S., Linke, C., Schnaiter, M., Saathoff, H., Stetzer, O., Wagner, R., Kramer, M., Mangold, A., Ebert, V., and Schurath, U.: Effect of sulfuric acid coating on heterogeneous ice nucleation by soot aerosol particles, J. Geophys. Res., 110, D11 210, doi:10.1029/2004JD005169, 2005.

Pan, L. L., Bowman, K. P., Atlas, E. L., Wofsy, S. C., Zhang, F., Bresch, J. F., Ridley, B. A., Pittman, J. V., Homeyer, C. R., Romashkin, P., and Cooper, W. A.: The Stratosphere-Troposphere Analyses of Regional Transport 2008 (START08) Experiment, Bull. Amer. Meteor. Soc., 91, 327-342, 2010.

Ravishankara, A. R.: Heterogeneous and Multiphase Chemistry in the Troposphere, Science, 276, 1997.

Rolf, C., Krämer, M., Schiller, C., Hildebrandt, M., and Riese, M.: Lidar observation and model simulation of a volcanic-ash-induced cirrus cloud during the Eyjafjallajökull eruption, Atmos. Chem. Phys., 12, 10281-10294, doi:10.5194/acp-12-10281-2012, 2012.

Salzmann, M., Ming, Y., Golaz, J.-C., Ginoux, P.A., Morrison, H., Gettelman, A., Krämer, M., and Donner, L.J.: Two-moment bulk stratiform cloud microphysics in the GFDL AM3 GCM: description, evaluation, and sensitivity tests, Atmos. Chem. Phys., 10, 8037 – 8064, doi:10.5194/acp-10-8037-2010, 2010.

Sassen, K. and Benson, S.: A Midlatitude Cirrus Cloud Climatology from the Facility for Atmospheric Remote Sensing. Part II: Microphysical Properties Derived from Lidar Depolarization, J. Atmos. Sci., 58, 2103 – 2112, 2001.

Sassen, K. and Campbell, J.R.: A Midlatitude Cirrus Cloud Climatology from the Facility for Atmospheric Remote Sensing. Part I: Macrophysical and Synoptic Properties, J. Atmos. Sci., 58, 481 – 496, 2001.

Schiller, C., Afchine, A., Eicke, N., Feigl, C., Fischer, H., Giez, A., Konopka, P., Schlager, H., Tuitjer, F., Wienhold, F. G., and Zöger, M.: Ice particle formation and sedimentation in the tropopause region: A case study based on in situ measurements of total water during POLSTAR 1997, Geophys. Res. Lett., 26, 14, 2219 – 2222, 1999.

Schiller, C., Krämer, M., Afchine, A., Spelten, N., and Sitnikov, N.: Ice Water Content of Arctic, midlatitude, and tropical cirrus, J. Geophys. Res., 113, D24208, doi: 10.1029/2008JD010342, 2008.

Schlicht, S.: Untersuchung zur Wasser-Patitionierung in Zirruswolken (in German), Ph.D. thesis, Univ. of Wuppertal, Wuppertal, Germany, 2006.

Schmitt, C. G. and Heymsfield, A. J.: The Size Distribution and Mass-Weighted Terminal Velocity of Low-Latitude Tropopause Cirrus Crystal Populations, J. Atmos. Sci., 66, 2013 – 2028, 2009.

Scott, S. G., Bui, P., Chan, K. R., and Bowen, S. W.: The Meteorological Measurement System on the NASA ER-2 Aircraft, J. Atmos. Ocean. Tech., 7, 4, 525 – 540, 1990.

Seifert, P., Ansmann, A., Mueller, D., Wandinger, U., Althausen, D., Heymsfield, A. J., Massie, S. T., and Schmitt, C.: Cirrus optical properties observed with lidar, radiosonde, and satellite over the tropical Indian Ocean during the aerosol-polluted northeast and clean maritime southwest monsoon, J. Geophys. Res., 112, D17205, doi:10.1029/2006JD008352, 2007.

Shapiro, M. A. and Kennedy, P. J.: Research aircraft measurements of jet stream geostrophic and ageostrophic winds, J. Atmos. Sci., 38, 2642 – 2652, 1981.

Sitnikov, N. M., Yushkov, V. A., Afchine, A. A., Korshunov, L. I., Astakhov, V. L., Ulanovskii, A. E., Kraemer, M., Mangold, A., Schiller, C., and Ravegnani, F.: The FLASH instrument for water vapor measurements on board the high-altitude airplane, Instrum. Exp. Tech., 50(1), 113 – 121, doi:10.1134/S0020441207010174, 2007.

Spichtinger, P. and Cziczo, D. J.: Impact of heterogeneous ice nuclei on homogeneous freezing events in cirrus clouds, J. Geophys. Res., 115, D14208, doi:10.1029/2009JD012168, 2010.

Spichtinger, P. and Gierens, K. M.: Modelling of cirrus clouds – Part1a: Model description and validation, Atmos. Chem. Phys., 9, 685 – 706, 2009a.

Spichtinger, P. and Gierens, K. M.: Modelling of cirrus clouds – Part 2: Competition of different nucleation mechanisms, Atmos. Chem. Phys., 9, 2319 – 2334, 2009b.

Spichtinger, P. and Krämer, M.: Tropical tropopause ice clouds: a dynamic approach to the mystery of low crystal numbers, Atmos. Chem. Phys., 13, 9801 – 9818, doi:10.5194/acp-13-9801-2013, 2013.

Stefanutti, L., Mackenzie, A. R., Santacesaria, V., Adriani, A., Balestri, S., Borrmann, S., Khattatov, V., Mazzinghi, P., Mitev, V., Rudakov, V., Schiller, C., Toci, G., Volk, C. M., Yushkov, V., Flentje, H., Kiemle, C., Redaelli, G., Carslaw, K. S., Noone, K., and Peter, T.: The APE-THESEO tropical campaign: An overview, J. Atmos. Chem., 48, 1 – 33, 10.1023/B:JOCH.0000034509.11746.b8, 2004.

Stone, R. G.: A compendium on cirrus and cirrus forecasting, Air Force Weather Service Technical Report, AWS TR, 105 – 130 , 1957.

Thomson, D. S., Schein, M. E., and Murphy, D. M.: Particle analysis by laser mass spectrometry WB-57F instrument overview, Aerosp. Sci. Technol., 33, 153, doi:10.1080/027868200410903, 2000.

Toon, O. B., Starr, D. O., Jensen, E. J., Newman, P. A., Platnick, S., Schoeberl, M. R., Wennberg, P. O., Wofsy, S. C., Kurylo, M. J., Maring, H., Jucks, K. W., Craig, M. S., Vasques, M. F., Pfister, L., Rosenlof, K. H., Selkirk, H. B., Colarco, P. R., Kawa, S. R., Mace, G. G., Minnis, P., and Pickering, K. E.: Planning, implementation, and first results of the Tropical Composition, Cloud and Climate Coupling Experiment (TC4), J. Geophys. Res., 115, D00J04, doi:10.1029/2009JD013073, 2010.

van Zadelhoff, G.-J., van Meijgaard, E., Donovan, D. P., Knap, W. H., and Boers, R.: Sensitivity of the shortwave radiative budget to the parameterization of ice crystal effective radius, J. Geophys. Res., 112, D08213, doi:10.1029/2006JD007791, 2007.

Vaughan, G., Schiller, C., MacKenzie, A. R., Bower, K., Peter, T., Schlager, H., Harris, N. R. P., and May, P. T.: SCOUT-O3/ACTIVE: High-altitude aircraft measurements around deep tropical convection, Bull. Amer. Meteor. Soc., 89, 647 – 662, doi:10.1175/BAMS-89-5-647.

Wang, P.K., Setvak, M., Lyons, W., Schmid, W., Lin, H.: Further evidences of deep convective vertical transport of water vapor through the tropopause, Atmos. Res., 94, 2009.

Weinstock, E. M., Hintsa, E. J., Dessler, A. E., Oliver, J. F., Hazen, N. L., Demusz, J. N., Allen, N. T., Lapson, L. B., and Anderson, J. G., New fast response photofragment fluorescence hygrometer for use on the NASA ER2 and the Perseus remotely piloted aircraft, Rev. Sci. Instrum., 65, 3544, doi: 10.1063/1.1144536, 1994.

Wylie, D. P.: Cirrus and Weather: A Satellite Perspective, in: Cirrus, Lynch, D. K., Sassen, K., Starr, D. O'C., Stephens, G. (Eds.), Oxford University Press, New York, New York, 136 - 146, 2002.

Wylie, D. P., and Menzel, W.P.: Eight Years of High Cloud Statistics Using HIRS, J. Climate, 12, 170 – 184, 1999.

Zöger, M., Afchine, A., Eicke, N., Gerhards, M.-T., Klein, E., McKenna, D. S., Mörschel, U., Schmidt, U., Tan, V., Tuitjer, F., Woyke, T., and Schiller, C.: Fast in situ stratospheric hygrometers: A new family of balloon-borne and airborne Lyman α photofragment fluorescence hygrometers, J. Geophys. Res., 104, D1, 1807 – 1816, 1999.

Appendix A: Supplementary Material

The following tables contain the coefficients for the ice water content probability distribution function fit curve described by Equations (3.1) and (3.2), and as shown in Fig. 3.5.

Table A1. Coefficients for IWC PDF fit curve 1 (left).

Temperature Bin (K)	PDF Curve Cross (ppmv)	y_0	A	x_c	w	t_0
180 – 194	0.310	-12.01382	143.82626	0.00232	0.04708	6.01119
195 – 200	0.210	0.04005	3.01381	0.06691	0.01104	0.21759
200 – 204	1.575	-21.05194	542.32027	-0.08534	0.24636	16.52809
205 – 209	2.820	-0.04896	174.02433	0.19308	0.05005	20.50805
210 – 214	3.130	-0.11413	511.28957	0.33684	0.13371	85.73126
215 – 219	2.120	-0.0421	65.15718	0.54913	0.16231	7.98491
220 – 224	5.520	0.03485	176.71533	1.01225	0.34463	19.09269
225 – 229	5.240	-0.09226	146.02093	2.0732	0.84991	14.57313
230 – 234	15.150	-2.45969E-4	905.42939	3.09583	0.74539	92.20203
235 – 249	20.655	-0.89462	687.5618	5.96274	3.47748	41.94154

Table A2. Coefficients for IWC PDF fit curve 2 (right).

Temperature Bin (K)	PDF Curve Cross (ppmv)	y_0	A	x_c	w	t_0
180 – 194	0.310	-0.04993	22.15607	0.15227	0.27243	1.18354
195 – 200	0.210	0.4352	93.60985	-0.10373	0.6196	8.99474
200 – 204	1.575	0.94322	134.26649	0.91332	0.45418	15.29113
205 – 209	2.820	1.17241	320.802	-0.24756	6.90152	27.62703
210 – 214	3.130	1.99588	592.03333	6.61255	7.18796	46.32476
215 – 219	2.120	0.88556	1051.38522	2.7375	15.44282	76.0587
220 – 224	5.520	-0.03553	1324.03447	5.23038	8.67946	85.97589
225 – 229	5.240	-1.20503	4091.10308	-5.03309	24.384	272.11367
230 – 234	15.150	-0.21949	3647.73046	20.82491	67.30492	136.20246
235 – 249	20.655	-1.1732	3924.81784	10.88579	25.94284	189.63804